DNA damage signalling in BRCA1-deficient mammary progenitor cells activates autologous p52/RelB NF-κB

Andrea Sau

Thesis submitted to the
Faculty of Graduate and Postdoctoral Studies
in partial fulfillment of the requirements
for the Doctorate in Philosophy degree in Cellular and Molecular Medicine.

Cellular and Molecular Medicine
Faculty of Medicine
University of Ottawa

ABSTRACT

Understanding the biological mechanisms underlying the initiation and progression of breast cancer is an important step for its prevention and treatment. We used an *in vitro* and *in vivo* model to demonstrate that p100/p52 and RelB are strongly activated in BRCA1-deficient mouse mammary progenitor cells and human BRCA1-mutation carriers. We found that NF-κB activation induces stem and progenitor cell expansion and inhibits differentiation. Knockdown and pharmacological inhibition showed that the progesterone-independent growth of BRCA1-deficient progenitor cells requires the alternative NF-κB activation mediated by ATM. Remarkably, treatment of mice with the NF-κB inhibitor dimethylaminoparthenolide (DMAPT) resulted in prolonged repression of BRCA1-deficient progenitor cell proliferation, revealing a possible approach to cyclic chemoprevention.

TABLE OF CONTENTS

LIST OF TABLES

LIST OF FIGURES

Introduction

Results

Discussion

Appendix

LIST OF ABBREVIATIONS

A: Alanine

ATM: ataxia telangiectasia mutated protein

ATP: adenosine triphosphate

ATR: ataxia telangiectasia and Rad3 related protein

BARD1: BRCA1 associated RING domain protein 1

bFGF: basic fibroblast growth factor

BMS: Bristol-Myers Squibb

BRCA1 KO: BRCA1 knockout

BRCA1 WT: BRCA1 wild type

BRCA1: breast cancer gene-1

BRCA2: breast cancer gene-2

BRCT: BRCA1 C Terminus

BSA: bovine serum albumin

C: cytosine

CD24: heat stable antigen (cell adhesion molecule)

CD29: integrin beta-1

CD49f: integrin alpha-6

Co-IP: co-immunoprecipitation

DDR: DNA damage response

DLL: delta-like protein

DMAPT: dimethylaminoparthenolide

DMBA: 7,12-dimethylbenz(a)anthracene

DMEM: Dulbecco’s modified Eagle medium

DNA: deoxyribonucleic acid

DSBs: double strand breaks

EGF: epidermal growth factor

Elf5: E74-like factor 5

EMT: epithelial-to-mesenchymal transition

EpCAM: epithelial cell adhesion molecule

ER: estrogen receptor

ERBB2: receptor tyrosine-protein kinase erbB-2

ERα: estrogen receptor alpha

FACS: fluorescence-activated cell sorting

FANCD2: Fanconi anemia group D2 protein

FBS: foetal bovine serum

GATA3: trans-acting T-cell-specific transcription factor 3

GEO: gene expression omnibus

H2AX: histone 2AX

HR: homologous recombination

HRP: horseradish peroxidase

i.p.: intra peritoneum

IgG: immunoglobulin G

IκB: inhibitors of kappa B

IKK: inhibitors of kappa B kinase

kDa: kilodalton

LEF: lymphoid enhancer factor

Lin neg.: lineage negative

LOH: loss of heterozygosity

MAPK: mitogen activated protein kinase

MRE-11: meiotic recombination 11 protein

NEMO: NF-κB essential modulator

NES: nuclear export sequences

NF-κB: nuclear factor kappa B

NGS: Normal goat serum

NHEJ: non-homologous end-joining

NICD: notch intracellular domain

NLS: nuclear localization signals

P4: progesterone

PARP-1: poly [ADP-ribose] polymerase 1

PBS: phosphate-buffered saline

PCNA: proliferating cell nuclear antigen

PCR: polymerase chain reaction

PI3K: phosphatidylinositol-3-kinase

PR: progesterone receptors

PR-B: progesterone receptors B isoform

PVDF: polyvinylidene fluoride

qPCR: quantitative polymerase chain reaction

RANK: receptor activator for nuclear factor kappa B

RANK-L: receptor activator for nuclear factor kappa B ligand

RHD: Rel homology domain

RING: really interesting new gene

RIPA: radioimmunoprecipitation assay

RNA: ribonucleic acid

RPMI: Roswell Park Memorial Institute medium

s.c.: sub cutaneous

Ser: serine

SERM: selective estrogen receptor modulator

shRNA: short hairpin ribonucleic acid

siRNA: small interfering ribonucleic acid

SSBs: single strand breaks

SUMO: small ubiquitin-like modifier

TAD: transcription activation domain

TBS-T: tris-buffered saline and tween

TCF: T-cell factor

TIC: tumor-initiating cells

TNBC: triple negative breast cancer

ACKNOWLEDGMENTS

First and foremost, I want to thank my supervisor, Christine Pratt. She has always been supportive from the beginning of my PhD, helping me not only scientifically but also personally in this new adventure in Canada. I will never forget our daily meetings. She represents the image of the perfect supervisor.

All of this would have never been possible without the help of my mom. She has been extremely supportive and has helped during the more difficult moments of my Canadian chapter. Her positivity and love for life has been the gasoline for this long trip. Thanks mom!

Also, the love of my life that I met in Rome and pushed me to move ahead in my life. Love was the reason I moved here: love for science but mostly love for my husband, with whom I share all the great and sad moments of my life. I would not be here if it were not for you. Thank you for everything you do for me.

To my lab members, past and present, with a special mention to Miguel Cabrita who helped me with all of my spelling mistakes. Special thanks to Rose Lau, who welcomed me in the lab with her passion and love for science. She helped me in the first year, and even if we live in different countries now, she continues to be in my life, and I am grateful for this.

Finally, I would like to thank Ghadi and Georges. They are, and continue to be, the only people, other than Rose, to be able to handle my Italian craziness.

INTRODUCTION

Breast cancer: from the Queen of Persia to present day

The word "cancer" was created in 400 BC by the famous Greek physician Hippocrates. He decided to use *karkinos* from the Greek word "crab", because swollen tumors surrounded by blood vessels reminded him of a crab dug in the sand with its legs in a circle. However, even before Hippocrates, ancient Egyptians and Greeks had described this disease. The first evidence that we have comes from a case of breast cancer illustrated in an ancient Egyptian papyrus. The author, an Egyptian doctor named Imhotep who lived in 2500 BC, described it as a "bulging mass in the breast, cool, hard, dense, and spreading insidiously under the breast". Under the section entitled "Therapy" the Egyptian physician wrote, "There is none". It would take more than two thousand years before breast cancer was written about again. In 440 BC, in the *Histories* written by Herodotus, the queen of Persia, Atossa noted a bleeding lump on her breast, which may have been the consequence of inflammatory breast cancer (Mukharjee, 2010).

Today, breast cancer is the most common cancer in women, with an estimated 1.7 million new cases worldwide in 2012. Women who live in developed countries tend to have a higher risk compared to those who live in developing countries and, as a consequence, the United States and Europe have higher rates of breast cancer. Although the reason for this difference is unclear, a major role is attributed to life-style and reproductive factors. However, low rates of screening and unreported cases of breast cancer could be the reason for the lower reported rates observed in developing countries (Bray et al., 2013).

Several studies have now demonstrated a direct link between lifestyle behaviors and cancer. In the EPIC-Norfolk study, it was demonstrated that the risk of death decreases as the number of positive health behaviours increase. They measured four factors: smoking, physical activity, alcohol consumption, fruit and vegetable intake, and then looked at the total mortality causes. After 11 years of follow up, they found that those who scored 4 (showing good behaviors for the 4 factors) had one quarter the mortality risk for cancer compared to those who scored 0 (Khaw et al., 2008). Another study published in the New England Journal of Medicine showed that a higher degree of adherence to Mediterranean diet was associated with reduction in death due to cancer (Trichopoulou et al., 2003). These findings were also confirmed by another study that demonstrate that adherence to Mediterranean diet, moderate alcohol consumption, physical activity, and non-smoking, were associated with lower incidence of mortality due to cancer (Knoops et al., 2004). All together, these findings demonstrate the importance of a balanced diet and life style in lowering the risk of cancer incidence.

Overview of mammary gland biology

Structure and physiology

Unlike other organs, which develop to a complete mature state during the embryonic stage, mammary glands fully develop only during the pregnancy/lactation status in the adult female (Medina, 1996). In mouse, the mammary epithelium is composed of blind-ended branched ducts that are embedded in the mammary adipose tissue (mammary fat pad). In human, every duct ends in the terminal ductal lobular unit and the mammary epithelium is embedded in collagenous stroma (Stingl, 2011) (Figure I A). The mammary epithelium is composed of two main cell lineages: luminal cells

surrounding the lumen, and myoepithelial/basal cells between the luminal cells and the basement membrane (Figure I B).

Mammary glands are under the constant stimulus of ovarian hormones. During every human menstrual cycle (28 days) and mouse estrous cycle (4 to 5 days), the hypothalamus induces changes in the ovarian hormone release. Both human and mouse cycles have a pre-ovulatory, follicular phase characterized by increased level of estrogen, and a post-ovulatory, luteal phase, characterized by a lower level of estrogen and a high level of progesterone (P4). The proliferative phase of the breast is during the post-ovulatory luteal phase, under the progesterone stimulus (Brisken, 2013; Longacre and Bartow, 1986; Masters et al., 1977; Walmer et al., 1992). If pregnancy is established, the level of progesterone rises even more to expand the gland followed by a prolactin stimulus, which induces mammary gland differentiation accompanied by the formation of milk-producing alveoli (Naylor et al., 2003).

Due to the complexity of hormonal regulation, the role of estrogen and progesterone in the mammary gland physiology has been controversial. The use of hormone ablation and replacement in mouse models has been extensively used to distinguish the effect of these two hormones. It has been demonstrated that the mammary epithelium ceases to proliferate and becomes atrophic after ovariectomy. However, the administration of estrogen to young ovariectomized mice induces a rudimentary growth in the pubertal mammary gland (Daniel et al., 1987). In contrast, in ovariectomized adult mice, estrogen does not induce proliferation in the mammary gland. Instead, only the combination of estrogen and progesterone can properly induce the mammary gland to undergo proliferation (Beleut et al., 2010; Wang et al., 1990). Estrogen has been shown

to be a permissive hormone, increasing the expression of progesterone receptor (PR) in mammary epithelial cells (Haslam and Shyamala, 1979; Stingl, 2011). Therefore, while estrogen can drive pubertal development, progesterone is the main stimulus for mammary epithelial cell proliferation in the adult mammary gland.

While it is well established that estrogen alone has a negligible effect in increasing breast cancer risk, the role of progesterone in the pathophysiology of the mammary glands has been controversial and only recently found to increase breast cancer risk (Brisken, 2014; Muti, 2014). More than a century ago, a case of regression of breast cancer after ovariectomy was reported (Beatson, 1896) and later in the 1960s inhibitors of estrogen and progesterone were developed. However, while estrogen inhibitors were introduced in 1970s and 1980s (such as tamoxifen and aromatase inhibitors), progesterone inhibitors failed clinical trials because of their elevated toxicity (Brisken, 2013). Dual estrogen and progesterone receptor agonists have also been developed and are currently used as contraceptive methods or for hormone replacement therapy (HRT); however, increasing evidence shows that oral contraceptives increase breast cancer risk (1996). Moreover, it has been demonstrated that estrogen-only HRT does not increase breast cancer risk or may even have a protective effect (Anderson et al., 2012). However, women taking combination of estrogen and progesterone for HRT show increased incidence in breast cancer risk, mainly due to the proliferative effect of progesterone on the mammary epithelium (Chlebowski et al., 2010; Hofseth et al., 1999). It has also been demonstrated that progesterone intake is correlated with increased breast density, one of the strongest risk factors for breast cancer (Boyd et al., 2007; Vachon et al., 2002). Since 30% of women in their forties have been shown to have ductal carcinoma in situ-like

lesions in their breasts (Nielsen et al., 1987), it is possible to speculate that the proliferative effect of progesterone in the mammary glands can promote progression of these pre-existing lesions to invasive cancer.

The mammary gland contains stem and progenitor cells

The first evidence of the presence of stem cells in the adult mammary gland came in 1959 when Deome and colleagues found that any portion of a normal mouse mammary gland transplanted into a cleared fat pad was able to regenerate a fully-developed mammary gland (Deome et al., 1959). Then in 1998 came the finding that a single cell was able to regenerate a ductal lobular outgrowth complete with luminal and myoepithelial cells (Kordon and Smith, 1998). Subsequent studies used flow cytometry in order to isolate and characterize the single stem cell able to regenerate a mammary gland *in vivo*. The differential expression of CD49f (integrin subunit α6) and CD24 (cell adhesion molecule) or EpCAM (epithelial cell adhesion molecule) was used to isolate stem cells. Indeed, two groups in the same year found that mammary stem cells express high levels of CD49f ($CD49f^{HI}$) and low levels of CD24 ($CD24^{LO}$), showing the same immunophenotype of basal and myoepithelial cells (Shackleton et al., 2006; Stingl et al., 2006).

Progenitor cells have been also identified in human and mouse mammary glands. In mouse, most of the progenitor cells are found in the luminal compartment. These progenitor cells express luminal and basal keratins at low levels and transcripts associated with transcription of milk proteins such as E74-like factor 5 (Elf5) (Asselin-Labat et al., 2006; Sleeman et al., 2007; Stingl et al., 2006). These progenitor cells can be defined as undifferentiated cells having an intermediate phenotype between the basal stem cells and

the luminal differentiated cells. Also, the expression of milk transcripts and Elf5 suggest that this population may be the pool of cells that will generate alveoli during pregnancy (Stingl, 2011). Indeed, lineage tracking studies found that cells in the luminal compartment can contribute to multiple lineages, confirming the presence of bipotent/progenitor cells in this compartment (Boulanger et al., 2005; Molyneux et al., 2010).

The controversy in the semantic definition of mammary stem, progenitor and differentiated cells perfectly reflects their nature: stem and progenitor cells are in constant flux between the basal and luminal compartment within the mammary gland (Figure I B). The most common technique used today to isolate stem and progenitor cells is through immunolabeling lineage-specific cell markers followed by cell separation using fluorescence-activated cell sorting (FACS). This technique allows the separation of basal and luminal populations based on the level of expression of membrane markers that are differentially expressed in these two populations. The basal/stem cell population has $CD49f^{HI}$ $CD24^{LO}$ or $EpCAM^{LO}$ immunophenotype while the luminal/progenitor cell population has $CD49f^{LO}$ $CD24^{HI}$ or $EpCAM^{HI}$ immunophenotype (Smalley et al., 2012). Enriched stem cells are found in the highest tip of the basal population, as they express high levels of CD49f while progenitor cells are in the highest tip of the luminal population (Stingl et al., 2006) (Figure II).

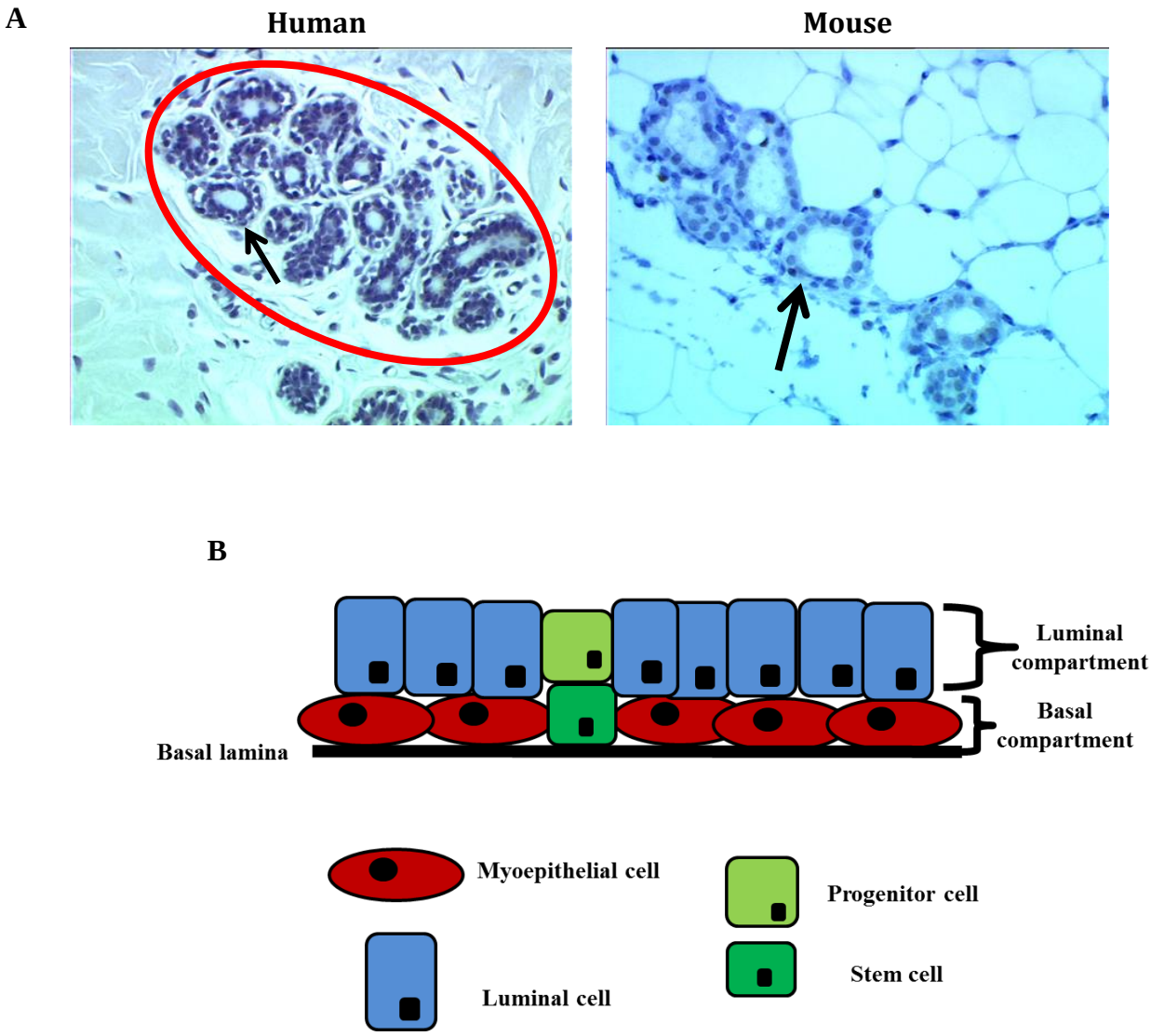

Figure I: Structure of human and mouse mammary glands

A. Left: Haematoxylin staining of a section of human mammary gland lobule and acini (Scale bar 25 μm).The red circle represents a lobule, while the arrow points an acinus. Right: Haematoxylin staining of a section of mouse mammary gland (Scale bar 15 μm). The arrow points an acinus. **B:** Graphic representation of cells composing human and mouse mammary gland ducts, lobules, and acini.

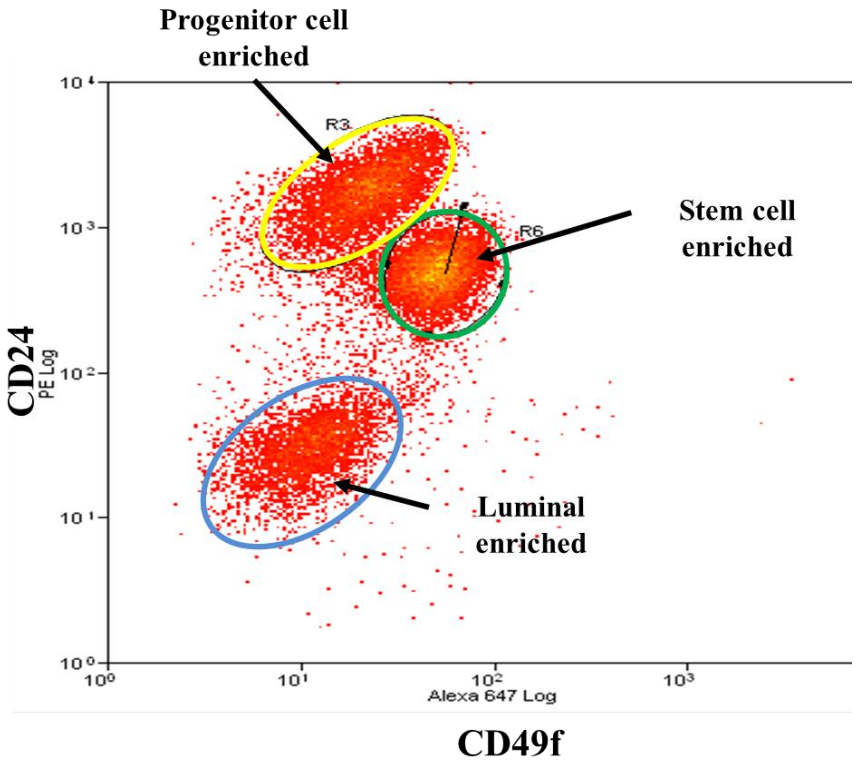

Figure II: CD49f CD24 flow-cytometry profile of mouse mammary epithelial cells

Three different populations can be separated based on CD49f and CD24 expression: Luminal cell population (within $CD49f^{LO}$ $CD24^{LO}$), stem cell population (tip of $CD49f^{HI}$ $CD24^{LO}$), and progenitor cell population (tip of $CD49f^{LO}$ $CD24^{HI}$).

Steroid hormones regulate the stem and progenitor cell proliferation

Mammary stem and progenitor cells are extremely responsive to steroid hormones even without expressing the PR or the estrogen receptor (ER). Several studies demonstrated that this was due to an indirect mechanism of action of estrogen and progesterone through paracrine signals (Asselin-Labat et al., 2006, 2010; Joshi et al., 2010; Lim et al., 2009). Indeed, it was shown that estrogen increases the release of amphiregulin from estrogen receptor α (ERα) positive cells that in turn can induce stromal cells to release growth factors necessary for stem cell proliferation (Booth et al., 2010; Mallepell et al., 2006).

As mentioned earlier, estrogen can induce the expression of PR changing the status of a cell from PR negative to PR positive (Haslam and Shyamala, 1979). Progesterone can then target PR positive cells and induce proliferation in a cyclin D1-dependent way (Beleut et al., 2010). However, this estrogen-mediated conversion of PR status is not necessary for progesterone to induce proliferation in PR negative cells. Indeed, in PR positive cells progesterone can increase the expression of the receptor activator for nuclear factor κB ligand (RANK-L), which can function as a progesterone mediator. RANK-L can then be secreted and bind its receptor RANK expressed on the PR negative stem and progenitor cells inducing proliferation and side branching during the mammary gland development (Cao et al., 2001; Mukherjee et al., 2010) (Figure III). A recent study also found that the elevated levels of progesterone during diestrus were able to induce an expansion of the stem cell compartment in the mouse mammary gland in a paracrine fashion via RANK-L release from luminal cells (Joshi et al., 2010). Moreover, Wnt expression is also downstream of progesterone signaling in PR negative

cells. Wnt signaling is important in stem cell differentiation. When Wnt ligands bind the receptor complex on the cellular membrane, β-catenin is stabilized and together with the T-cell factor/lymphoid enhancer factor (TCF/LEF) moves into the nucleus to target genes such as CCND1 (cyclin D1) and MYC (Myc) (Karamboulas and Ailles, 2013; Komiya and Habas, 2008). Progesterone can induce the expression of Wnt4, which can in turn induce proliferation in PR negative cells in a paracrine fashion (Brisken et al., 2000).

Whether alone or through the activation of intermediary pathways, progesterone is the main hormone in the mammary gland that is able to induce proliferation in differentiated PR positive cells and PR negative stem and progenitor cells.

Luminal progenitors are the cells of origin for breast cancer

Based on their gene-expression profile, human breast cancers have been categorized into five subtypes: luminal A, luminal B, receptor tyrosine-protein kinase erbB-2 (ERBB2) positive, basal-like, normal-like (Perou et al., 2000; Vargo-Gogola and Rosen, 2007). These five molecular subtypes have prognostic and predictive value: the basal-like and ERBB2 positive subtypes show the worst prognosis while within the ER positive subtypes, luminal B has a worse prognosis than luminal A subtype (showing the most favorable outcome). Among those five subgroups, the basal-like cancers have the peculiarity in that they lack the expression of ER, PR, and ERBB2; for this reason they are also defined as triple negative breast cancer (TNBC) (Sørlie et al., 2003).

The concept that cancer might arise from a population of cells with stem cell properties was first proposed almost 140 years ago (Cohnheim, 1875). This cancer stem cell hypothesis was then evoked in 1961 when it was postulated that tissue-specific "primitive" cells might be the cells of origin of cancer (Till and McCulloch, 1961). Over

the last 50 years several studies have supported this hypothesis (Foreman et al., 2009; Tuma, 2012; Wicha et al., 2006). Because of their long life span, adult stem cells can accumulate mutations required for tumor formation, making them good candidates for the cells of origin of tumors. Several groups had suggested that the stem cell population was the target for transformation events that lead to a variety of tumors (Dontu et al., 2003a; Tu et al., 2002). However, recent studies have shown that different cells of origin might give rise to the different breast cancer subtypes (Figure IV). Indeed, while the normal-like breast cancers show a gene expression signature in alignment with that of stem cells, the basal-like breast cancers show a gene expression signature that resembles more closely the luminal progenitor cells (Prat et al., 2010; Shehata et al., 2012). The remaining subtypes (luminal A, luminal B, ERBB2-positive) are more difficult to categorize. Although the luminal A has a profile resembling mature luminal cells, it is possible that a subset of this population could represent the target of transformation (Visvader and Stingl, 2014). The cell of origin for familial breast cancers (i.e. tumors arising in breast cancer associated 1 gene (BRCA1) mutation carriers) has also been studied. Genetic profiling of normal versus BRCA1-mutation carriers (Lim et al., 2009), generation of a p53/BRCA1 mouse model (Molyneux et al., 2010), and two other studies (Bai et al., 2013; Proia et al., 2011) have demonstrated that the luminal progenitors are the cells of origin for the basal-like breast cancer originating from BRCA1-mutation carriers. These observations also suggest that progenitor cells within the luminal linage can be reprogrammed to a more stem/basal-like phenotype (Guo et al., 2012).

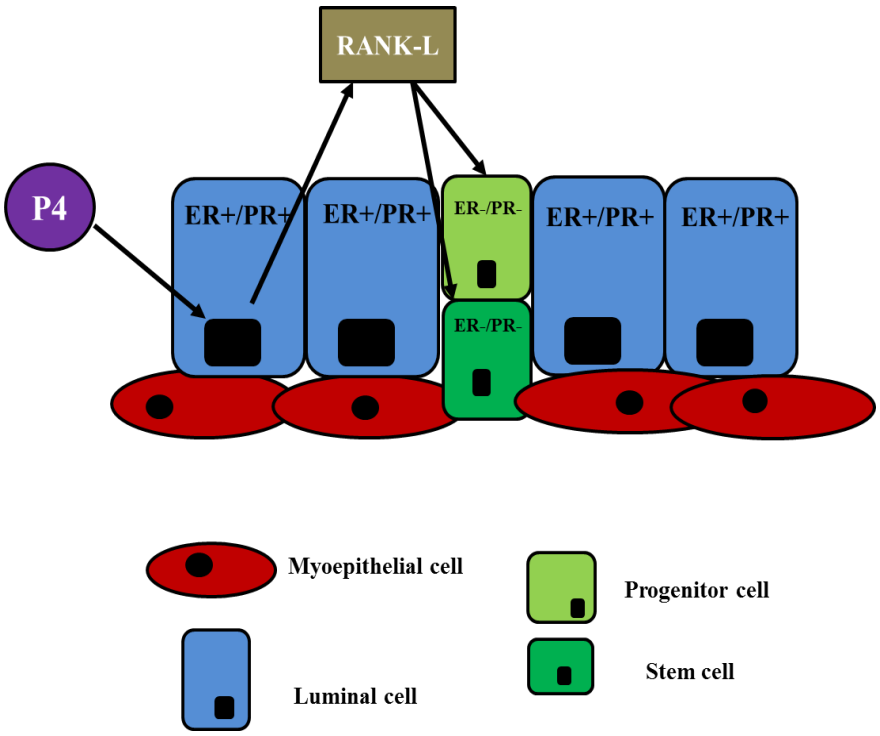

Figure III: Progesterone signaling in the mammary gland

Progesterone (P4) targets ER^+/PR^+ luminal cells where induces RANK-L release that in turn binds RANK on stem and progenitor cells (ER^-/PR^-) leading to NF-κB activation and cell proliferation.

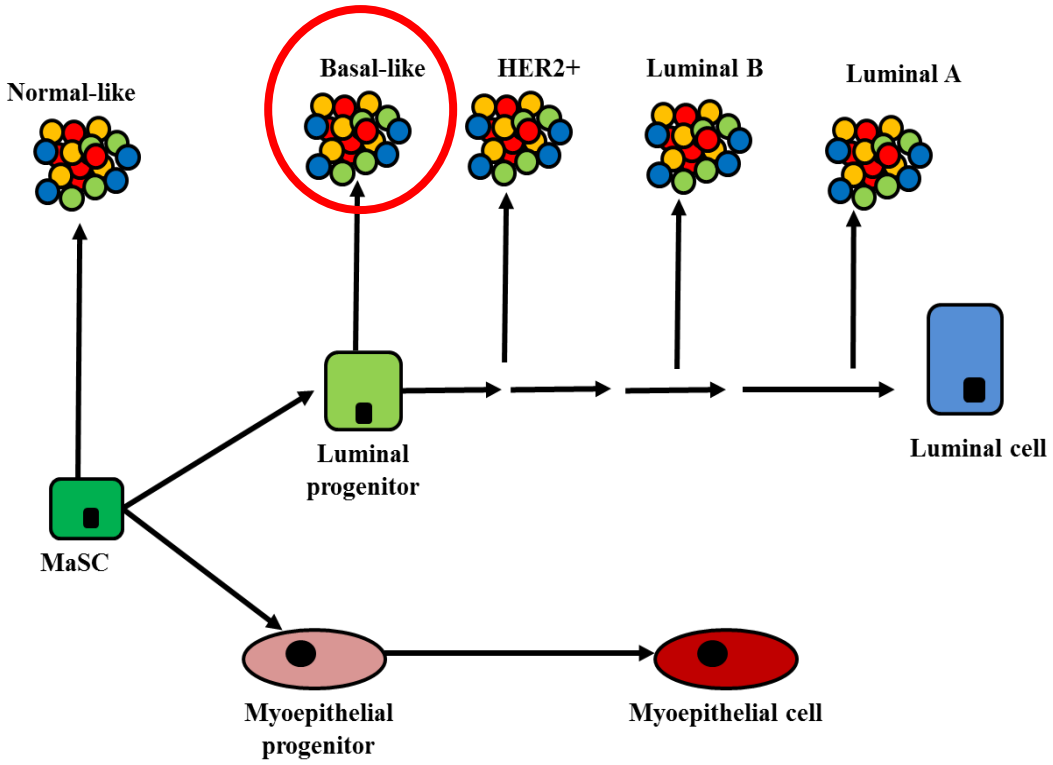

Figure IV: Breast cancer subtypes

Schematic representation of the cells of origin of the 5 breast cancer subtypes. MaSC (Mammary stem cell). Red circle: BRCA1-associated breast cancers belong to the basal-like subtype and it has been demonstrated that they originate from luminal progenitor cells. Adapted from Visvader and Stingl, 2014.

Breast cancer associated gene 1

Protein structure and function

The BRCA1 gene was originally mapped in 1990 and cloned in 1994 (Hall et al., 1990; King, 2014; Miki et al., 1994). The human gene has 24 exons, which encode for 1863 amino acids. BRCA1 contains multiple functional domains: a highly conserved N-terminal really interesting new gene (RING) finger, exon 11-13, and a C-terminal BRCA1 C Terminus (BRCT) domains (Clark et al., 2012). The N-terminal RING domain has an E3-ubiquitin ligase activity and mediates interactions between BRCA1 and other proteins, with BRCA1 associated RING domain protein 1 (BARD1) being the major BRCA1 binding partner. The BRCA1 E3-ubiquition ligase activity is increased by the formation of BRCA1/BARD1 heterodimers that are essential for BRCA1 tumor suppressor activity (Greenberg, 2011). Exons 11-13 cover the majority of the BRCA1 sequence, encoding for two nuclear localization signals (NLS) and binding sites for different proteins (Myc, Rad51, and more). Many clinically relevant mutations are associated with this region, however little is known about the structure and function of this region compared to the RING and BRCT domain (Deng and Brodie, 2000). The BRCT domain is present as tandem repeats and functions to mediate phosphoprotein interactions between BRCA1 and protein phosphorylated by ataxia telangiectasia mutated protein (ATM) and ataxia telangiectasia and Rad3 related protein (ATR). It is also been shown that BRCT plays a role in binding DNA double-strand breaks (DSBs) (Yamane et al., 2000). Mutations on the BRCT domain inhibits the ability of BRCA1 to recognize phosphoprotein and as such its ability to repair DNA damage (Leung and Glover, 2011).

BRCA1 plays an important role in maintaining global genomic stability (Zhang and Powell, 2005). Single or double DNA strand breaks (SSBs or DSBs) can occur during normal cellular replication or during exposure to genotoxic compounds. In mammalian cells, DSBs can be repaired by two main DNA repair systems: non-homologous end-joining (NHEJ), which is error-prone and mainly occurs in G1 phase of the cell cycle when sister chromatids are not available; or by homologous recombination (HR), which is error-free and occurs in late S and G2 phase of the cell cycle when sister chromatids are available as a template for repair (Kim et al., 2005). If HR is not functional, the DSBs cannot be repaired leading to chromosome rearrangement and genomic instability. BRCA1 plays a key role in HR-mediated DSBs repairs, acting as a scaffold protein to assemble a cohort of other DNA repair proteins into large physical complexes. After DNA damage, BRCA1 is recruited to the site of DSBs together with Rad50, Rad51, and many other proteins, which leads to repair of the DSBs through HR (Ciccia and Elledge, 2010). The role of BRCA1 in preventing global genomic instability is also achieved by activation of various checkpoints during normal cell cycle proliferation. BRCA1/BARD1 complex can activate G1/S, S-phase, and G2/M checkpoints and induce cell cycle arrest. While the mechanism of S-phase and G2/M checkpoints activation by BRCA1 is less understood, during the G1/S-checkpoint BRCA1 is required for ATM or ATR-mediated phosphorylation of p53 on serine (Ser) 15, which is necessary for the activation of p21 leading to cell cycle arrest to facilitate DNA repair (Fabbro et al., 2004).

During replication, cells can be subjected to DNA damage by both endogenous factors (such as by-products of cellular metabolism) and exogenous factors (such as UV

and chemical mutagens). Nicks, gaps, and stretches in the single strand of DNA can also be the cause of replication stress that together with DNA damage can impair the progression of replication forks (Zeman and Cimprich, 2014). BRCA1 has been found to participate in the protection of stalled replication forks in a HR-dependent and independent manner (Nagaraju and Scully, 2007). Together with the Fanconi anemia group D2 protein (FANCD2), BRCA2, and Rad51, BRCA1 can protect stalled forks to prevent nucleotide degradation during replication. Indeed, BRCA1 localizes to the replication foci containing the proliferating cell nuclear antigen (PCNA) followed by the co-localization of FANCD2 and Rad51. Moreover, BRCA1-defective mouse embryonic stem cells show shortened nascent filaments with replication stalling, confirming the importance of BRCA1 in maintaining stable replication forks (Schlacher et al., 2012). Together these data show the varied, critical and complex role that BRCA1 has in maintaining global genomic stability during normal cell replication and under stressed conditions (Figure V).

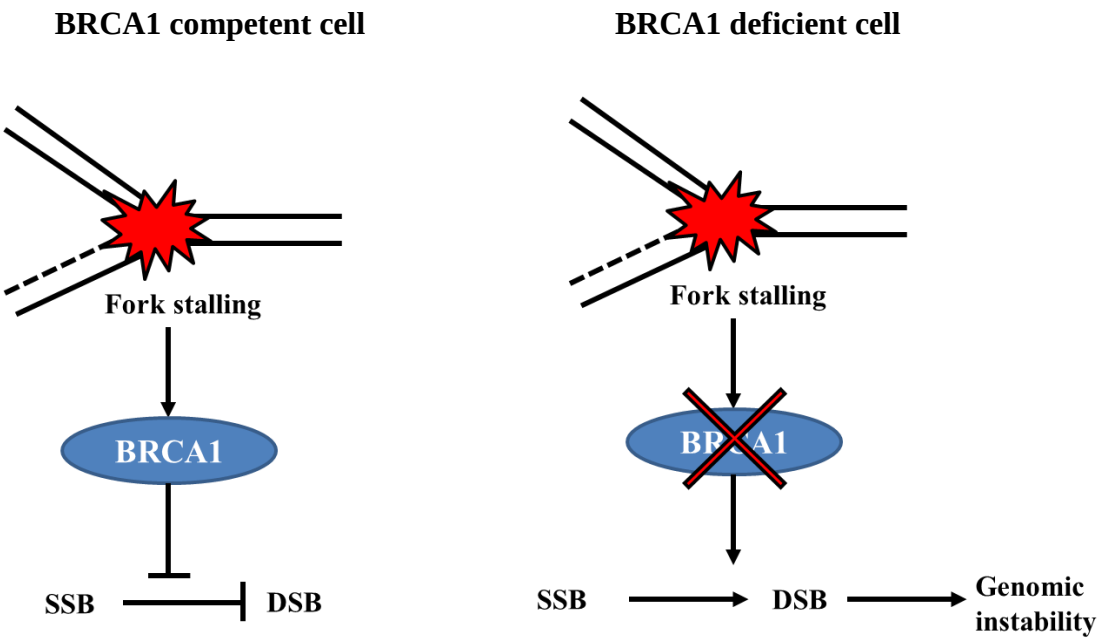

Figure V: BRCA1 and fork stalling

Role of BRCA1 in fork stalling. Replication stress can induce fork stalling. When BRCA1 is functional, it can protect and repair DNA damage caused by replication stress. When BRCA1 is mutated or lost, homologous recombination (HR) cannot properly function leading to single and double strand breaks that can result in genomic instability.

Role of BRCA1 in the mammary gland

The first evidence implicating BRCA1 in regulating mammary gland development and differentiation came only one year after its discovery. In 1995, Marquis and colleagues showed that BRCA1 was expressed in rapidly proliferating cells undergoing differentiation. Indeed, BRCA1 expression was induced during puberty, pregnancy, and after hormone treatment in ovariectomized animals. They concluded that BRCA1 was involved in the proliferation and differentiation of the mammary gland, specifically in response to ovarian hormones (Marquis et al., 1995). Other studies also confirmed the correlation between high mRNA and protein levels of BRCA1 and mammary gland differentiation (Rajan et al., 1996, 1997), while a BRCA1 tissue-specific conditional knockout mouse model showed impaired development of mammary glands (smaller mammary glands and abnormal ductal morphogenesis) (Xu et al., 1999).

Using the stem-like mouse mammary epithelial cell line HC11 as a model, it has been demonstrated that BRCA1 levels are increased when this cell line is induced to differentiate in the presence of lactogenic hormones (Kubista et al., 2002). Furuta and colleagues demonstrated that BRCA1 loss is responsible for impaired differentiation and increased proliferation in the non-tumorigenic human mammary epithelial cell line MCF-10A. They were also able to demonstrate that the C-terminal BRCT domain, but not the N-terminal RING domain, was crucial for normal differentiation. Gene expression profiling experiments also showed that depletion of BRCA1 up-regulates proliferative genes but down-regulates those involved in differentiation (Furuta et al., 2005). BRCA1 has also been shown to regulate the expression of ERα through the direct binding of its

promoter: when BRCA1 is lost or mutated, ERα expression is repressed (Hosey et al., 2007).

BRCA1 has also been found to regulate the stem and progenitor cell fate of mammary glands. Loss of BRCA1 function results in aberrant luminal differentiation and accumulation of stem and progenitor cells (Liu et al., 2008). BRCA1 has been reported to regulate Notch, a signaling pathway involved in proliferation and differentiation of stem and progenitor cells. The Notch pathway is composed of four receptors (Notch1, Notch2, Notch3, Notch4) and five ligands (three delta-like protein DLL1, DLL2, DLL3 and two Jagged proteins JAG1 and JAG2). When a ligand binds the Notch receptor, two proteases induce a cleavage of Notch receptor leading to the release of an active intracellular domain (NICD) that translocates into the nucleus to activate gene expression (Karamboulas and Ailles, 2013). Notch activation in mammary epithelial cells is known to be associated with the transition from a bipotent/progenitor to a more differentiated luminal cell, with Notch 3 expression being essential (Raouf et al., 2008). BRCA1 can increase the expression of the Notch ligand JAG1 in the basal/stem cell compartment, and this can in turn signal to the surrounding cells. Notch inhibition was also associated with an increase in the stem and progenitor cells and loss of terminal differentiation markers (Buckley et al., 2011). Moreover, BRCA1 can interact with and co-regulate target genes with trans-acting T-cell-specific transcription factor 3 (GATA3), a transcription factor known to be up-regulated by Notch and have a key role in maintaining the luminal lineage. This finding provides another mechanism through which BRCA1 can regulate the luminal commitment (Kouros-Mehr et al., 2006; Tkocz et al., 2012). While the up-regulation of the *JAG1* gene in the basal compartment enforces a basal-cell commitment,

the activation of Notch in the surrounding luminal cells leads to the adoption of a luminal-cell fate. Taken together these data demonstrate that BRCA1 is a key regulator of the stem and progenitor cell fate, able to orchestrate proliferation, differentiation and cell lineage commitment in the mammary gland.

BRCA1 also plays a key role in breast cancer; indeed, mutations in one copy of the BRCA1 gene in the germ line lead to the hereditary breast and ovarian cancer syndrome, which is inherited in an autosomal-dominant fashion. This syndrome is characterized by early onset of breast and ovarian cancer (before the age of 50), and increased risk of pancreatic, stomach, and prostate cancer. It has been estimated that the mutation rate for BRCA1 carriers is around 1/800 (Mann et al., 2006). BRCA1-associated breast cancer account for 5-7 % of all breast cancers and BRCA1-mutation carriers have up to 80 % risk of developing breast cancer by the age of 70 (Easton et al., 1995; Roy et al., 2012). Approximately 15 % of all breast cancer belongs to the basal-like subtype and more than 90 % of these are BRCA1-associated breast cancers (Foulkes et al., 2003; Garber, 2009). In a study conducted in 2010, 57 unique BRCA1 variants were classified as deleterious (based on the presence of premature stop codons or missense alterations at critical residues in functional domains), the majority of which affect the BRCT domain. Moreover, another 110 mutations were found and classified as variants with unknown clinical significance. Unfortunately, classifying these unknown variants remains a great challenge, because they outnumber the known deleterious mutations and may include both unidentified deleterious mutations and neutral variants with no clinical importance (Borg et al., 2010).

NF-κB

NF-κB protein family and function

Originally discovered as a B-cell nuclear factor that binds the DNA sequence of immune globulin nearly 30 years ago (Sen and Baltimore, 1986; Singh et al., 1986), the nuclear factor (NF)-κB has been shown to have a key role in the immune system. Indeed, pro-inflammatory stimuli and byproducts of microbial and viral infection can activate NF-κB, which in turn regulates the transcription of genes involved in apoptosis, proliferation, and secondary immune response (Karin and Lin, 2002).

NF-κB can operate through two different signaling pathways: the canonical pathway and the alternative pathway. The activation of both pathways consists of series of phosphorylation, ubiquitination, and degradation reactions involving inhibitor of κB (IκB) proteins, which release NF-κB hetero- or homo-dimers. Once in the nucleus, NF-κB dimers bind the κB elements in the promoters and/or enhancers of target genes and regulate transcription through recruitment of coactivators or corepressors. The NF-κB transcription factor family is composed of five members: p105/p50 (NFKB1), p100/p52 (NFKB2), p65 (RelA), c-Rel, and RelB, which all share the N-terminal Rel homology domain (RHD) responsible for DNA binding and dimerization. RelA, RelB, and c-Rel are the only members of the family to have a transcription activation domain (TAD), which positively regulate gene transcription. Due to the lack of TAD, p52 and p50 repress transcription unless they hetero-dimerize with the Rel proteins or other coactivators. When inactive in the cytoplasm, NF-κB proteins are associated with one of the three IκB proteins (IκBα, IκBβ, IκBε) and the precursor proteins p100 and p105. These IκB proteins contain nuclear export sequences (NES) and multiple ankyrin repeat domains

that bind the RHD of NF-κB dimers to prevent their nuclear translocation (Hayden and Ghosh, 2008a) (Figure VI).

Activation of the canonical NF-κB pathway begins with the activation of inhibitors of κB kinase (IKK) proteins. The IKK complex contains IKKα and IKKβ kinases, mostly found as hetero-dimeric complexes, and a regulatory subunit IKKγ, also known as NF-κB essential modulator (NEMO). IKKβ is the main kinase activated by pro-inflammatory stimuli and it is normally sufficient to phosphorylate IκBα at Ser 32 and Ser 36 and IκBβ at Ser 19 and Ser 23. These phosphorylations result in the poly-ubiquitination of IκB by E3 ubiquitin ligase and its proteasome degradation (Karin and Ben-Neriah, 2000). Following the degradation of IκB, the NF-κB dimer (mainly p65/p50) moves into the nucleus where it can activate or repress gene transcription (Hayden and Ghosh, 2004). Conversely, the activation of the alternative NF-κB pathway depends only on IKKα kinase and does not require IKKβ or NEMO (Claudio et al., 2002). However, another study demonstrated that NEMO and IKKα can form a functional IKK complex that can activate the alternative NF-κB pathway (Solt et al., 2007). The p100 precursor acts as an IkB-like protein that inhibits RelB nuclear localization (Solan et al., 2002). Thus, IKKα can phosphorylate p100 inducing its ubiquitin-dependent partial proteolytic processing that results in p52 generation and p52/RelB nuclear localization (Ghosh and Karin, 2002; Senftleben et al., 2001) (Figure VII).

NF-κB has been shown to respond to various stresses mainly through induction of cell proliferation and survival (Ak and Levine, 2010). While the activation of NF-κB followed by extracellular stimuli is well characterized, little is known about its activation induced by intracellular genotoxic stresses. Recent studies have revealed a novel role of

NF-κB during DNA damage or replication stress (Wu and Miyamoto, 2008; Wu et al., 2010). After DNA damage, cells are able to activate an orchestrated response termed DNA damage response (DDR). The DDR is involved in the detection of the specific DNA damage, activation of the repair mechanisms, cell cycle checkpoints, and transcriptional responses. The result of the DDR may be the lesion repair and cell survival or the activation of apoptotic cell death if the DNA damage is too excessive (Ciccia and Elledge, 2010).

During DNA damage, the main kinase activated after DSBs is ATM, which phosphorylates H2AX leading to the recruitment of several other proteins involved in DDR. Several studies have demonstrated the activation of NF-κB following DSBs (Janssens and Tschopp, 2006; Wu and Miyamoto, 2007), but the first that showed an ATM-dependent NF-κB activation came in 1999, when a group found that cells from patients with ataxia telangiectasia had defective NF-κB activation in response to the DNA damaging agent camptothecin (Piret et al., 1999). Two years later another group showed that wild type but not ATM-null mice were able to activate IKKs after whole body radiation. They concluded that ATM is essential for NF-κB activation in response to DSBs but not pro-inflammatory stimuli (Li et al., 2001). More recently, it has been demonstrated that ATM is necessary but not sufficient in DNA damage induced NF-κB activation, with NEMO taking a central stage in the ATM-mediated NF-κB activation.

After DNA damage, NEMO is retained in the nucleus through ATM-independent SUMOylation (small ubiquitin-like modifier). This nuclear localization results in ATM-dependent phosphorylation followed by monoubiquitination of NEMO that ultimately leads to IKK activation (Huang et al., 2003) (Figure VIII). The ATM-dependent NEMO

phosphorylation seems to be essential for nuclear export. Indeed, the NEMO-Ser85Ala mutant that can not be phosphorylated by ATM, can be SUMOylated efficiently but fails to be monoubiquitinated and exported into the cytoplasm (Wu et al., 2006).

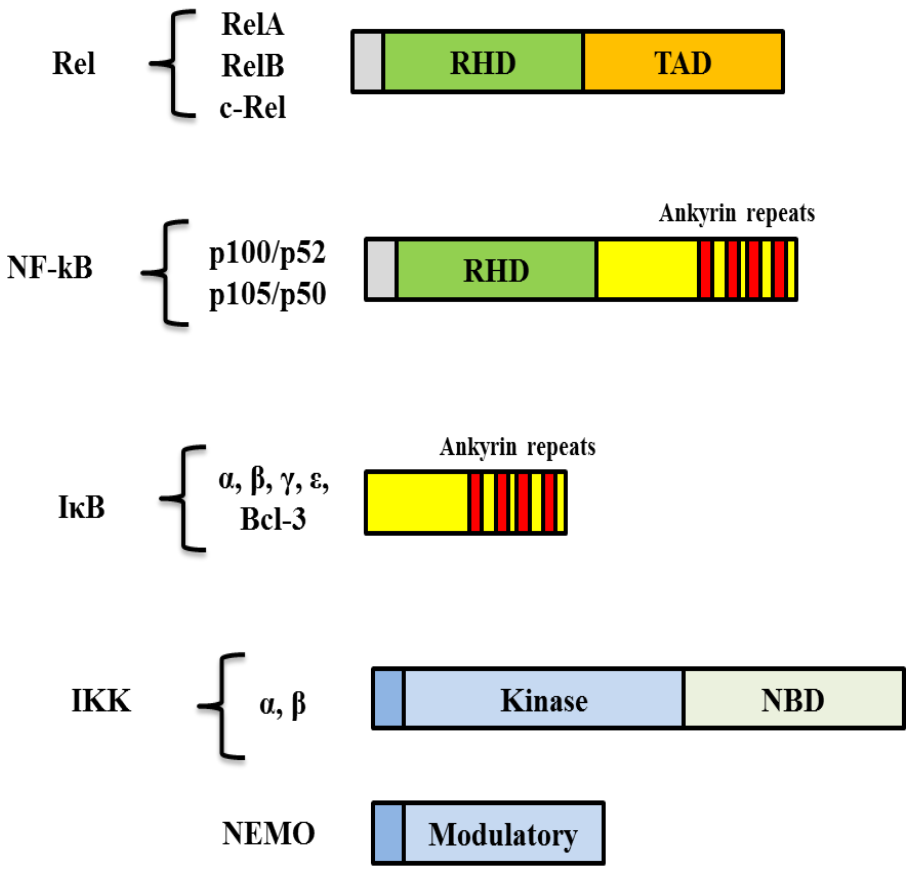

Figure VI: NF-κB family members

Schematic representation of NF-κB protein family members. RHD: Rel Homology Domain; TAD: Transactivation Domain; NBD: NEMO Binding Domain.

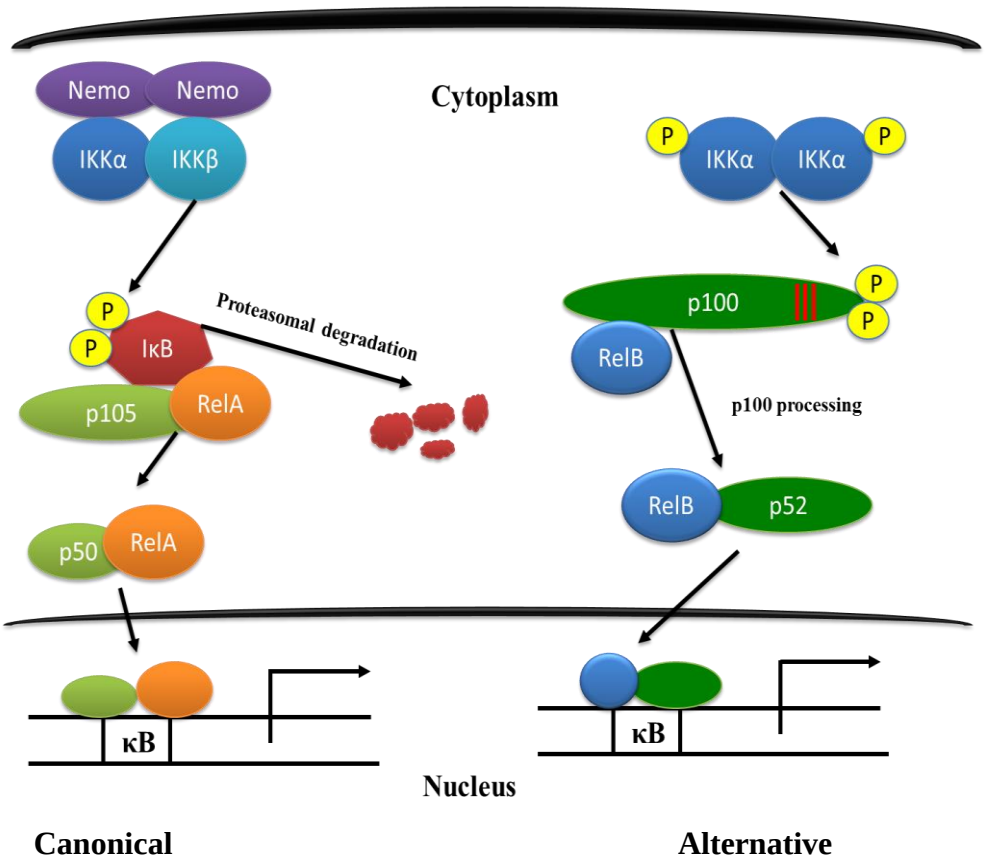

Figure VII: The canonical and alternative NF-κB pathways

Schematic representation of the canonical (left) and alternative (right) NF-κB pathways. In the canonical NF-κB pathway, IKK-dependent IκB phosphorylation induces the release of p50/RelA heterodimer that can move into the nucleus and activate gene transcription. In the alternative NF-κB pathway, IKKα homodimers induce the partial proteolytic degradation of p100 that results in p52/RelB nuclear translocation.

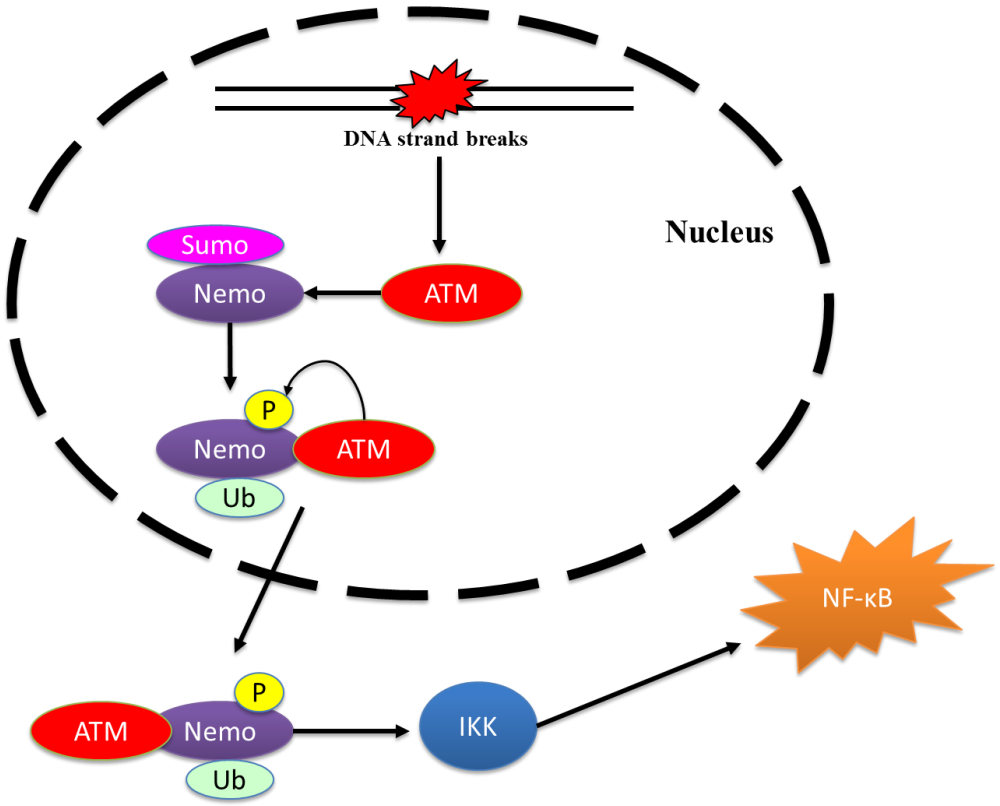

Figure VIII: Induction of NF-κB activation by DNA damage

Schematic representation of DNA damage-induced NF-κB activation. As a consequence of DNA strand breaks, ATM is activated and induces the nuclear export of NEMO. Once in the cytoplasm, the ATM/NEMO complex can induce IKK-mediated NF-κB activation.

NF-κB and breast cancer

Even before the discovery of NF-κB**,** a link between inflammation and cancer was suggested by Virchow in the nineteen century (David, 1988). However, only recently we have developed a better understanding of the role played by NF-κB in cancer initiation and progression (Coussens and Werb, 2002; Karin, 2006). Tumorigenesis requires six essential alterations: self-sufficiency in growth signal, insensitivity to growth inhibition, evasion to apoptosis, immortalization, sustained angiogenesis, and tissue invasion and metastasis (Hanahan and Weinberg, 2011). NF-κB has been shown to regulate many of these key features. For instance, NF-κB can control cell proliferation (Cao et al., 2001), increase apoptotic inhibition (Karin and Lin, 2002), and also increase metastasis and angiogenesis (Huang et al., 2000).

Several studies have shown that NF-κB is activated in breast cancers and this activation is increased with hormone independence. NF-κB was found to be constitutively active in the nucleus of human breast cancer cells, while no detectable levels were found in normal cells (Sovak et al., 1997). The canonical NF-κB pathway has been found mostly active specifically in ER positive breast cancers (Biswas et al., 2004; Nakshatri et al., 1997; Pratt et al., 2003, 2009). More studies followed these original findings, trying to address the role of NF-κB in breast cancer initiation and progression *in vivo*. Indeed, it has been found that NF-κB inhibition in transgenic mouse models increases the breast cancer latency and decrease the breast tumor burden (Connelly et al., 2011; Pratt et al., 2009). NF-κB can also regulate epithelial-to-mesenchymal transition (EMT), a key process in breast cancer progression (Huber et al., 2004). It has been found that the MCF-10A cell line undergoes EMT when p65 is overexpressed. This

phenomenon was linked to the suppression of E-cadherin and induction of mesenchymal markers such as vimentin (Chua et al., 2007). More recently it was demonstrated that both the canonical and alternative NF-κB pathways are required for the self-renewal and proliferation of tumor-initiating cells, as a consequence of NF-κB-directed stimulation of genes involved in EMT (Kendellen et al., 2014).

Not only the canonical, but also the alternative NF-κB pathway has a role in breast cancer. It was demonstrated that p100/p52 and p52/Bcl-3 hetero-dimers were both highly expressed in breast cancer cell lines and human breast cancers (Cogswell et al., 2000; Dejardin et al., 1995). Moreover, p52/RelB expression was also found increased in breast tumors induced by 7,12-dimethylbenz(a)anthracene (DMBA) (Demicco et al., 2005). A direct link between the alternative NF-κB activation and breast cancer initiation came from a mouse model in which p100 was overexpressed in the mammary gland. This mouse model showed a delay in the mammary gland development but also reduction in ductal branching during pregnancy. These mice had thickening of primary ducts, loss of epithelial cell organization and hyperplasia. Most importantly, no change in the p65 nuclear localization was detected in this mouse model, demonstrating that these phenotypic changes were only due to the alternative NF-κB deregulation (Connelly et al., 2007). Elevated levels of RelB have also been found increased in ERα-negative breast cancer. Indeed, RelB is necessary to maintain the mesenchymal phenotype of ERα-negative breast cancer cells (Wang et al., 2007).

The link between the alternative NF-κB pathway and BRCA1-mutated tumors has only recently been proposed. A microarray gene expression analysis experiment performed on 249 human breast tumors revealed that the p100/p52 and RelB genes

(components of the alternative NF-κB pathway) were mostly expressed in TNBC, the same subtype to which the BRCA1-associated breast cancers belong (Pratt et al., 2009). Moreover, the same year another study showed that p100/p52 and RelB gene expression was higher in BRCA1-mutated tumors compared to other subtypes (Fernández-Ramires et al., 2009).

NF-κB and mammary gland development

The unique development of the mammary gland reflects its special function to synthesize and deliver milk for the newborn offspring. This gland completes its development after birth, during the pregnancy/lactation phase (Medina, 1996). During puberty, under hormonal stimuli the mammary epithelium proliferates and branches extending through the entire stroma. Each round of pregnancy induces a more extensive growth and differentiation. After nursing, the majority of the epithelium undergoes apoptosis in a process called involution (Furth, 1999).

Since its discovery, NF-κB has been found to induce proliferation, differentiation, and apoptosis in several tissues (lymphocytes, lung, liver, skin, and bone) (Bendall et al., 1999; Hu et al., 1999; Tanaka et al., 1999). NF-κB has been also found to regulate the normal post-natal morphogenesis of the mammary gland as well. Indeed, NF-κB activity is high during pregnancy, decreases during lactation and increases again during involution. This pattern demonstrates the regulatory role that NF-κB has during the proliferative and apoptotic phases of the mammary gland (Brantley et al., 2000; Clarkson et al., 2000). The link between progesterone-mediated proliferation in the mammary gland and NF-κB came only recently to light. As stated earlier, progesterone can activate NF-κB in autocrine and paracrine fashion through RANK (Schramek et al., 2010). In a

previous study it was found that deletion of RANK or RANK-L resulted in a normal mammary gland development after birth. However, mammary glands showed increased apoptosis and failed to form lobulo-alveolar mammary structures during pregnancy (Fata et al., 2000). As in p100 transgenic mice, mice that overexpress RANK fail to develop a functional mammary gland, showing increased proliferation during pregnancy, impaired differentiation and decreased expression of the milk protein β-casein. Moreover, due to this constitutive overexpression of RANK, these mice developed mammary gland hyperplasia at advanced age (Gonzalez-Suarez et al., 2007). This lactation defect of RANK-null mice most closely resembled the lactation defect found in progesterone receptor B (PRB)-null mice. Indeed, PRB-null mice failed to form lobulo-alveolar structures during pregnancy and also showed decreased level of RANK-L expression (Mulac-Jericevic et al., 2003). Moreover, the knock-in $IKK\alpha^{AA}$ mice, in which the kinase function of IKKα has been deactivated, also show the same lactation defect as RANK-null mice (Cao et al., 2001).

A recent study proposed a mechanism through which a mammary gland responds to hormonal stimuli as follows: progesterone-induced proliferation occurs in two phases, an immediate phase that mostly relies on cyclin D1, and a second phase that mostly relies on RANK-L. PR positive cells quickly respond to progesterone stimulus by increasing the level of cyclin D1 and RANK-L. While cyclin D1 elicits proliferation in the small portion of PR positive cells (approximately 20%), RANK-L induces proliferation in a paracrine fashion targeting the PR negative cells (approximately 80%) (Beleut et al., 2010). All together these data demonstrate that the RANK/NF-κB axis is a key regulator of mammary epithelial cell proliferation.

Previous observations

NF-κB is known to be important during normal mammary development; however whether or not the canonical or non-canonical pathways play distinct roles in this process is unclear. Our laboratory performed a bioinformatic analysis of microarray data derived from human bipotent progenitor, early luminal progenitor, and differentiated luminal cell populations for NF-κB family proteins [Gene Expression Omnibus (GEO) accession number GSE11395] (Raouf et al., 2008). This analysis demonstrated that the gene expression of p100/p52 was higher in the bipotent and early progenitor cells compared to the more differentiated luminal cells (Figure 34 in the Appendix). This observation led to the hypothesis that the alternative NF-κB pathway has a major role in the early phase of the mammary epithelial cell commitment wherein it is necessary for the proliferation and differentiation of early progenitor cells.

Statement of the problem

The activation of the alternative NF-κB pathway has been demonstrated to play a role in the initiation and progression of breast cancer (Pratt et al., 2009; Schramek et al., 2010). Since NF-κB induces proliferation and differentiation of mammary epithelial cells, it has been proposed that its altered expression in breast cancer may be a consequence of its deregulated role in mammary gland development. NF-κB can be activated by a variety of extracellular stimuli and intracellular genotoxic stimuli (such as DNA damage) (Hayden and Ghosh, 2008b; Miyamoto, 2011). However, little is known about the DNA damage-directed NF-κB activation in breast cancer.

BRCA1 is a protein that has a key role in maintaining the global genomic stability and in regulating mammary gland development (Xu et al., 1999; Zhang and Powell,

2005). BRCA1 loss or mutation is associated with high risk of developing breast and ovarian cancer. BRCA1-associated breast cancers have a basal-like phenotype and are hormone independent (Garber, 2009; Mann et al., 2006). While the role of BRCA1 in DNA damage is well studied (Deng, 2006), little is known about its role in the initiation and progression of breast cancers. Moreover, there are no studies that link BRCA1 loss, DNA damage and proliferative signaling through NF-κB activation.

Hypothesis

Based on these previous observations, we propose that BRCA1 loss or mutation will activate the alternative NF-κB pathway in response to the increase in DNA damage. Moreover, the alternative NF-κB activation plays a role in the proliferation of progenitor cells leading to an expansion of this genetically unstable cell population in the mammary gland (Figure IX).

Objectives

1. To determine if BRCA1 loss or mutation induces the NF-κB pathway activation and if this activation is mediated by DNA damage.
2. To determine if the alternative NF-κB pathway activation is responsible for luminal progenitor cell expansion in the mouse mammary glands.

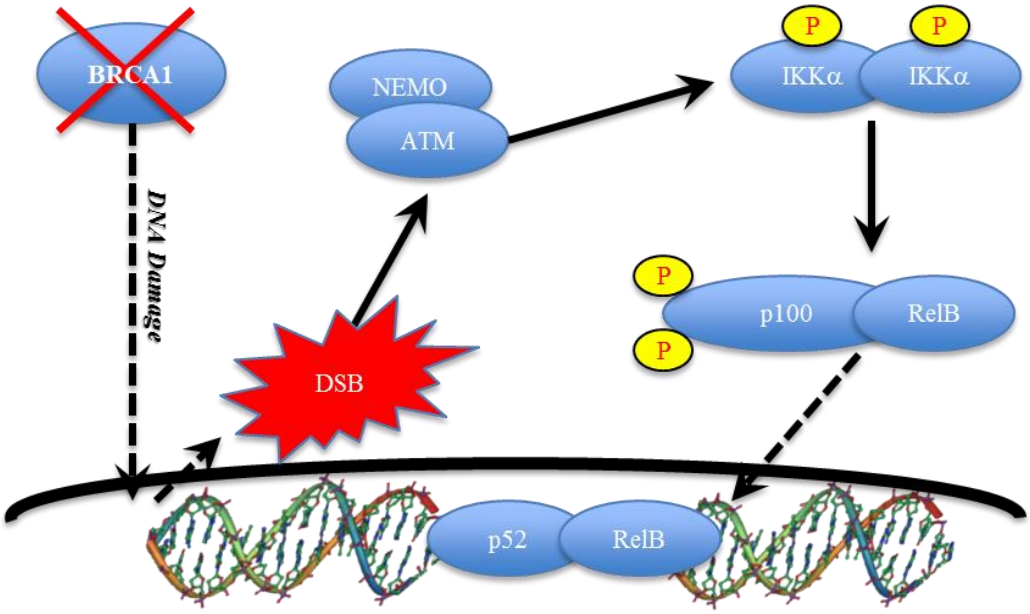

Figure IX: Schematic representation of the hypothesis

After BRCA1 loss or mutation, DNA damage-induced NF-κB activation would result in luminal progenitor cell expansion in the human and mouse mammary glands.

MATERIALS AND METHODS

Reagents

BMS-345541 and progesterone were purchased from Sigma. Dimethylaminoparthenolide (DMAPT) was a kind gift from Dr. Peter Crooks (Department of Pharmaceutical Sciences, College of Pharmacy, University of Arkansas).

Cell culture

MCF-10A, MCF-7, MDA-MB-231, HCC1937, HC11, 293T and PT67 were purchased from the American Type Culture Collection. MCF-10A human mammary epithelial cells were maintained in Ham's F12:DMEM (1:1) (GIBCO), 20 ng/mL epidermal growth factor (EGF) (Sigma), 10 μg/mL insulin (Sigma), 500 ng/mL hydrocortisone (Sigma), 100 μg/mL cholera toxin (Sigma), and 5% horse serum (GIBCO). MCF-7 cells were maintained in DMEM high glucose (HyClone) supplemented with 5% foetal bovine serum (FBS) (GIBCO). MDA-MB-231 cells were maintained in DMEM low glucose supplemented with 5% FBS. HCC1937 cells were maintained in RPMI (HyClone) supplemented with 10% FBS. HC11 mouse mammary epithelial cells were maintained in RPMI supplemented with 5 μg/mL insulin, 10 ng/ml EGF and 10% FBS. 293T and PT67 were grown in DMEM high glucose supplemented with 10% FBS.

Lentivirus and retrovirus preparation

Lentiviruses were prepared in 293T cells transfected using polyethyleneimine (4 μg/ml) with lentiviral vector and packaging plasmids psPax2 and pMD2G. After 48 and 72 hours media containing virus was collected and filtered through 0.45 μm filter and the virus concentrated using Lenti-X Concentrator (Clonotech #631231). Lenti-X

Concentrator was mixed with the filtered supernatant at a ratio 1:3 and left on ice for 1 hour. After this incubation, the supernatant was centrifuged at 1 500 x g for 1 hour at 4 °C. The white pellet obtained after centrifugation was resuspended in 400 µL of filtered 1% BSA and stored at -80 °C. 15 µL of concentrated virus was used to infect 60 to 100 mm plates. For reconstitution experiments, pBABE-puro HA-BRCA1 (Addgene #14999) was transfected into PT67 cells and media containing retrovirus collected after 72 hours, filtered through 0.45 µm filter and used for cell infection. In Table 1 are shown all plasmids used for lentiviral packaging.

Table 1: List of primers and shRNA sequences used for lentiviral packaging

1	Clone ID: V2LHS_254648
2	F: GCTGCTAAATGCTGCTCAGAA R: TTCTGAGCAGCATTTAGCAGC
3	Clone ID: V3LMM_485472
4	(Pratt et al., 2009)
5	F: GTGGAAAGGACGAAACACCGCTTGAGGCTGATCCATATCTTCAAGAGAGAATAT R: GTGGAAAGGACGAAACACCGCTTGAGGCTGATCCATATTCTTCAAGAGAGAATAT
6	F: GTGGAAAGGACGAAACACCGGTTCGATGTCCCAATTCTGTTCAAGAGACAGAAT R: TCCAGCTCGAGAAAAAGGTTCGATGTCCCAATTCTGTCTCTTGAACAGAAT
7	F: TGGAGATGATGACCGAGTTA R: TAACTCGGTCATCATCTCCTTTTTTC
8	F: TGAATTTCTATCACCAGCAA R: TTGCTGGTGATAGAAATTCTTTTTTC
9	Clone ID: V3LMM_514338
10	F: ATCTCGCTTGGGCGAGAGTAAG R: CTTACTCTCGCCCAAGCGAGAG
11	F: CAACAAGATGAAGAGCACCAA R: TTGGTGCTCTTCATCTTGTTG

[1] human/mouse pGIPZ shBRCA1 (Thermo Scientific). [2] Human/mouse pLKO3.G shp100 (TRC#0000006512). [3] Mouse pGIPZ shp100 (Thermo Scientific). [4] Mouse pLenti-GFP-S32/36A IκBα^{SR}. [5] Mouse pFLRU-shATM and [6] pFLRU shNT (kind gift of Dr. B. Sleckman) (Gapud et al., 2011). [7] and [8] Mouse LentiLox Puro shMyc (Kind gift of Dr. B. Amati) (Smith et al., 2009). [9] Mouse pGIPZ shCyclin D2 (Thermo Scientific). [10] pGIPZ shNT (Thermo Scientific). [11] pLKO.1 shNT (Sigma).

Transfection

siRNA transfections were performed in 60 mm dishes. One mL of serum free media was added to the dish and mixed with 5 nM siRNA and 7.5 µL of Dharmafect I (Dharmacon) and then incubated for 15 minutes. Cells were seeded in the dish and after 6 hours an equal amount of media was added. After 24 hours, media was changed and cells were harvested after 72 hour of transfection. The following siRNAs were used: BRCA1 (SMARTpool #M-003461–02–0005), ATM (SMARTpool #M-003201-04-0005), non-targeting siRNA #1 (siGENOME #D-001210–01–05) (Dharmacon).

For the differentiation assay, HC11 cells were transfected with pcDNA3 empty vector and p52 cFlag pcDNA3 (Addgene #20019) using GeneJuice transfection reagent (EMD Millipore) according to the manufacturer's instructions. HC11 were then selected in media containing Gentamicin (GIBCO) at a final concentration of 400 µg/ml. After antibiotic selection, cells were induced to differentiate.

Differentiation assay

Differentiation assays were performed with HC11 by plating 150 000 cells in a six well plate in the above medium for 3 days. Once cells reached confluency, EGF was removed for 24 hours and then the lactogenic hormones dexamethasone (10 µM, Sigma) and ovine-prolactin (5 µg/ml, Sigma) were added to the media without EGF. After 4 days in this differentiation media, cells were photographed for dome formation and protein collected for immunoblotting analysis.

Alamar Blue viability assay

MCF-10A and HCC1937 were plated in 96 well plates at a density of 4 000 cells per well. When cells were 80 % confluent BMS-345541 (Sigma) and DMAPT were

added at a final concentration of 10 μM for 48 and 72 hours. At each time point, Alamar Blue (Invitrogen) was added to the media as per manufacturer's instructions. After 1 hour of incubation, fluorescence was read using Synergy H1 microplate reader using the following settings: excitation 560 nm and emission 590 nm.

Immunoblotting analysis

Whole-cell extracts were prepared in radioimmunoprecipitation assay (RIPA) buffer (1% Nonidet P-40[NP-40], 0.5% deoxycholate, 0.1% sodium dodecyl sulfate [SDS], Complete Protease Inhibitor Cocktail tablets [Roche] and PhosSTOP Phosphatase Inhibitor Cocktail tablet [Roche]). Cells in RIPA were incubated on ice for 10 minutes, vortexed, and centrifuged for 15 minutes at 15 000 x g at 4 °C. Protein concentrations were determined using the Biorad D_c Protein Assay kit (Biorad). Between 20 to 40 μg of protein were denaturated in sample buffer (50 mM Tris-HCl pH 6.8, 100 mM dithiothreiotol [DTT], 2% SDS, 0.1% bromophenol blue, 10% glycerol) heated at 100 °C for 5 minutes. Protein were loaded on SDS polyacrylamide gels (ranging from 6-15%) by electrophoresis (Laemmli, 1970). Gels were transferred to polyvinylidene fluoride (PVDF) membranes (Millipore) at 100 V for 1.5 hours (with the exception of ATM and BRCA1, where gels were transferred to PVDF membrane at 12 V overnight at 4 °C). Membranes were then blocked for 1 hour with 5% non-fat skim milk powder dissolved in Tris-buffered saline (20 mM Trsi-HCl pH 7.6, 137 mM NaCl) containing 0.1% Tween-20 (TBS-T) and then incubated with primary antibody following the manufacturer's instructions. Membranes were then incubated for 1 hour with horseradish peroxidase (HRP)-conjugated secondary antibody (Jackson ImmunoResearch). The membranes were

then washed with TBS-T and protein detected with Immobilon Western Chemiluminescent HRP Substrate (Millipore) using radiography film.

Antibodies

The following primary antibodies were used for immunoblot analysis: anti-actin #A-2066 (Sigma); anti-NF-κB p52 #06-413 (Millipore); anti-BRCA1 (I-20) #sc-646, anti-phospho-ATM (10H11.E12) (S1981) #sc-47739, anti-RelB (C-19) #sc-226, β-casein (H-7) #sc-166520, anti-Ki67 (H-300) #sc-15402 (Santa Cruz); anti-IKKα #2682, phospho-IKKα/β (Ser176/180) #2697, anti-phospho-H2AX (S139) #2577, anti-E-caderin #3195, anti-cyclin D2 #3741 (Cell Signaling); anti-Myc #ab32072 (Abcam). Quantification of immunoreactive bands on immunoblots was performed using ImageJ software (www.rsb.info.nih.gov/ij/). The area under the curve (AUC) of the specific signal was corrected for the AUC of the loading control.

Co-immunoprecipitation experiments

MCF-7 cells (infected with lentivirus expressing either BRCA1 shRNA or non-targeting shRNA for 72 hours) and HCC1937 cells were harvested in co-immunoprecipitation (co-IP) buffer (25 mM Tris-HCl pH 7.5, 150 mM NaCl, 50 mM NaF, 0.5 mM EDTA pH8, 0.5% Triton-X, 5 mM β-glycerophosphate, 5% glycerol, 1 mM DTT, 1 mM PMSF, and 1 mM $NaVO_3$). Cells were then left rotating for 30 minutes at 4 °C, and then spun 15 minutes at 14,000 x g at 4 °C. The supernatant was collected and protein quantified as described in the immunoblotting section. 200 to 300 µg of protein were used for each immunoprecipitation reaction and incubated with antibody overnight with rotation at 4 °C. To immunoprecipitate ATM, two different antibodies were used in a 1:1 ratio at a final concentration of 2 µg (1 µg of mouse monoclonal ATM

[Clone MAT3-4G10/8 Sigma #A1106] and 1 µg of rabbit polyclonal ATM [Clone Ab-3 819-844 Calbiochem #PC-116]). Anti-mouse and rabbit IgG (Immunoglobulin G) (Jackson ImmunoResearch) were used as negative controls. The following day 20 µL of protein A/G PLUS-Agarose (Santa Cruz #2003) were added and incubated for 3 hours at 4 °C with rotation. All tubes were then centrifuged. Next, protein A/G agarose bound to immunoreactive complexes were washed 4 times with co-IP buffer, each time rotating for 5 minutes at 4 °C followed by centrifugation at 200 x g for 2 minutes. After the final wash, immunoprecipitated complexes were eluted in 50 µL of 2X sample buffer and boiled for 5 minutes. 40 µL of each sample was analyzed using SDS-PAGE as described above with 20 µg of input protein.

Mice

Brca1$^{loxP/loxP}$ [FVB;129-Brca1tm2Brn] mice, bearing loxP sites in introns 4 and 13 of the Brca1 gene (obtained from the NCI-Frederick National Laboratories Mouse Repository) were bred to MMTV-Cre mice (kind gift from Dr. W.J. Muller, McGill University, Montreal, Canada) (Andrechek et al., 2000; Clark-Knowles et al., 2007). Nine to 12 week-old MMTV-Cre$^{+/-}$;BRCA1$^{loxP/loxP}$ and MMTV-Cre$^{-/-}$;BRCA1$^{loxP/loxP}$ or MMTV-Cre$^{-/-}$;BRCA1$^{WT/WT}$ littermates were used for isolation of CD24/CD49f cells. DMAPT injections were administrated intra-peritoneum (i.p.) at 40 mg/Kg every other day for 15 days (total of 6 injections). Progesterone injections were administrated subcutaneous (s.c.) at 10 mg/Kg for 3 consecutive days. Mammary glands were collected the day after the last injections for DMAPT and progesterone.

C57/Bl6 IKKα $^{AA/AA}$ and C57/Bl6 IKKα $^{WT/WT}$ mice were obtained from Dr M. Karin (University of California, San Diego, USA). Serine 176 and serine 180 of IKKα were replaced with alanines (A), blocking IKKα kinase activity (Cao et al., 2001).

Mouse genotypes were determined by PCR. Animal husbandry was conducted in accordance with Policy 31 of the University of Ottawa and the Canadian Council on Animal Care guidelines.

Stem/progenitor cell isolation

Isolation of mammary epithelial subpopulations was performed on the 4th inguinal mammary glands of 8 to 12 week-old MMTV-Cre$^{+/-}$; BRCA1$^{loxP/loxP}$ or MMTV-Cre$^{-/-}$; BRCA1$^{loxP/loxP}$ mice. Mammary glands were subjected to overnight enzymatic digestion using gentle collagenase/hyaluronidase (1:10 dilution in EpiCult^{TM}-B Mouse media) (Stem Cell technology #07919). The day after, a single cell suspension was generated using 0.25% trypsin (GIBCO) and 5mg/ml dispase (Stem Cell technology #07913). For the mammosphere and Matrigel assay, a lineage negative (Lin neg.) cell population was isolated using EasySep^{TM} kit (Stem Cell Technology #19757) according to the manufacturer's instructions. Lin neg. is a cell population depleted of non-epithelial cells (such as endothelial and hematopoietic cells) found within the freshly dissociated mammary glands. For the immunostaining of stem and progenitor cell populations, luminal progenitor cells (CD49f^{LO} CD24^{HI}) and stem cells (CD49f^{HI} CD24^{LO}) were isolated from dissociated mammary glands using CD24 antibody, clone M1/69, PE-conjugated (Stem Cell technology #19757) and CD49f antibody, clone GoH3, Alexa647-conjugated (AbD Serotec). Luminal progenitor and stem cells were sorted using a

BeckmanCoulter MoFlo instrument (Ottawa Hospital Sprott Centre for Stem Cell research) and then cytospun onto slides followed by immunostaining.

Mammosphere assay

Single cell suspensions of Lin neg. cells were plated in 96 well low-attachment plate (Corning #3474). Cells were cultured in EpiCult^{TM}-B Mouse media containing 10 ng/mL basic fibroblast growth factor (bFGF) (Stem Cell technology #02634), 10 ng/mL EGF (Stem Cell technology #02633), 4 µg/mL heparin (Stem Cell technology #07980), and 1:50 B27 (BD Biosciences). Primary mammosphere formation was scored after 7 days, counted under microscope and then collected, dissociated using trypsin and re-plated again. After another week, secondary mammosphere formation was scored and spheres were counted again.

Matrigel assay

Lin neg. cells were seeded at a density of 2 000 cell per well mixed in 20 µl of Matrigel (BD Biosciences) and acini formation was scored after 15 days. For Matrigel assay DMEM:F12 (1:1) media containing 5 µg/ml insulin, 0.5 µg/ml hydrocortisone, 20 ng/ml EGF, 20 ng/ml cholera toxin (Sigma) and 1:50 B27 supplement (BD Bioscience) was added to the culture. The diameter of at least 30 of the largest acini in each well was measured under a Zeiss microscope using Northern Eclipse software. In order to confirm lentiviral infection, all acini were scored to detect GFP positivity under the microscope before size was calculated.

Immunofluorescence analysis

Cells were directly plated on coverslips while primary cells from mouse mammary glands were plated after sort (see section above: *Stem/progenitor cell*

isolation). Cells were then fixed with 4% paraformaldehyde for 15 minutes at room temperature, permeabilized with 0.5% TritonX-100 for 5 minutes at room temperature, and blocked 1 hour at room temperature with 1% bovine serum albumin (BSA). Primary and secondary antibodies were diluted in Antibody dilution buffer (DAKO #S0809) and incubated as per manufacturer's instructions. Cy3-AffiniPure donkey secondary anti-rabbit (Jackson Immunoresearch # 711-165-152) was incubated 1 hour at room temperature, protected from light. Cells were then covered with VECTASHIELD® Mounting Media with DAPI (Vector H-1200) and images were taken using a Zeiss Axioskop 2 *mot* plus microscope.

Human and mouse mammary gland paraffin-embedded sections

Mouse paraffin-embedded sections, were prepared by the University of Ottawa Department of Pathology and Laboratory Medicine. Human paraffin blocks were obtained from the Queensway Carleton Hospital in compliance with the University of Ottawa Research Ethics Board. Slides were hydrated in toluene, 100% ethanol, 95% ethanol, 70% ethanol, and water 10 minutes each. Antigen retrieval was done in the presence of 10 mM sodium citrate pH 6. Slides were then blocked for 1 hour at room temperature in blocking solution containing 2% normal goat serum (NGS), 1% BSA, 0.3% Triton X-100. Primary, secondary antibody, and image acquisition were performed as described above. Patients' information is provided in Table 2. All samples were sectioned from histologically normal breast tissue from paraffin blocks. For those patients with diagnosed contralateral cancers, tissue was confirmed normal from the other breast by pathology.

Table 2: Medical information corresponding to patient samples

BRCA1 wild type carriers		
#1	52 years	contralateral invasive ductal cancer ER+/PR+ (SERM neoadjuvant)
#2	53 years	contralateral infiltrating ductal cancer ER+/PR- (SERM neoadjuvant)
#3	66 years	contralateral infiltrating ductal cancer ER+/PR- (SERM neoadjuvant)
BRCA1-mutation carriers		
#1	49 years	contralateral ER-/PR-/HER2- invasive ductal carcinoma (medullary features). (neoadjuvant chemotherapy)
#2	35 years	prophylactic mastectomy
#3	38 year	prophylactic mastectomy

SERM: Selective Estrogen Receptor Modulator

Immunohistochemistry analysis

Human and mouse paraffin-embedded sections were subjected to the same protocol as the immunofluorescence experiment described above with the following differences. After the primary antibody was added, slides were incubated 1 hour at room temperature with DAKO Envision + Peroxidase (DAKO K4002), then developed for 5 to 30 minutes using 1 drop of DAB Chromogen per mL of substrate buffer (DAKO K3467). Slides were then rinsed in distilled water. Counterstaining was performed by dipping the slides for 10 seconds in filtered hematoxylin (Fisher), followed by 2 minutes in distilled water. Dehydration was performed in 70, 95, and 100% ethanol followed by toluene. Slides were finally covered with permanent mounting media (Permount™, Fisher).

Quantitative PCR analysis

Cells were seeded in triplicate in 6 well plates. Total RNA extraction was performed using Trizol (Invitrogen) according to the manufacturer's instructions. RNA concentration was measured using H1 Multi mode plate reader using optical density at 260 nm. Reverse transcription-quantitative PCR (qPCR) reactions were performed using the QuantiTect SYBR Green RT-PCR kit (Qiagen) with 100 ng of RNA and 0.5 μM of the respective primers, according to manufacturer's protocol. Reverse transcription was performed at 50 °C for 30 minutes followed by 15 minutes at 95 °C for initial PCR activation. A total of 40 cycles (each cycle composed of denaturating step at 94 °C for 30 seconds, annealing step at 55 °C for 30 seconds, extension step at 72 °C for 30 seconds) were performed.

Forward and reverse primers for BRCA1, ATM, ABCB1, Cyclin D2, CD44 and β-Actin were designed using the Roche website (Universal ProbeLibrary Assay Design Center) and showed in Table 3.

Statistical Analyses

Experimental results obtained *in vivo* and *in vitro* represent a minimum of three independent trials. Values presented are means ± S.E. Student's t-test was used for statistical analysis with two levels of significance: (*) $p<0.05$ and (**) $p<0.01$. Comparisons between multiple groups were performed by two-way analysis of variance (ANOVA). Tukey tests were used to determine the differences between groups. A p value < 0.05 was considered significant.

Table 3: List of primers used for qPCR

	Forward 5’ to 3’	Reverse 5’ to 3’
BRCA1 (Human)	GCGTCCCCTCACAAATAAAT	CTTGACCATTCTGCTCCGTT
BRCA1 (Mouse)	TGACAGTGCCAAAGAACTCG	GATACGCTGGTGCTCTCCTC
ATM (Mouse)	AGGATCTCCCTGGAAACGAG	CGGTGCAGAGAACACACAAG
ATM (Human)	TTTCTTACAGTAATTGGAGCATTTTG	GGCAATTTACTAGGGCCATTC
β-Actin (Mouse)	CTAAGGCCAACCGTGAAAAG	ACCAGAGGCATACAGGGACA
β-Actin (Human)	CCAACCGCGAGAAGATGA	CCAGAGGCGTACAGGGATAG
CyclinD2 (Mouse)	AAGCCTGCCAGGAGCAAA	ATCCGGCGTTATGCTGCTCT
CD44 (Mouse)	GGCTCATCATCTTGGCATCT	GCTTTTTCTTCTGCCCACAC

RESULTS

BRCA1 knockdown activates the alternative NF-κB pathway *in vitro*

BRCA1 plays a key role in maintaining the global genomic stability and in DNA damage repair through HR (Deng, 2006). It has also been shown that NF-κB can be activated after DNA damage induced by ionizing radiation and chemotherapeutic drugs as a result of ATM/NEMO-mediated signaling to IKK (Hadian and Krappmann, 2011; Miyamoto, 2011). We therefore hypothesized that NF-κB would be activated in BRCA1-deficient cells as a consequence of increased DNA damage. To test this, BRCA1 was knocked down using both siRNA and shRNA on three different cell lines: MCF-10A (human non-tumorigenic mammary epithelial cell line), MCF-7 (human breast adenocarcinoma cell line, luminal subtype), and MDA-MB-231 (human breast adenocarcinoma cell line, basal subtype). Since activation of the alternative NF-κB pathway is detected by nuclear localization of p52 and RelB, after BRCA1 knockdown with either siRNA or lentiviral infection with shRNA, immunofluorescence analysis was performed in order to detect the subcellular localization of the NF-κB components p100/p52 and RelB. BRCA1 knockdown in MCF-7 and MCF-10A resulted in a high level of nuclear p52 and RelB (Figure 1). Confirmation of BRCA1 knockdown in both cell lines was performed by immunofluorescence and showed in Figure 2. Phosphorylation of p100 induces its partial proteasome-mediated degradation that can be visualized on SDS-page as a series of fragments with a size range from 100 KDa (uncleaved p100) to 52 KDa (active p52). After BRCA1 knockdown, proteins were collected from MCF-10A, MCF-7, and MDA-MB-231 and western blot analysis performed. Increased p100 processing, resulting in two to six-fold increases in p52

formation, was detected in all the cell lines after BRCA1 knockdown, demonstrating alternative NF-κB pathway activation (Figure 3). To confirm the efficacy of siRNA and lentiviral shRNA BRCA1 knockdown, qPCR was performed on all the three cell lines and more than 60 % reduction in BRCA1 mRNA levels was detected after 72 hours of transfection with siRNA and infection with lentiviral shRNA (Figure 3).

These experiments confirmed the activation of the alternative NF-κB pathway after BRCA1 knockdown; however, it was interesting to examine the effect of a deleterious BRCA1 mutation in modulating the activation of NF-κB. The BRCA1-mutated breast cancer cell line HCC1937 has a cytosine (C) insertion at the nucleotide 5382 on the BRCA1 gene that causes a truncation of 34 amino acids at the C-terminus of the BRCA1 protein, making it non-functional (Scully et al., 1999). Reconstitution experiments were performed by infecting the HCC1937 cells with a retrovirus carrying wild type BRCA1. After infection, proteins were collected and western blot analysis showed an 80 % decrease in p52 processing (Figure 4 A). Immunofluorescence analysis also showed the same decrease in RelB and p52 nuclear localization after BRCA1 wild type reconstitution (Figure 4 B). Confirmation of the reconstitution showing the increased level of BRCA1 was done by western blot and immunofluorescence (Figure 5). All together these results show that the alternative NF-κB pathway is activated after BRCA1 is knocked down or mutated.

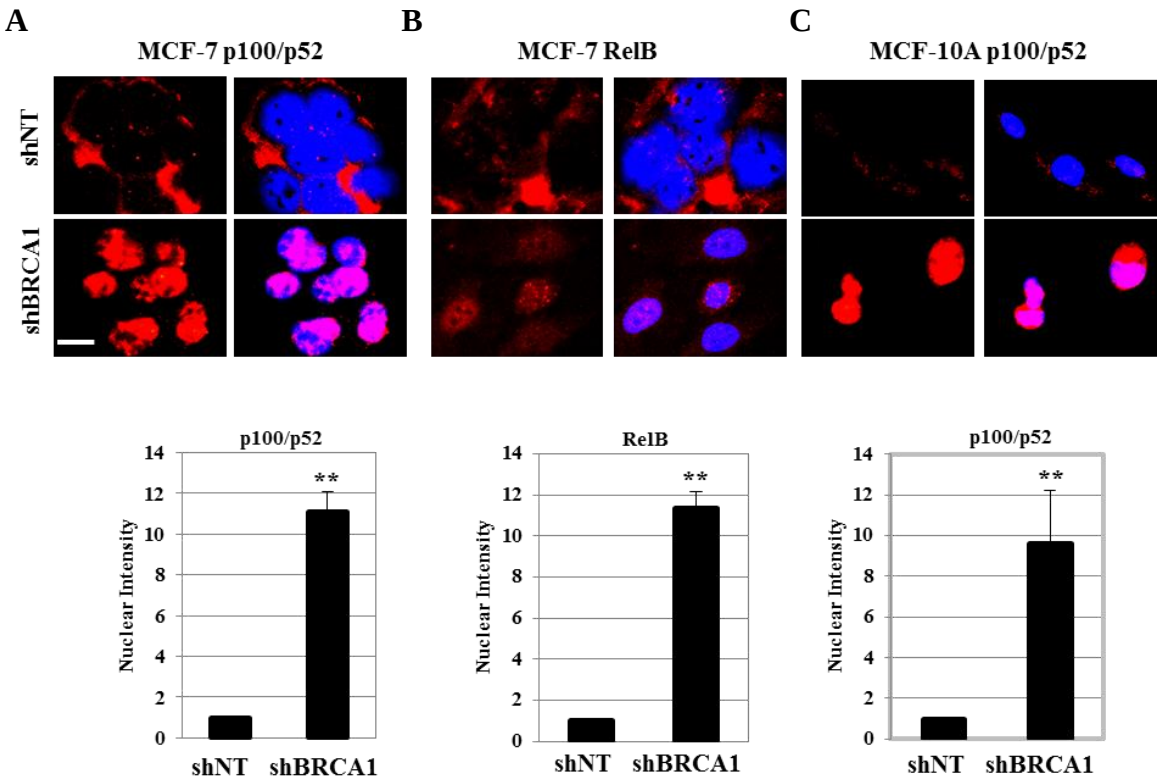

Figure 1: The alternative NF-κB pathway is activated after BRCA1 knockdown

MCF-7 and MCF-10A cells infected for 72 hours with lentivirus carrying non-targeting (NT) or BRCA1 shRNA. MCF-7 were immunostained for **A.** p100/p52 and **B.** RelB. MCF-10A were immunostained for **C.** p100/p52. The graph underneath each image represents fluorescence intensity calculated with ImageJ normalized to shNT levels (mean ± S.E). (**) refers to $p<0.01$ by Student's t-test. Scale bar 10 µm. Immunofluorescence images are representative of a minimum of three independent experiments.

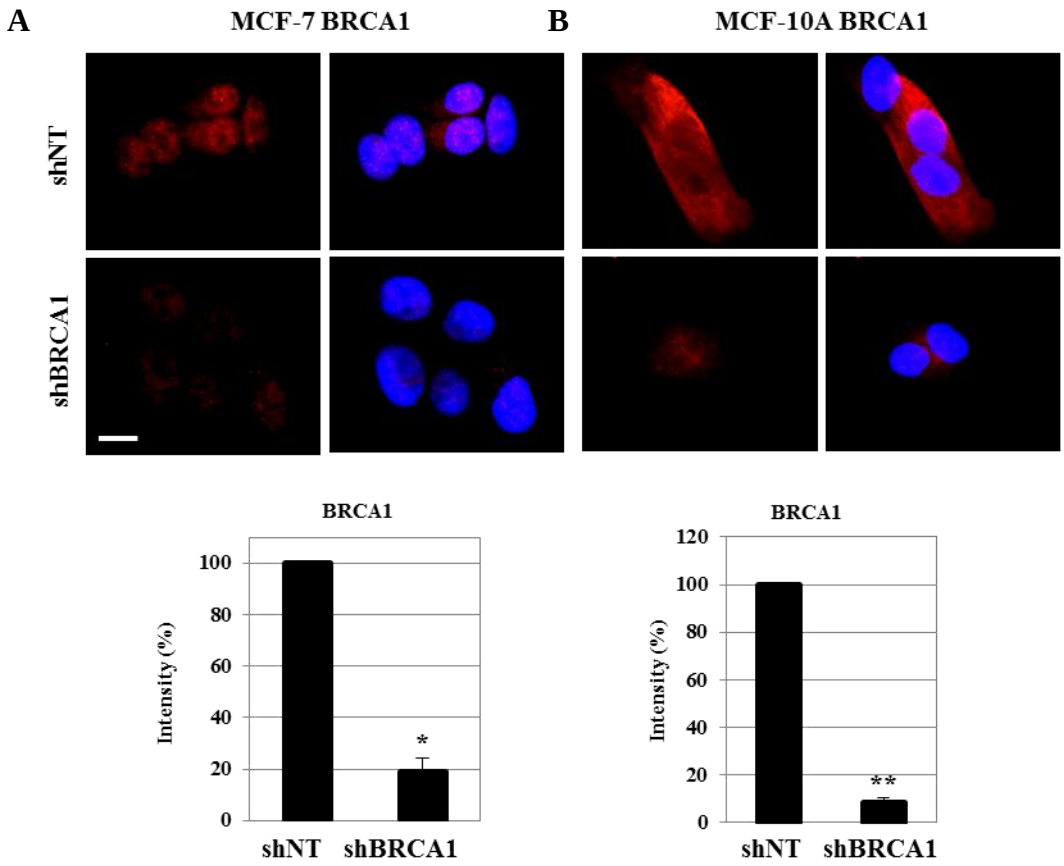

Figure 2: Confirmation of BRCA1 knockdown

MCF10-A and MCF-7 cells infected for 72 hours with lentivirus carrying non-targeting (NT) or BRCA1 shRNA. **A.** MCF-10A and **B.** MCF-7 were immunostained for BRCA1. The graph underneath each image shows BRCA1 intensity calculated with ImageJ normalized to shNT levels and expressed as percentage (mean ± S.E). (**) refers to $p<0.01$ and (*) refers to $p<0.05$ by Student's *t*-test. Scale bar 10 µm. Immunofluorescence images are representative of a minimum of three independent experiments.

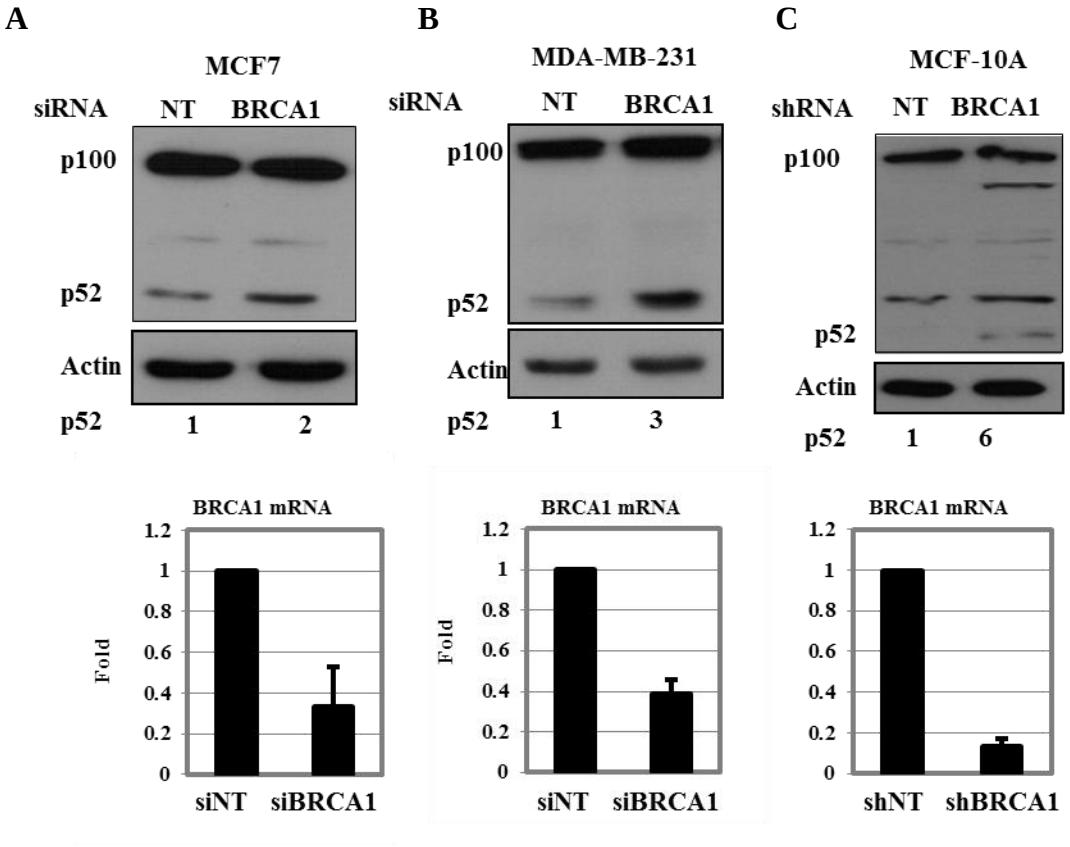

Figure 3: BRCA1 knockdown increases p52 formation

MCF-10A cells were infected for 72 hours with lentivirus carrying non-targeting (NT) or BRCA1 shRNA, MDA-MB-231, and MCF-7 were transfected for 72 hours with non-targeting (NT) or BRCA1 siRNA. Whole cell lysates from **A.** MCF7, **B.** MDA-MB-231, and **C.** MCF-10A were immunoblotted for p100/p52. Actin was used as loading control. Numbers underneath actin represent p52 protein level quantification with ImageJ normalized to non-targeting (shNT or siNT) levels. The graph underneath each blot represents confirmation of BRCA1 knockdown by qRT-PCR. mRNA levels were quantified using primers specific for BRCA1 and beta-actin (the endogenous control). Data in the graphs are normalized to non-targeting (shNT or siNT) levels (mean ± S.E). Immunoblot images are representative of a minimum of three independent experiments.

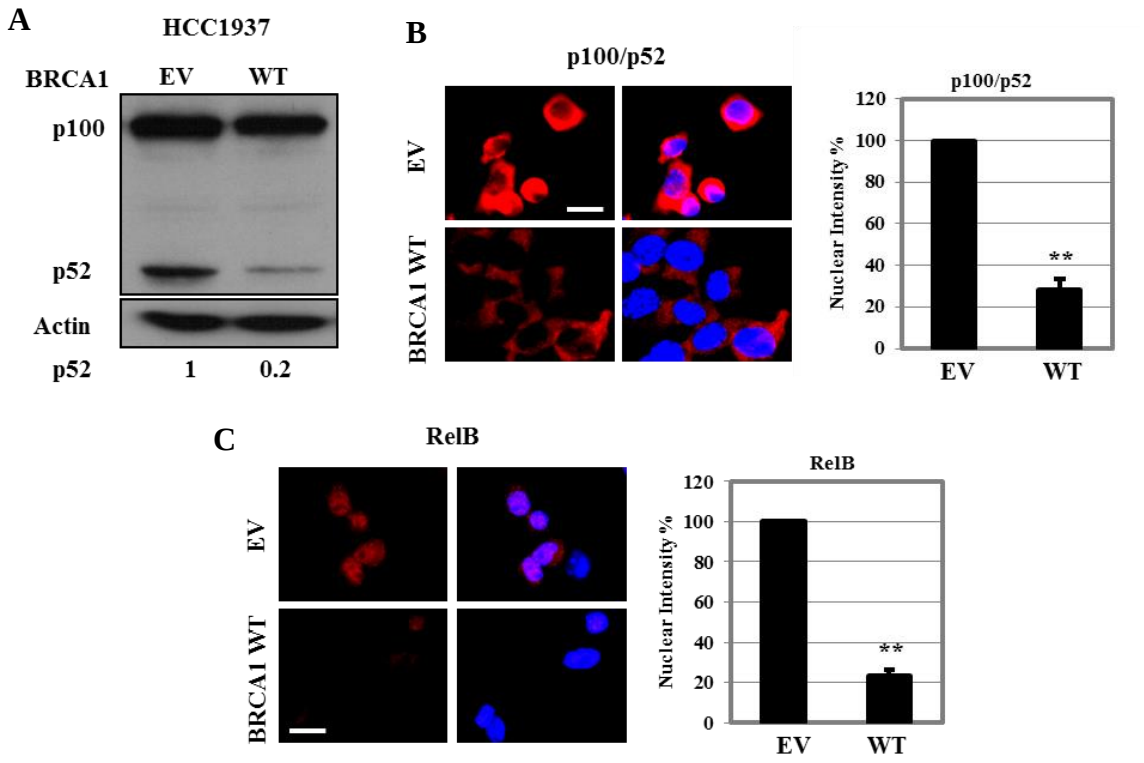

Figure 4: BRCA1 reconstitution reduces p100 processing

HCC1937 cells were infected for 72 hours with retrovirus carrying BRCA1 wild type (WT) expression vector or empty vector (EV). **A.** Whole cell lysates were immunoblotted for p100/p52. Actin was used as loading control. Numbers underneath actin represent p52 protein level quantification by ImageJ software normalized to empty vector (EV). HCC1937 cells were immunostained for **B.** p100/p52 and **C.** RelB. The graph on right to each image represents fluorescence intensity calculated with ImageJ normalized to empty vector (EV) levels and expressed as percentage (mean ± S.E). Scale bar 10 µm. (**) refers to $p<0.01$ by Student's *t*-test. Immunoblot and immunofluorescence images are representative of a minimum of three independent experiments.

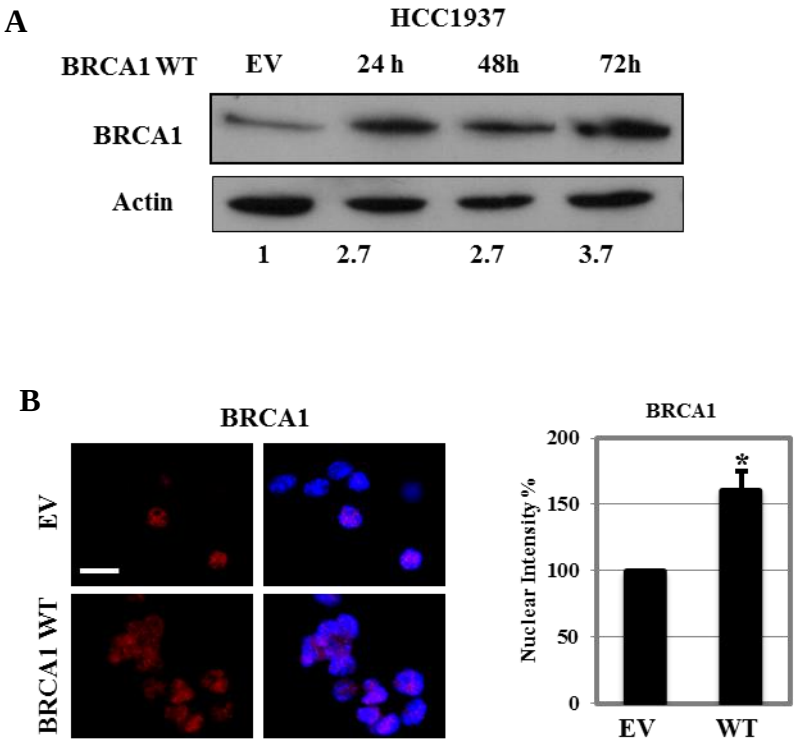

Figure 5: Confirmation of BRCA1 reconstitution

HCC1937 were infected with retrovirus expressing empty vector (EV) or BRCA1 wild type (WT) vector for 24, 48, and 72 hours. **A.** HCC1937 whole cell lysates were immunoblotted for BRCA1. Actin was used as loading control. Numbers underneath actin represent BRCA1 protein level quantification calculated with ImageJ normalized to empty vector. **B.** HCC1937 were immunostained for BRCA1 after 72 hours of infection. Graph on right represents quantification of BRCA1 nuclear intensity calculated with ImageJ normalized to retrovirus empty vector (EV) levels and expressed as percentage (mean ± S.E). Scale bar 10 μm. (*) refers to $p<0.05$ by Student's *t*-test. Immunoblot and immunofluorescence images are representative of a minimum of three independent experiments.

BRCA1 loss or mutation induces the alternative NF-κB pathway activation *in vivo*

To test if the alternative NF-κB pathway was also activated in primary mammary epithelial cells, stem and progenitor cells were collected from MMTV-Cre$^{-/-}$; BRCA1$^{loxP/loxP}$ (BRCA1 WT) and MMTV-Cre$^{+/-}$; BRCA1$^{loxP/loxP}$ (BRCA1 KO) mice mammary glands. Mammary glands were digested overnight as described in materials and methods, and then the single cell suspension obtained was sorted using FACS. Progenitor-enriched (CD49f^{LO} CD24^{HI}) and stem-enriched (CD49f^{HI} CD24^{LO}) cell populations were pooled after sorting and plated on coverslips. The following day immunofluorescence was performed. Stem- and progenitor-enriched cell populations collected from BRCA1 KO mice showed increased phospho-IKKα, p52, and RelB nuclear localization compared to those collected from BRCA1 WT (Figure 6 A-C). Moreover, a lineage negative (lin neg.) cell population was isolated from mouse mammary glands for protein extraction. Lin neg. is a mammary epithelial cell population depleted of non-epithelial cells (such as endothelial and hematopoietic cells) and its isolation is described in material and methods. After three days in culture, lin neg. cells are sub-confluent and proteins and/or RNA can be extracted. Western blot analysis showed 6-fold increase in IKKα/β phosphorylation and p52 formation in lin neg. cells obtained from BRCA1 KO mouse mammary glands compared to those obtained from the BRCA1 WT (Figure 7 A,B). In a cell, IKKβ is mostly found in hetero-dimeric complex with IKKα and it has been shown that IKKα phosphorylation induces IKKβ phosphorylation as well (Hayden and Ghosh, 2008b). Since IKKβ is the main kinase of the canonical NF-κB pathway, p65 (RelA) protein levels were analyzed in the stem- and progenitor-enriched cell populations. When the canonical NF-κB pathway is inactive, p65

is kept into the cytoplasm bound to p50; however, after activation, p50/p65 hetero-dimers move to the nucleus. An increased level of nuclear p65 is a sign of increased activation of canonical NF-κB. When immunofluorescence was performed, low level of p65 were detected in the nuclei of stem- and progenitor-enriched cells isolated from BRCA1 KO and BRCA1 WT mouse mammary glands (Figure 7 C). BRCA1 knockout was confirmed in the enriched stem and progenitor cell compartment by immunofluorescence (Figure 7 D).

In order to confirm that the alternative NF-κB pathway was activated also in the whole mouse mammary gland, immunofluorescence was performed on paraffin-embedded mouse mammary glands obtained from BRCA1 KO and WT mice. When inactive, the alternative NF-κB pathway shows cytoplasmic localization of p100/RelB hetero-dimers; once activated, p52/RelB complexes are found in the nucleus. As expected, BRCA1 WT mouse mammary glands showed a normal pattern of p100 and RelB expression, mostly localized in the cytoplasm of basal and luminal mammary epithelial cells, with low or no level of p52 and RelB in their nuclei. However, in the basal and luminal cells of BRCA1 KO mouse mammary glands an overall increase was found in the expression of p52 and RelB, with higher level of nuclear localization compared to the BRCA1 WT (Figure 8 A,B). To exclude the canonical NF-κB activation, paraffin-embedded mouse mammary glands were also subjected to immunofluorescence to determine the level of p65 in the whole mammary gland. Both BRCA1 KO and BRCA1 WT mammary glands showed only cytoplasmic localization of p65 in the basal and luminal cells, with no differences in the level of expression (Figure 8C). This data

confirms that BRCA1 knockout in the mouse mammary gland can specifically induce the alternative NF-κB pathway without affecting the activation of the canonical pathway.

In order to determine if alternative NF-κB pathway was also activated in human mammary tissue with BRCA1 mutation, immunofluorescence was performed on paraffin-embedded sections obtained from three BRCA1-mutation carriers and compared them to three BRCA1 wild type carriers (patients' information is described in Table 2). Two out of three BRCA1-mutation carriers showed strong expression of p100/p52 and RelB in their lobules, while low or no-expression was found in all BRCA1 wild type carriers (Figure 9 A,B). Interestingly, in the BRCA1-mutation carriers the intensity of p100/p52 and RelB was lobule specific, some of them showing higher levels than others and some being negative (Figure 10). Overall, more than 50% of the lobules stained positive for p100/p52 and RelB in two out of three BRCA1-mutation carriers.

These findings demonstrate that BRCA1 loss or mutation induces the alternative NF-κB pathway activation in the mouse stem- and progenitor-enriched cell populations and that this NF-κB activity can also be differentially detected in the mouse and human mammary tissues.

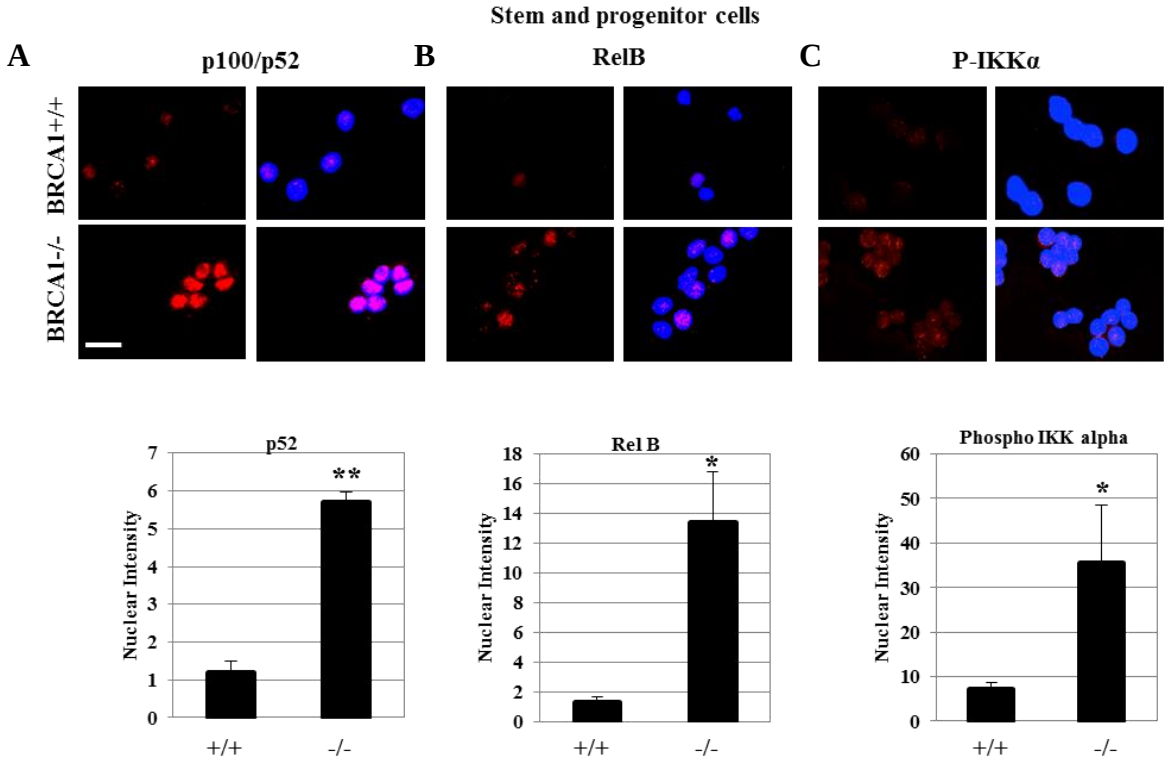

Figure 6: The alternative NF-κB pathway is activated in BRCA1-deficient stem and progenitor cells

Stem-enriched ($CD49f^{HI}$ $CD24^{LO}$) and progenitor-enriched ($CD49f^{LO}$ $CD24^{HI}$) cell populations were isolated from BRCA1 wild type (+/+) and BRCA1 knockout (-/-) mouse mammary glands (as described in materials and methods), sorted by FACS, and cytospun on slides for immunofluorescence. Stem and progenitor cells were immunostained with **A.** p100/p52, **B.** RelB, and **C.** phospho IKKα. The graph underneath each image represents quantification of nuclear fluorescence by ImageJ normalized to BRCA1 +/+ (mean ± S.E.). Scale bar 10 μm. (**) refers to $p<0.01$ and (*) refers to $p<0.05$ by Student's *t*-test. Immunofluorescence images are representative of a minimum of three independent experiments.

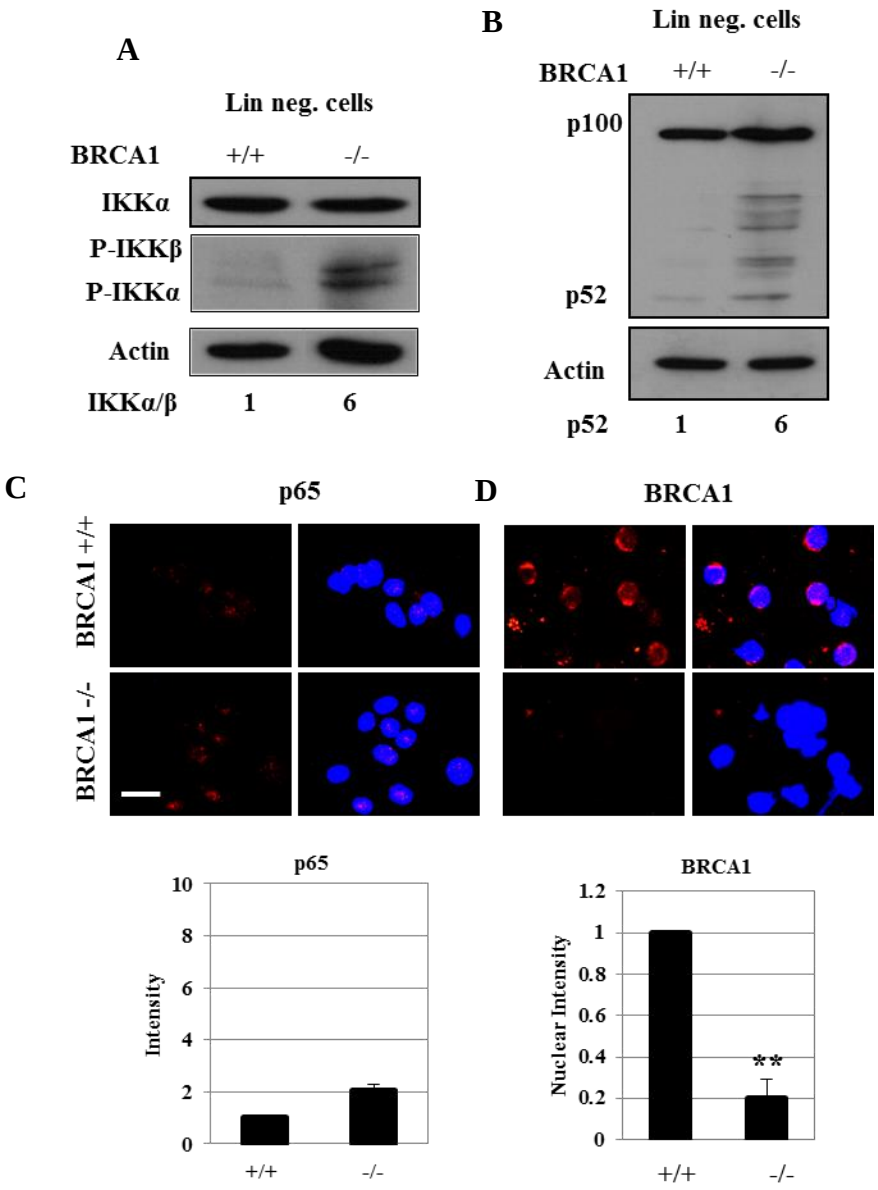

Figure 7: Lin neg. cells from BRCA1 knockout mammary glands show alternative NF-κB activation

(A and B) Lin neg. cells were isolated from BRCA1 wild type (+/+) or BRCA1 knockout (-/-) mouse mammary glands using EasySep™ and cultured until they reached 80 % confluence. Whole cell lysates from lin neg. cells were immunoblotted for **A.** phospho IKKα/β (serines 176/180) and **B.** p100/p52. Actin was used as loading control. Numbers underneath the actin represent protein quantification calculated with ImageJ and normalized to BRCA1 +/+. **(C and D)** Stem-enriched ($CD49f^{HI}$ $CD24^{LO}$) and progenitor-enriched ($CD49f^{LO}$ $CD24^{HI}$) cell populations were isolated from BRCA1 wild type (+/+) and BRCA1 knockout (-/-) mouse mammary glands, sorted by FACS, and cytospun on slides for immunofluorescence. Stem and progenitor cells were immunostained for **C.** p65 and **D.** BRCA1. The graph below each image represents fluorescence quantification calculated with ImageJ normalized to BRCA1 +/+ (mean ± S.E.). (**) refers to $p<0.01$ by Student's *t*-test. Scale bar 10 µm. Immunoblot and immunofluorescence images are representative of a minimum of three independent experiments.

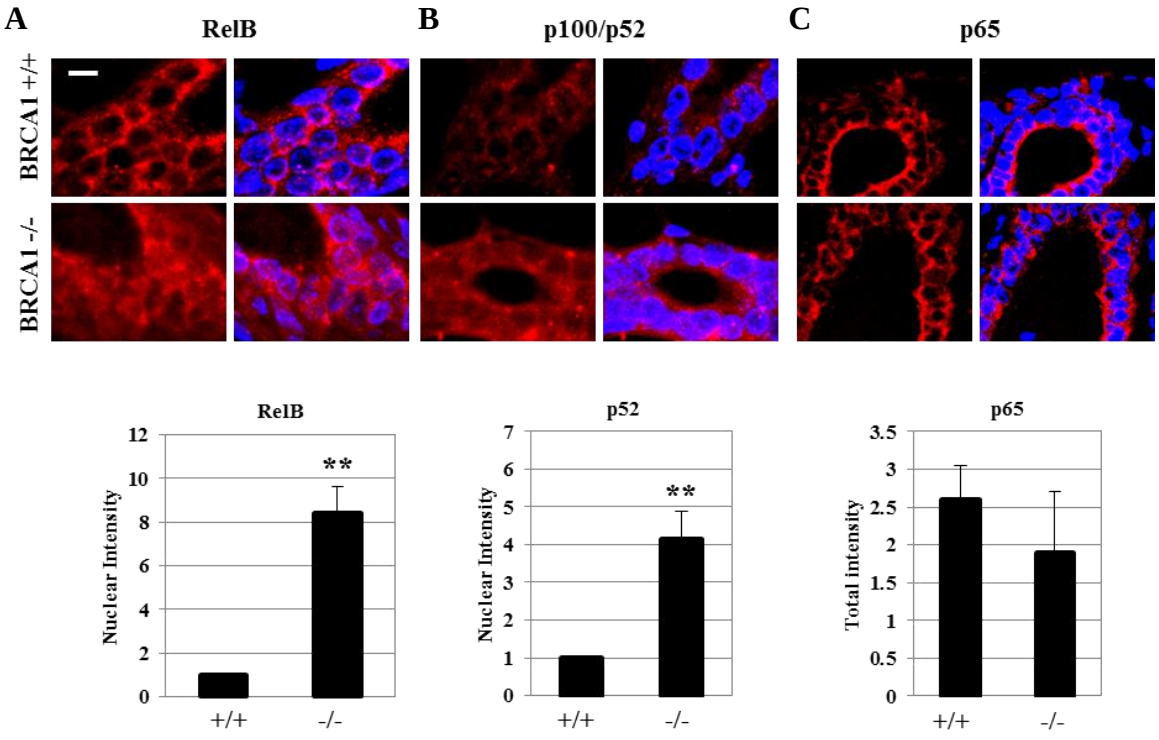

Figure 8: The alternative but not the canonical NF-B pathway is activated in BRCA1 knockout mouse mammary glands

Paraffin-embedded sections of whole mouse mammary glands isolated from BRCA1 wild type (+/+) and BRCA1 knockout (+/+) mice. Sections were immunostained for **A.** RelB, **B.** p100/p52, and **C.** p65. The graph underneath each image represents fluorescence intensity calculated with ImageJ normalized to BRCA1 +/+ (mean ± S.E.). Scale bar 5 µm. (**) refers to $p<0.01$ by Student's *t*-test. Immunofluorescence images are representative of a minimum of three independent experiments.

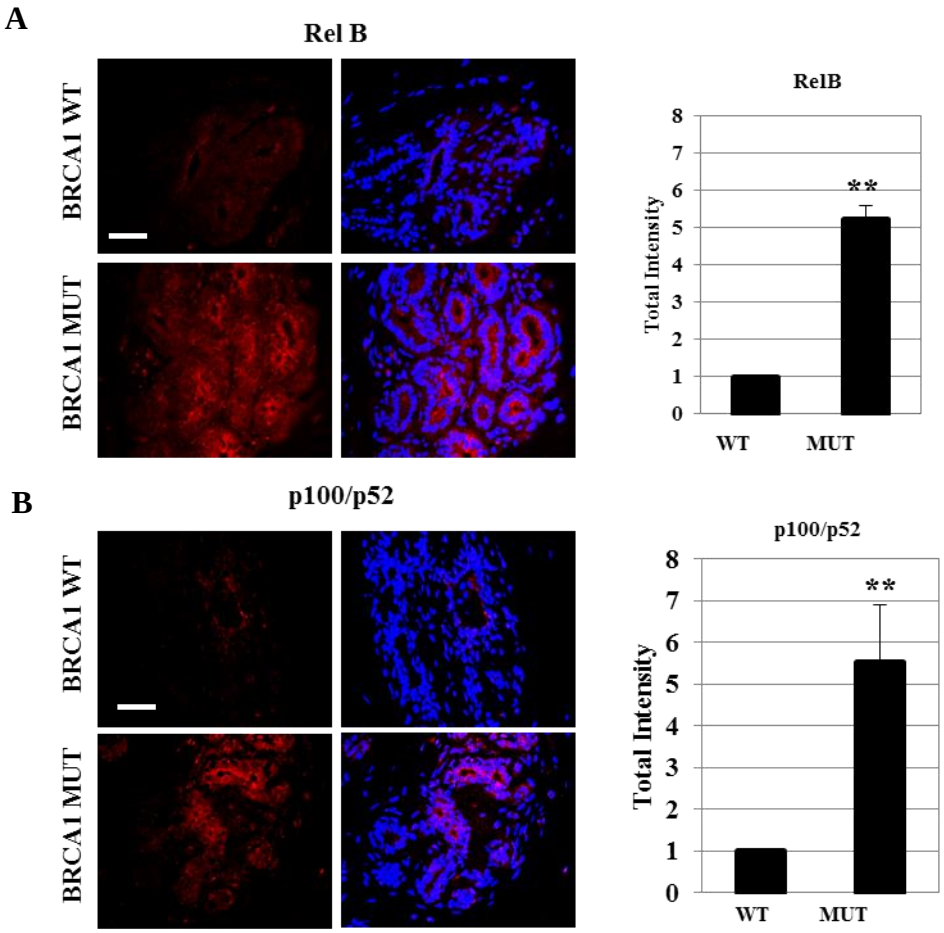

Figure 9: Increased expression of p100/p52 and RelB in BRCA1-mutated human mammary glands

Paraffin-embedded sections of human mastectomies from BRCA1 wild type (WT) or BRCA1-mutation (MUT) carriers. Sections were immunostained for **A.** RelB and **B.** p100/p52. The graph to the right of each image represents fluorescence intensity of each stain calculated with ImageJ normalized to BRCA1 WT (mean ± S.E.). (**) refers to $p<0.01$ by Student's *t*-test. Scale bar 25 μm. Images are representative of the three BRCA1-mutation carriers and BRCA1 wild type.

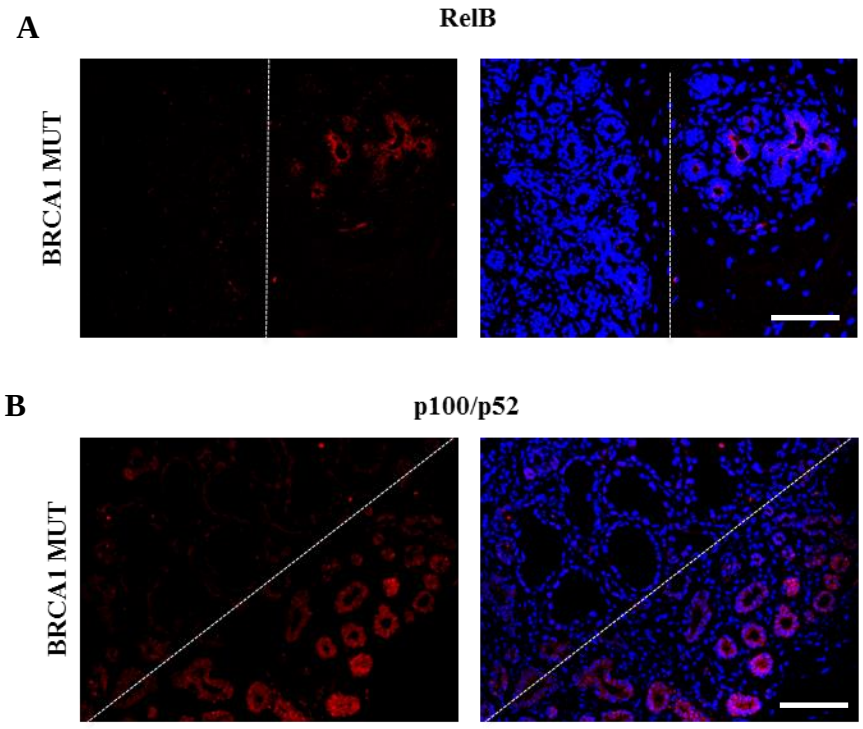

Figure 10: Lobule-restricted expression of RelB and p100/p52 in BRCA1-mutated human mammary glands

Paraffin-embedded sections of human mastectomies from BRCA1-mutation (MUT) carriers. Sections were immunostained for **A.** RelB and **B.** p100/p52. Scale bar 50 μm. The dotted line in the image divides positive areas from negative areas.

NF-κB over-activation increases stemness and blocks differentiation

BRCA1 plays an important role in the differentiation process of stem and progenitor cell populations in the mammary gland. It has been demonstrated that BRCA1 inhibition is responsible for a block in the differentiation and the accumulation of luminal progenitor cells in the human and mouse mammary glands (Furuta et al., 2005; Lim et al., 2009; Liu et al., 2008) . It has also been previously shown that the alternative NF-κB pathway plays a critical role in the normal progenitor cell expansion and differentiation (Connelly et al., 2007; Demicco et al., 2005).

To confirm the presence of a skewed population of progenitor cells in the BRCA1 KO versus BRCA1 WT mouse mammary glands, cell sorting was performed in order to determine the percentage of stem- and progenitor-enriched cell populations. The differential expression of CD24 and CD49f was used to distinguish stem- and progenitor-enriched cell population. Cells that express high level of CD49f and medium or low level of CD24 have been functionally characterized as bipotent/stem cells, while cells that express medium or low level of CD49f and high level of CD24 have been characterized as progenitor/early committed luminal cells. FACS analysis revealed that BRCA1 KO mice had higher percentage of $CD24^{LO}$ $CD49f^{HI}$ (stem/bipotent cells) compared to the BRCA1 WT mice, while the percentage of $CD24^{HI}$ $CD49f^{LO}$ (luminal progenitor cells) was not changed (Figure 11 A). To further confirm this finding, the protein and mRNA levels of CD44 were analyzed in the cell lysate obtained from the cultured lin neg. cells obtained from mouse mammary glands. Indeed, the expression of CD44 has been found increased in the mammary epithelial stem cells while it is down-regulated during differentiation, having a role in the regulation of stem cell proliferation during pregnancy,

lactation and involution (Fillmore and Kuperwasser, 2007; Hebbard et al., 2000). BRCA1-deficient cells (lin neg. cells isolated from BRCA1 KO mammary glands) showed 14-fold increase in CD44 mRNA level accompanied by 2-fold increase in its protein levels compared to the BRCA1-competent ones (Figure 11 B,C). To test if the increase in CD44 levels was a consequence of BRCA1 loss of function, the HC11 mouse mammary epithelial cell line was infected with lentivirus carrying shBRCA1 and CD44 mRNA levels were examined. After BRCA1 knockdown, HC11 showed 5-fold increase in CD44 mRNA levels, confirming that BRCA1 inhibition was inducing an increase in cell stemness (Figure 11 D). BRCA1 knockdown in HC11 was confirmed by q-PCR showed in Figure 11 E.

Another technique commonly used to determine the stemness of a cell population is the mammosphere assay. Lin neg. cells isolated from the mouse mammary gland were plated on low-adherent plates, allowing the growth of stem cells, the only cells able to form spheres (mammosphere) in suspension. The higher the number of primary and secondary mammospheres, the higher the proliferative capacity of a stem cell population (Dontu et al., 2003b). In order to understand the role of NF-κB in the mouse mammary stem cell population, the IKK-α/β inhibitor BMS-345541 was used. Lin neg. cells isolated from mouse mammary glands were plated in low-adherent conditions in the presence or absence of 10 μM of BMS-345541. After a week primary spheres were counted, then collected, dissociated to a single cell suspension, and re-plated for secondary sphere formation in the presence or absence of 10 μM BMS-345541. BRCA1-deficient cells formed more secondary mammospheres compared to BRCA1-competent cells. Moreover, BMS-345541 blocked primary and secondary sphere formation of both

BRCA1-deficient and BRCA1-competent cells (Figure 12 A). This data suggests that BRCA1 KO mice have stem cells with higher self-renewal capacity and that NF-κB is an important mediator of stem cell proliferation in either the presence or absence of a functional BRCA1.

The presence of expanded stem and progenitor cell populations from the mammary tissue of human BRCA1-mutation carriers was previously described (Lim et al., 2009; Liu et al., 2008; Proia et al., 2011). Moreover, it was demonstrated that a subset of mammary gland sections from patients with a BRCA1 mutation contained whole histologically normal lobular units that over express the stem/progenitor cell marker ALDH1. This group surmised that these ALDH1 positive cells represent the expanded progenitor cell population within these glands (Liu et al., 2008). To detect ALDH1, immunofluorescence was performed in the three BRCA1-mutation carriers and BRCA1 wild type carriers. One of the three BRCA1-mutation carriers was positive for ALDH1, while none of the BRCA1 wild type carriers expressed ALDH1 (Figure 12 B). Interestingly, when the ALDH1 staining was compared with the previous p100/p52 staining, it was found that the same lobules of the same BRCA1-mutation carrier stained positively for both. Moreover, when the images of the same lobule stained with p100/p52 and ALDH1 were overlapped, it was found that the same acini within the lobule that were positive for ALDH1 were also positive for p100/p52 (Figure 13). This finding indicates that NF-κB is active in the ALDH1-positive expanded stem/progenitor cell populations found in BRCA1-mutation carriers.

NF-κB has been implicated in proliferation as well as differentiation of stem/progenitor cells (Connelly et al., 2007; Demicco et al., 2005). To test the effect of

NF-κB activation on mammary epithelial cell differentiation, the HC11 mouse mammary epithelial cell line was used. This cell line is able to undergo differentiation and synthesize the β-casein milk protein in response to treatment with lactogenic hormones (Perotti et al., 2009). HC11 cell line was stably transfected with pcDNA3 empty vector or pcDNA3 p52-expressing vector and then induced to differentiate using prolactin and dexamethasone (as described in materials and methods). After 4 days in differentiation media, dome formation (indicative of differentiation) was assessed by microscopy and proteins were collected from cell lysate. Overexpression of p52 blocked dome formation (Figure 14 A) and strongly reduced the expression of β-casein, which is produced following prolactin-mediated differentiation (Figure 14 B). p52 overexpression was confirmed by western blot analysis (Figure 14 C). This demonstrates that when NF-κB is overexpressed, stem and progenitor cells are not able to fully differentiate.

All together these findings suggest that BRCA1 plays an important role in the stem and progenitor cell compartment, and that BRCA1-mediated NF-κB activation induces an expansion of mammary epithelial stem cells in the human and mouse mammary glands, while repressing differentiation.

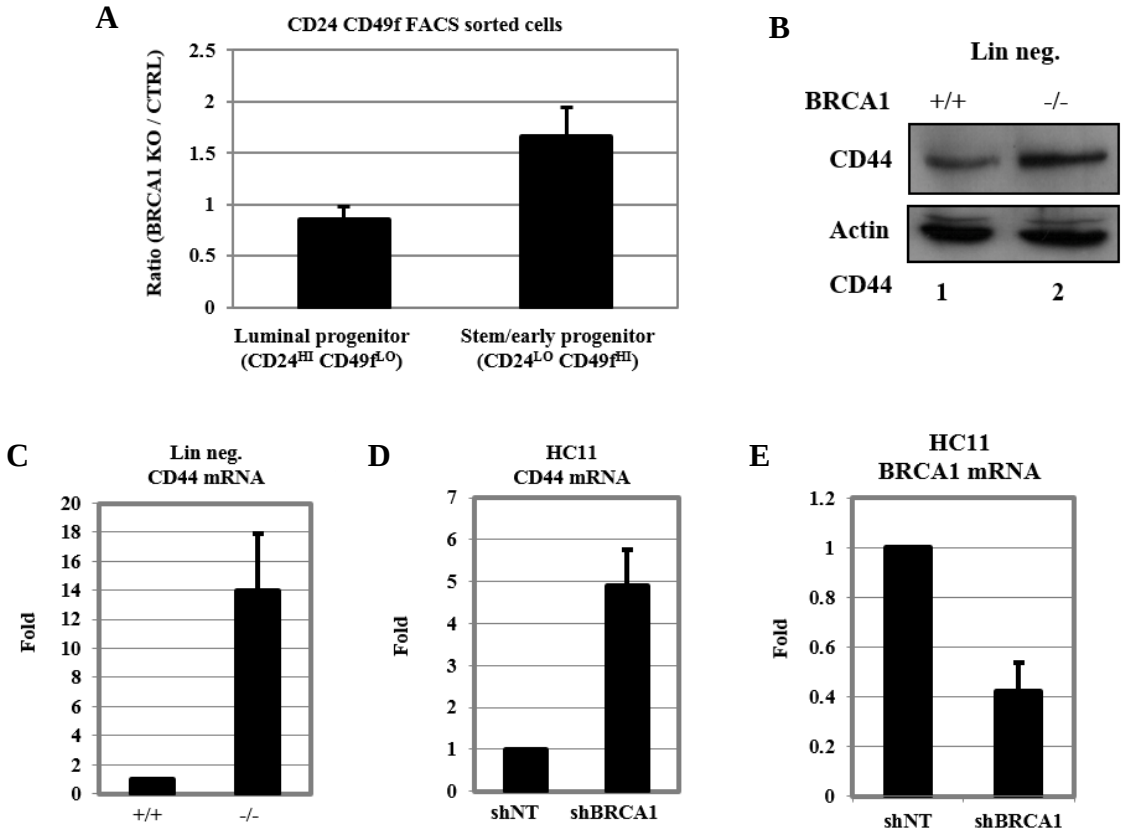

Figure 11: BRCA1 loss increases stemness

A. Stem-enriched ($CD49f^{HI}$, $CD24^{LO}$) and progenitor-enriched ($CD49f^{LO}$, $CD24^{HI}$) cell populations isolated from BRCA1 wild type (+/+) and BRCA1 knockout (-/-) mouse mammary glands. The graph represents the percentage of stem- and progenitor-enriched cell population in BRCA1 +/+ versus BRCA1 -/- mouse mammary glands calculated by FACS and normalized to BRCA1 +/+ (means ± S.E.). Data was collected from 5 BRCA1 +/+ and 5 BRCA1 -/- mice. **B.** Lin neg. cells were isolated from BRCA1 wild type (+/+) and BRCA1 knockout (-/-) mouse mammary glands. Whole cell lysates were isolated and immunoblotted for CD44. Actin was used as loading control. Numbers underneath actin represent CD44 protein level quantification calculated with ImageJ normalized to BRCA1 +/+ levels. **C.** mRNA was extracted from the same lin neg. cells used for immunoblot analyses and qRT-PCR was performed for CD44 mRNA levels. mRNA levels were quantified using primers specific for CD44 and beta-actin (the endogenous control). The graph represents CD44 mRNA levels compared to BRCA1 +/+ levels (mean ± S.E.). **D.** HC11 cells were infected with lentivirus carrying non-targeting (NT) or BRCA1 shRNA for 72 hours and then mRNA was collected for qRT-PCR analysis. mRNA levels were quantified using primers specific for CD44 and beta-actin (the endogenous control). The graph represents CD44 mRNA levels compared to BRCA1 +/+ levels (mean ± S.E.). **E.** Confirmation of BRCA1 knockdown in HC11 cells. mRNA levels were quantified using primers specific for BRCA1 and beta-actin (the endogenous control). The graph represents BRCA1 mRNA levels compared to shNT levels. Images are representative of a minimum of three independent experiments.

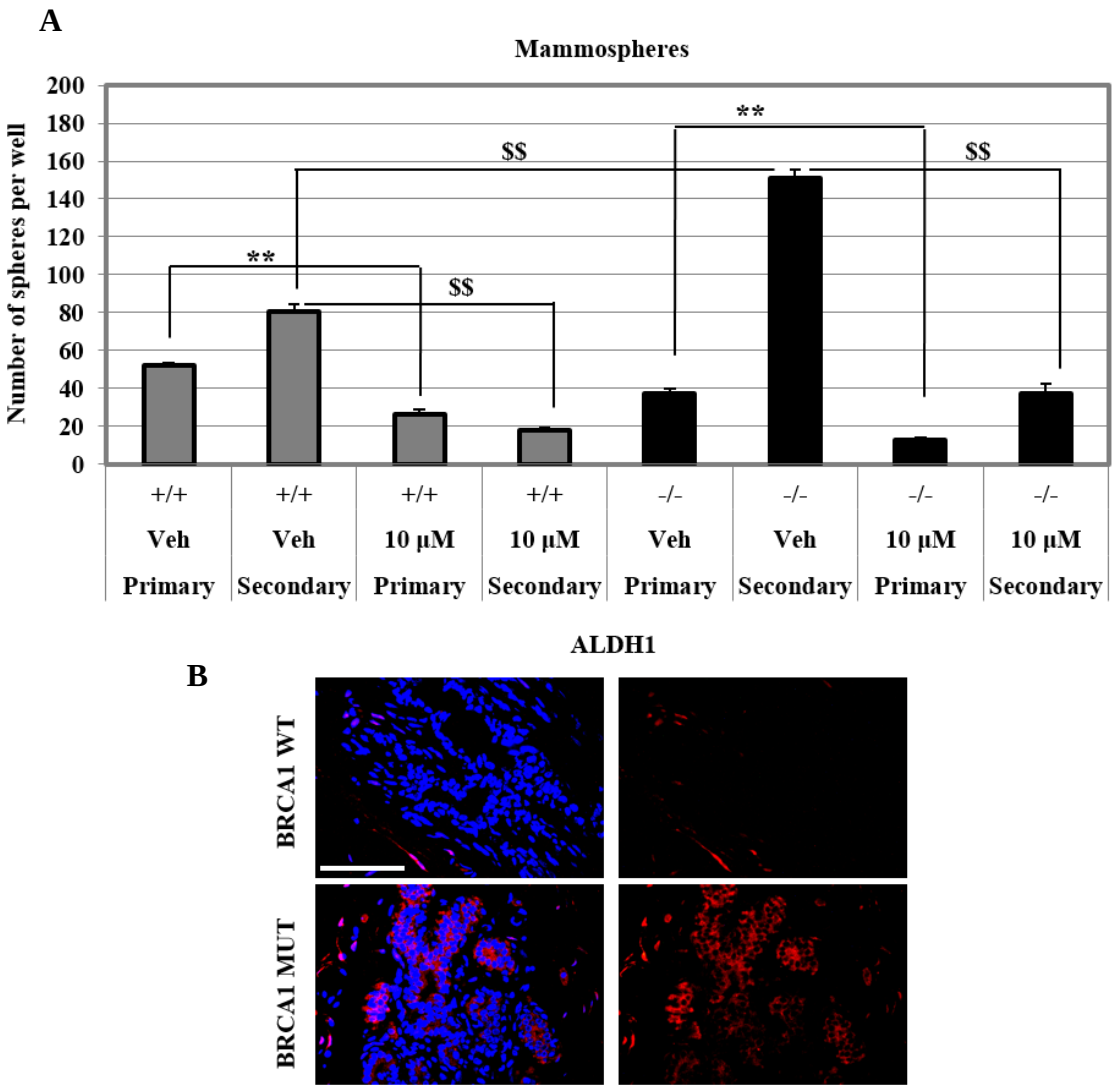

Figure 12: BRCA1 loss or mutation increases stemness in mouse and human mammary glands

A. Lin neg. cells were isolated from BRCA1 wild type (+/+) and BRCA1 knockout (-/-) mouse mammary glands and plated in 96 well low-adherent plates (2,000 cell per well). Spheres (mammospheres) were counted under a light microscope after one week (Primary), collected, dissociated and re-plated. After another week, mammosphere formation was counted again (Secondary). Cells were cultivated in the presence of vehicle (Veh) or 10 µM of BMS-345541. The graph represents the total number of spheres per well counted under a light microscope (mean ± S.E.). (**) refers to $p<0.01$ in primary spheres and ($$) refers to $p<0.01$ in secondary spheres by two-way ANOVA analysis, followed by Tukey test. **B.** Paraffin-embedded sections from human mastectomies of BRCA1 wild type (WT) and BRCA1-mutation carriers (MUT) were immunostained for ALDH1. Scale bar 25 µm. The graph and the image are representative of a minimum of three independent experiments

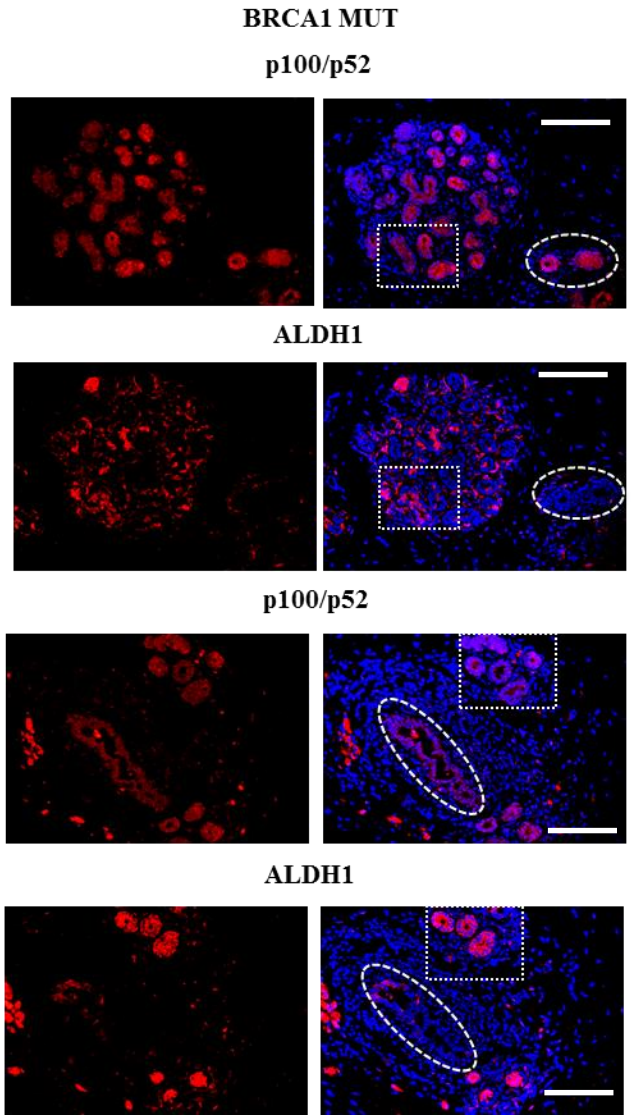

Figure 13: p100/p52 and ALDH1 expression co-localize in BRCA1 mutated human mammary glands

Two representative images from serial sections of a BRCA1-mutation carrier (MUT) immunostained for p100/p52 and ALDH1. Squares represent the same area positive for both ALDH1 and p100/p52 while ovals represent the same area positive for p100/p52 but negative for ALDH1. Scale bar 50 μm.

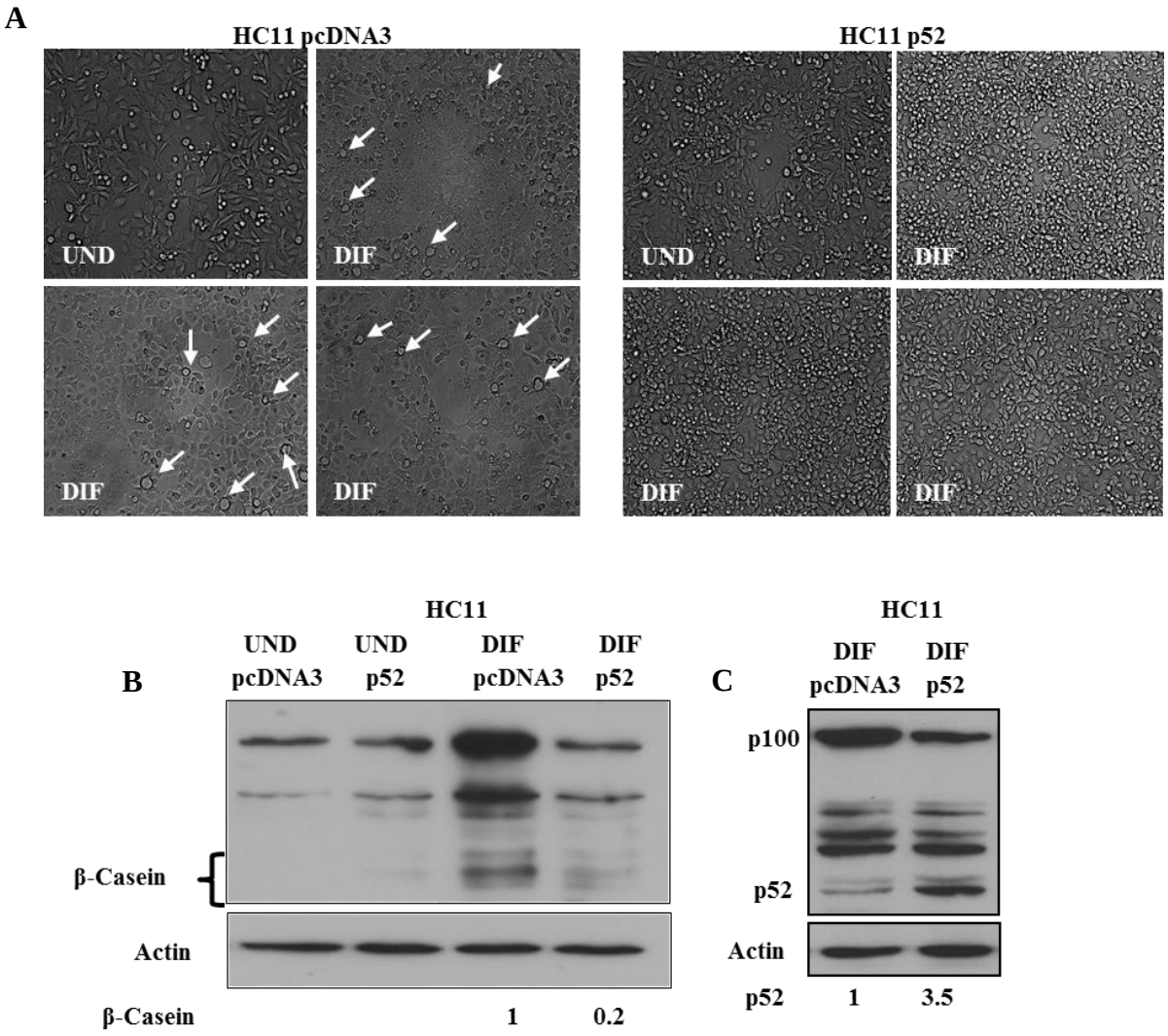

Figure 14: p52 overexpression blocks differentiation in the HC11 mouse cell line

HC11 cells were stably transfected with pcDNA3 empty vector or pcDNA3-p52 expressing vector and induced to differentiate as described in materials and methods. **A.** Images of HC11 undifferentiated (UND) or differentiated (DIF). Arrows indicate dome formation (indication of differentiation). Whole cell lysates from HC11 cells were immunoblotted for **B.** β-casein and **C.** p100/p52. Actin was used as loading control. Numbers underneath actin represent quantification of protein levels calculated with ImageJ normalized to pcDNA3 transfected HC11 DIF levels. Images are representative of at least three independent experiments.

The alternative NF-κB pathway induces the expansion of mouse mammary luminal progenitor cells

BRCA1-associated breast cancers are believed to originate from luminal progenitor cells (Lim et al., 2009; Visvader and Stingl, 2014). To better understand the role of NF-κB in the mammary progenitor cell population, the Matrigel acini assay was employed, in which progenitor cells grow and form acini in a 3D-collagen matrix. It has previously been shown that luminal progenitor cells obtained from BRCA1 wild type human carriers did not form acini in Matrigel in the absence of B27 (a supplement rich in progesterone). Conversely, luminal progenitor cells isolated from human BRCA1-mutation carriers had the ability to grow in Matrigel and form acini even in absence of B27, showing a progesterone-independent growth. Based on their ability to overcome the necessity of progesterone to grow, this population has been defined "aberrant" luminal progenitor cell population (Lim et al., 2009). When lin neg. cells isolated from the mouse mammary gland are plated in Matrigel, only the luminal progenitor cells are able to form acini.

First, confirmation of the progesterone-independent growth of progenitor cells obtained from BRCA1 KO mouse mammary glands was performed. After isolation from the mouse mammary glands, lin neg. cells were plated in a thick layer of Matrigel covered by media supplemented with or without B27. As previously reported, BRCA1-deficient progenitor cells were able to form acini in absence of B27 while the BRCA1-competent ones failed to do so (Lim et al., 2009). In order to understand the role of NF-κB in the luminal progenitor cells, the IKK-α/β inhibitor BMS-345541 was used. When progenitor cells were cultivated in Matrigel in the presence of two different

concentrations of BMS-345541 (10 μM and 20 μM), acini formation was blocked at both concentrations, demonstrating the necessity of the NF-κB activity for the progenitor cells in order to proliferate (Figure 15 A and Figure 35). Moreover, p52 levels were reduced in the BRCA1-mutated HCC1937 cell line treated with 10 μM BMS-345541 (Figure 15 B). Confirmation of NF-κB inhibition by BMS-345541 in lin neg. cells is shown in Figure 15 C.

A second NF-κB inhibitor, the IKK-α/β inhibitor dimethylamino-parthenolide (DMAPT), was then tested (Neelakantan et al., 2009). This compound has been shown to selectively target cancer stem cells, through its activation of p53 while inhibiting NF-κB. Moreover, DMAPT can also inhibit the mitogen activated protein kinase (MAPK) pathway, JAK/STAT, phosphatidylinositol-3-kinase (PI3K), reducing tumor formation and progression *in vivo* (Ghantous et al., 2013). To compare the efficacy of DMAPT versus BMS-345541 in causing cell death, the BRCA1 wild type MCF-10A and the BRCA1 mutated HCC1937 cell lines were used. Both cell lines were plated at the same density and then treated with either 10 μM of DMAPT, 10 μM BMS-345541, or vehicle. After 48 hours of treatment, cell viability was assessed using the colorimetric Alamar Blue assay. While MCF-10A viability was not affected by either BMS-345541 or DMAPT treatment, after only 48 hours of treatment HCC1937 showed a 40 % decrease in viability with 10 μM BMS-345541 and 80 % decrease with 10 μM DMAPT (Figure 16 A). Western blot analysis confirmed p100/p52 inhibition after DMAPT treatment on HCC1937 (Figure 16 B). This result demonstrates that even if both BMS-345541 and DMAPT target the IKK complex, they show different effects on cell viability, likely due to the fact that DMAPT inhibits several pathways in addition to NF-κB.

Based on this previous data, the effect of DMAPT was next assessed on acini formation. BRCA1-deficient and BRCA1-competent progenitor cells obtained from mouse mammary glands were cultivated in Matrigel in the presence or absence of 1 μM and 2.5 μM of DMAPT. At both concentrations, DMAPT resulted in a decrease in acini sizes formed by BRCA1-deficient and competent progenitor cells. However, the strongest effect was achieved on BRCA1-deficient progenitor cells grown in absence of B27 (with no progesterone) treated with 2.5 μM of DMAPT (Figure 17 A and Figure 36). Western blot analysis also confirmed the efficacy of DMAPT in the NF-κB inhibition, showing a decrease in p100 levels in lin neg. cells treated with 1 μM and 2.5 μM of DMAPT (Figure 17 B).

Inhibition of progenitor cell proliferation *in vivo* would be predicted to reduce acini formation in Matrigel. To test this, mice were injected intra peritoneum (i.p.) with DMAPT at 40 mg/Kg every other day for 2 weeks. The day after the last injection, lin neg. cells were collected and plated in Matrigel. Remarkably, cells from DMAPT i.p. injected mice had strongly reduced the acini sizes (Figure 18 A and Figure 37). Moreover, a partial rescue was observed in the acini sizes formed by the recovered cells after the mice were left untreated for 15 days after the last injection (Figure 18 B and Figure 37). Confirmation of NF-κB inhibition in the lin neg. cells obtained from mice injected with DMAPT is shown in the western blot in Figure 18 C.

Since both NF-κB inhibitors (BMS-345541 and DMAPT) are able to block the alternative and canonical NF-κB pathways, the effect of a specific alternative NF-κB pathway inhibitor was examined. Therefore, a lentivirus carrying p100/p52 shRNA (lenti-shp100) was produced. After progenitor cells were plated in Matrigel and infected with

lenti-shp100 or lenti-shNT, a strong reduction in acini formation from BRCA1-deficient progenitor cells grown in the absence of B27 was observed. A much smaller reduction was still observed in the presence of B27, while BRCA1-competent progenitor cells infected with lenti-shp100 were still able to form acini of sizes comparable to those infected with lenti-shNT (Figure 19 A and Figure 38). Confirmation of p100/p52 knockdown in lin neg. cells was assessed by western blot and shown in Figure 19 B.

To further test the role of the alternative NF-κB pathway in the luminal progenitor cell proliferation in Matrigel, a knock-in mouse model that lacks IKKα catalytic activity was used. These mice express $IKK\alpha^{AA}$ knock-in allele containing alanines instead of serines in the activation loop (Ser176Ala and Ser180Ala). Homozygous $IKK\alpha^{AA}$ females have been shown to have defect in the lobuloalvealor proliferation and differentiation that prevents them from lactation (Cao et al., 2001). Lin neg. cells were isolated from $IKK\alpha^{AA}$ and IKKα wild type ($IKK\alpha^{WT}$) mouse mammary glands and plated in Matrigel for acini assay. Progenitor cells from $IKK\alpha^{WT}$ were able to form acini, and as expected required the progesterone-enriched B27 supplement (as the BRCA1 WT). However, acini size was reduced when progenitor cells from $IKK\alpha^{AA}$ were plated in the presence or in the absence of B27 (Figure 20 A and Figure 39). We also confirmed by western blot that $IKK\alpha^{AA}$ lin neg. cells had lover levels of p52 formation compared to $IKK\alpha^{WT}$ lin. neg cells (Figure 20 B).

To exclude any involvement of the canonical NF-κB pathway in the proliferation of luminal progenitor cells, p65/p50 activation was inhibited using lentivirus expressing the Inhibitor of κB super repressor ($I\kappa B\alpha^{SR}$) or empty vector. Progenitor cells were plated in Matrigel and after infection no changes were detected in the acini size in any condition

(Figure 21 A). Expression of IκBα^{SR} in the lin neg. cells as well as HC11 cells was confirmed by western blot (Figure 21 B).

Taken together this set of data demonstrates that the alternative NF-κB pathway, but not the canonical, is essential for the progesterone-independent expansion of the aberrant luminal progenitor cell population found in the BRCA1 KO mouse mammary glands.

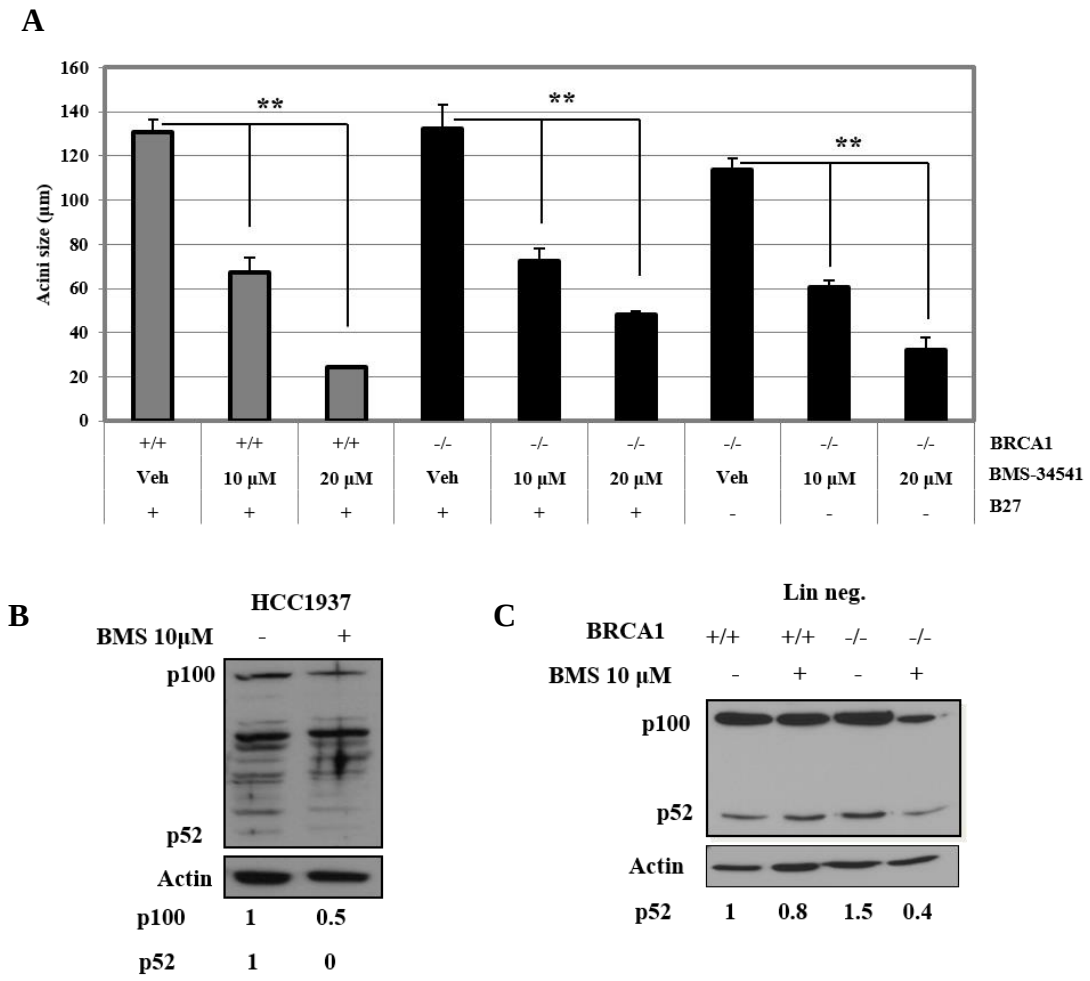

Figure 15: BMS-345541 reduces acini size in Matrigel

A. Lin neg. cells were isolated from BRCA1 wild type (+/+) or BRCA1 knockout (-/-) mouse mammary glands and plated on a thick layer of Matrigel (2,000 cells in 20 µL of Matrigel). Cells were then grown in media containing vehicle (Veh), 10 µM, or 20 µM of BMS-345541 in the presence (+) or absence (-) of B27 supplement. After 15 days acini size was measured using Northern Eclipse. The graph shows the average of the thirty largest acini in the microscopy field (mean ± S.E.). **B.** Whole cell lysates from HCC1937 treated with vehicle (-), 10 µM BMS-345541 (+) were immunoblotted for p100/p52. Actin was used as loading control. Numbers underneath the actin represent quantification of p100/p52 protein levels calculated with ImageJ compared to vehicle-treated (-) levels. **C.** Whole cell lysates from lin neg. cells were immunoblotted for p100/p52. Actin was used as loading control. Numbers underneath the actin represent quantification of p52 protein levels calculated with ImageJ normalized to BRCA1 +/+ vehicle-treated levels. (**) refers to $p<0.01$ calculated by two-way ANOVA analysis, followed by Tukey test. The graph and immunoblots are representative of at least three independent experiments.

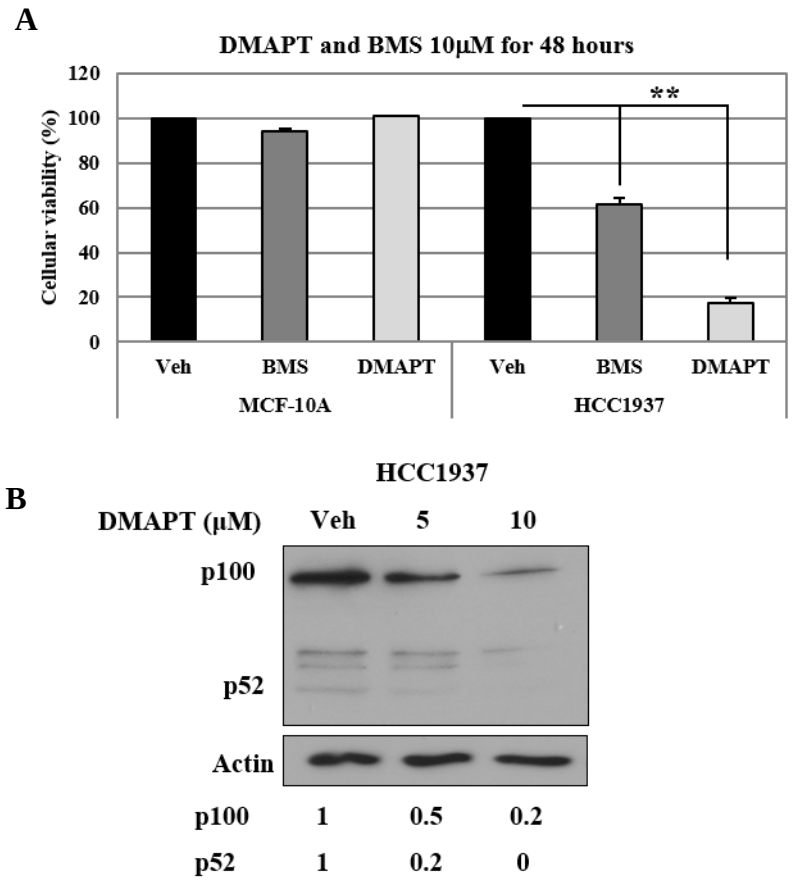

Figure 16: DMAPT blocks p52 formation and reduces cell viability in HCC1937

HCC1937 and MCF-10A cells treated with BMS-345541 or DMAPT for 48 hours. **A.** MCF-10A and HCC1937 were plated at the density of 4.000 cells in 96 well-plate, treated with vehicle (Veh), 10 μM BMS-345541, or 10 μM DMAPT for 48 hours and Alamar Blue assay performed as described in materials and methods. The graph represents cell viability expressed as percentage and normalized to vehicle-treated (Veh) cells (mean ± S.E.). **B.** Whole cell lysates from HCC1937 treated with vehicle (Veh), 5 μM, or 10 μM DMAPT were immunoblotted for p100/p52. Actin was used as loading control. Numbers underneath the actin represent quantification of p100/p52 protein levels calculated with ImageJ normalized to vehicle-treated levels. (**) refers to $p<0.01$ calculated by two-way ANOVA analysis, followed by Tukey test. The graph and immunoblot are representative of at least three independent experiments.

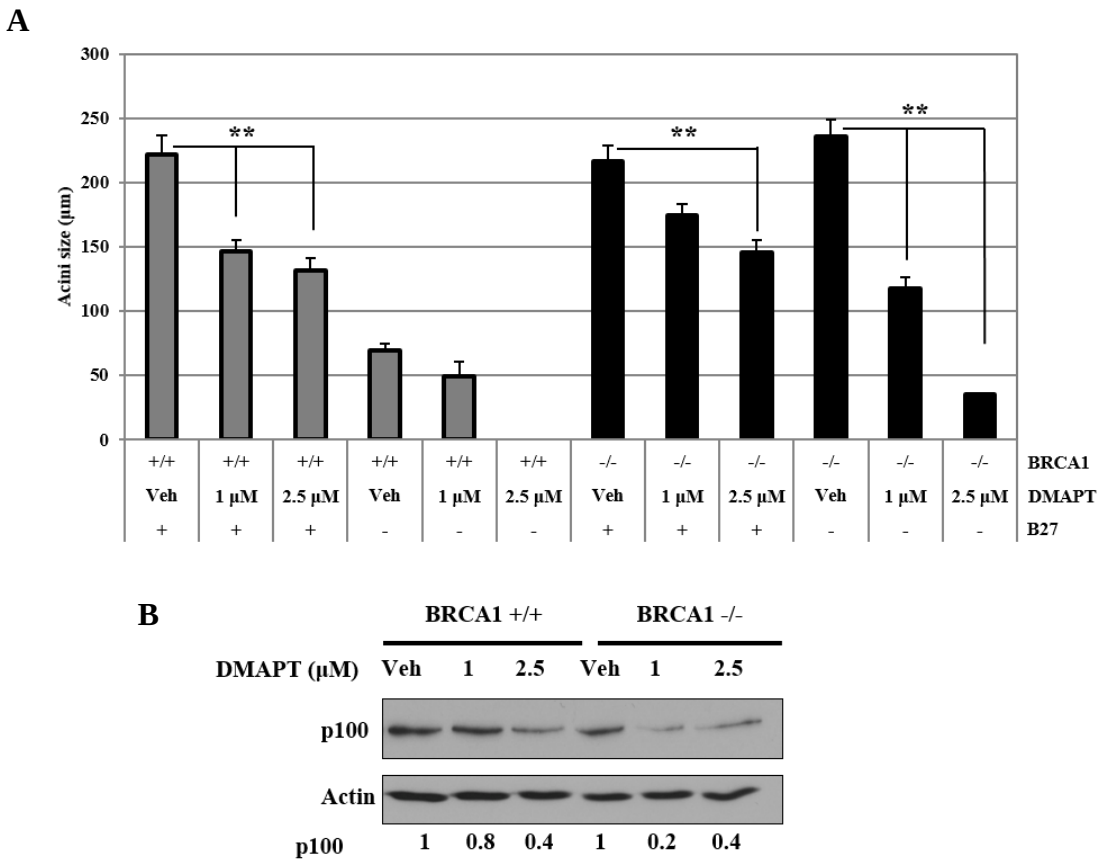

Figure 17: DMAPT blocks luminal progenitor cells from forming acini *in vitro*

Lin neg. cells were isolated from BRCA1 wild type (+/+) and BRCA1 knockout (-/-) mouse mammary glands and plated in Matrigel **A.** Lin neg. cells were plated on a thick layer of Matrigel (2,000 cells in 20 µL Matrigel). Cells were grown in media containing vehicle (Veh), 1 µM DMAPT, or 2.5 µM DMAPT in the presence (+) or absence (-) of B27 supplement. After 15 days acini size was measured using Northern Eclipse. The graph shows the average of the thirty largest acini in the microscopy field (mean ± S.E.). **B.** Whole cell lysates from lin neg. cells were immunoblotted for p100. Actin was used as loading control. Numbers underneath actin represent p100 protein level quantification calculated with ImageJ and normalized to vehicle-treated levels. (**) refers to $p<0.01$ calculated by two-way ANOVA analysis, followed by Tukey test. The graph and immunoblot are representative of at least three independent experiments.

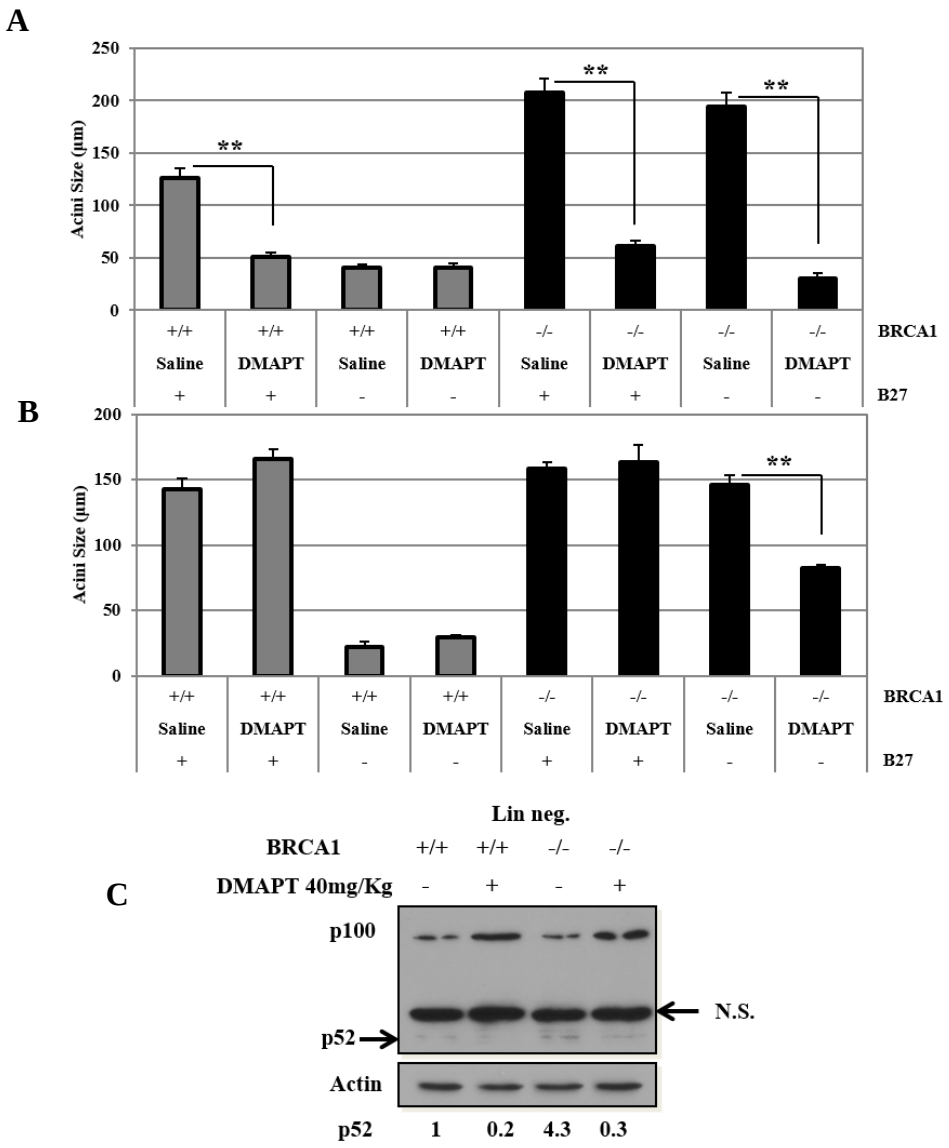

Figure 18: DMAPT injections prevents BRCA1-deficient luminal progenitor cells from forming acini in Matrigel

BRCA1 wild type (+/+) and BRCA1 knockout (-/-) mice were injected i.p. with saline or DMAPT at 40 mg/Kg. **A.** The day after the last injection and **B.** two weeks after the last injection lin neg. cells were isolated from mouse mammary glands and plated on a thick layer of Matrigel (2,000 cells in 20 µL of Matrigel). Cells were grown in media with (+) or without (-) B27 supplement. After 15 days acini size was measured using Northern Eclipse. The graphs show the average of the thirty largest acini in the microscopy field (mean ± S.E.). **C.** lin neg. cells from DMAPT injected mice were immunoblotted for p100/p52. Actin was used as loading control. Numbers underneath actin represent p52 protein level quantification calculated with ImageJ. Values were normalized to saline-treated (-). N.S. (non-specific band). (**) refers to $p<0.01$ calculated by two-way ANOVA analysis, followed by Tukey test. The graphs are representative of at least three independent experiments.

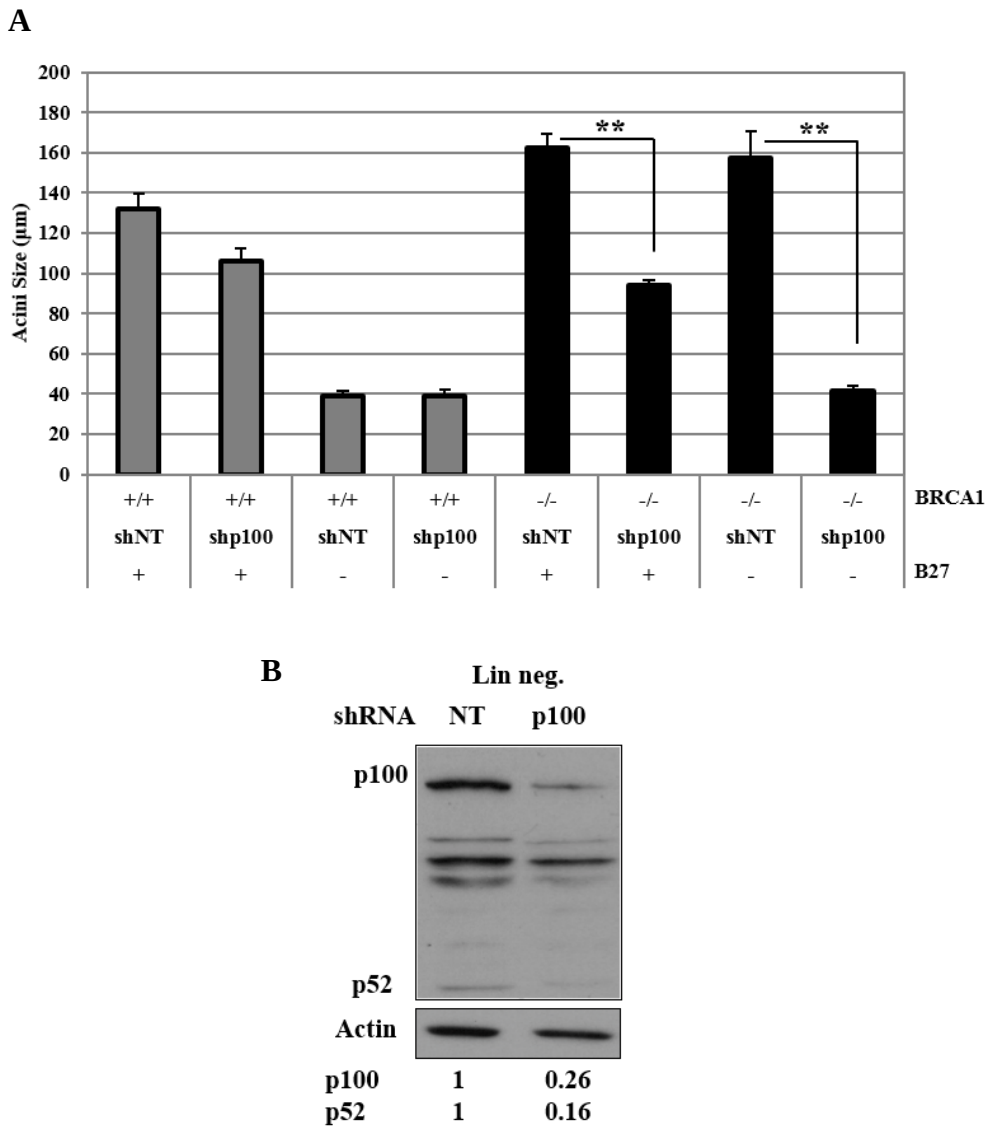

Figure 19: The alternative NF-κB pathway inhibition blocks the progesterone-independent growth of BRCA1-deficient luminal progenitor cells

Lin neg. cells isolated from BRCA1 wild type (+/+) and BRCA1 knockout (-/-) mouse mammary glands and plated in Matrigel **A.** Lin neg. cells were plated on a thick layer of Matrigel (2,000 cells in 20 µL of Matrigel). Cells were infected with lentivirus carrying non-targeting (NT) or p100 shRNA and grown in the presence (+) or absence (-) of B27 supplement. After 15 days acini size was measured using Northern Eclipse. The graph shows the average of the thirty largest acini in the microscopy field (mean ± S.E.). **B.** Whole cell lysates from BRCA1 deficient lin neg. cells infected with lentivirus carrying shNT or shp100 were immunoblotted for p100/p52. Actin was used as loading control. Numbers underneath actin represent p100/p52 protein levels quantification calculated with ImageJ. Values were normalized to shNT levels. (**) refers to $p<0.01$ calculated by two-way ANOVA analysis, followed by Tukey test. The graph and immunoblot are representative of at least three independent experiments

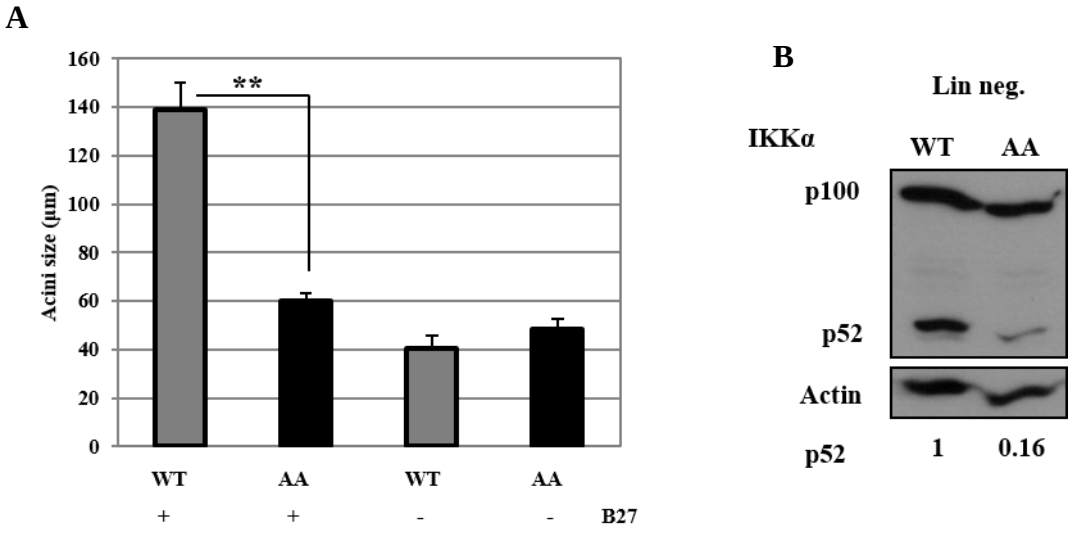

Figure 20: IKKα inhibition prevents luminal progenitor cells to form acini in Matrigel

Lin neg. cells were isolated from IKKα wild type (WT) and IKKα knock-in (AA) mouse mammary glands and plated in Matrigel. **A.** Lin neg. cells were plated on a thick layer of Matrigel (2,000 cells in 20 µL of Matrigel) and grown in the presence (+) or absence (-) of B27 supplement. After 15 days acini size was measured using Northern Eclipse. The graph shows the average of the thirty largest acini in the microscopy field (mean ± S.E.). **B.** Whole cell lysates from lin neg. cells were immunoblotted for p100/p52. Actin was used as loading control. Numbers underneath actin represent p52 protein levels quantification calculated with ImageJ and normalized to WT levels. (**) refers to $p<0.01$ calculated by two-way ANOVA analysis, followed by Tukey test. The graph and immunoblot are representative of at least three independent experiments.

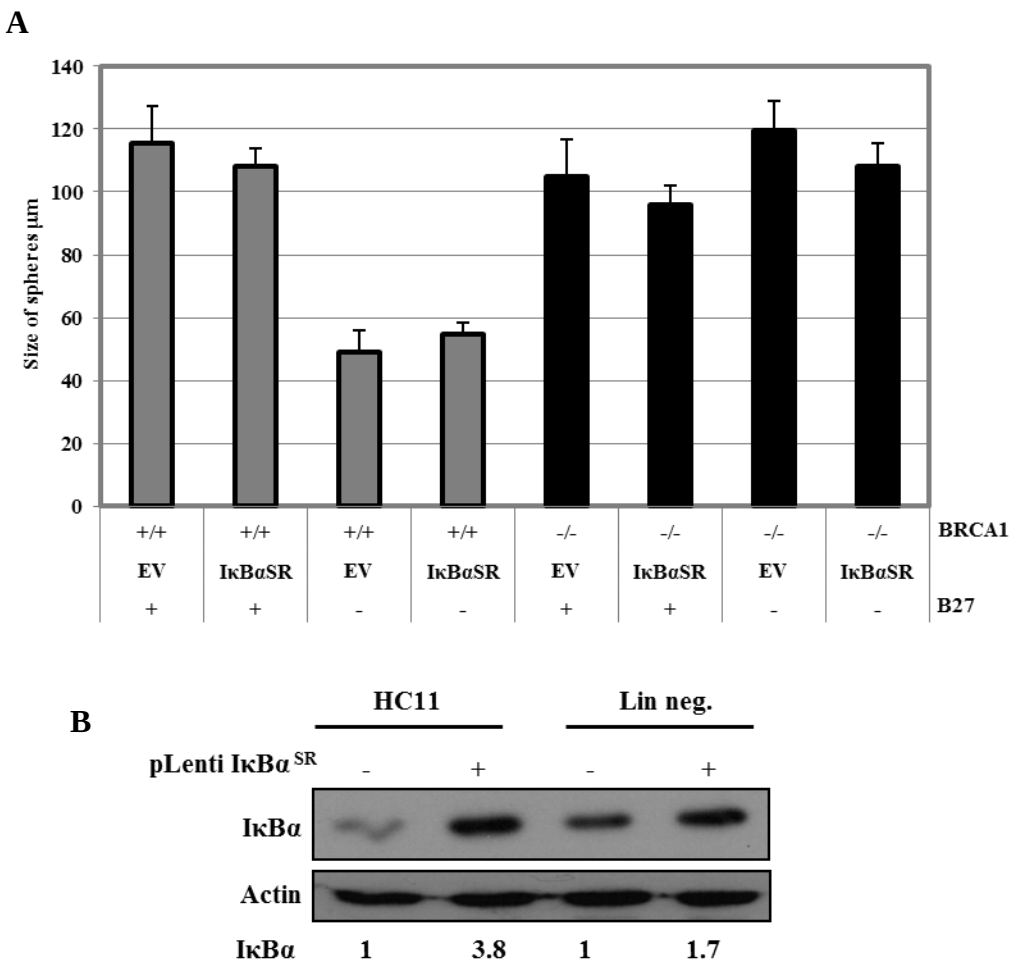

Figure 21: The canonical NF-κB pathway inhibition does not affect acini formation in Matrigel

Lin neg. cells were isolated from BRCA1 wild type (+/+) and BRCA1 knockout (-/-) mouse mammary glands and plated in Matrigel **A.** Lin neg. cells were plated on a thick layer of Matrigel (2.000 cells in 20 µL of Matrigel). Cells were infected with lentivirus expressing empty vector (EV) or IκBα^{SR} and grown in the presence (+) or absence (-) of B27 supplement. After 15 days acini size was measured using Northern Eclipse software. The graph shows the average of the thirty largest acini in the microscopy field (mean ± S.E.). **B.** Whole cell lysates from lin neg. cells and HC11 cells were immunoblotted for IκBα. Actin was used as loading control. Numbers underneath actin represent IκBα protein levels quantification calculated with ImageJ and normalized to EV levels. The graph and immunoblot are representative of at least three independent experiments

DNA damage induces NF-κB activation in the absence of BRCA1

BRCA1 is a key protein for the maintenance of genomic stability and DNA repair, playing an important role during G1 and S phase to prevent stalling at the replication forks (Deng, 2006; Jasin, 2002; Willis et al., 2014). The induction of the DNA damage response pathway following BRCA1 knockdown was first assayed in MCF-7 cells. Immunofluorescence analysis performed on MCF-7 cells infected with lenti-shBRCA1 for 72 hours showed high levels of phosphorylated ATM and H2AX while being undetectable in MCF-7 cells infected with lenti-shNT (Figure 22 A,B). BRCA1 knockdown was confirmed by immunofluorescence and showed in Figure 22 C. The DNA damage pathway activity was also examined in the stem- and progenitor-enriched cell populations isolated from mouse mammary glands. Stem- and progenitor-enriched cell populations obtained from BRCA1 KO mouse mammary glands showed elevated levels of phosphorylated ATM and H2AX foci while those obtained from BRCA1 WT mice did not (Figure 23 A,B). To translate this finding in human tissue, immunofluorescence for phosphorylated ATM was also performed on the sections from human BRCA1-mutation carriers. Two out of three BRCA1-mutation carriers showed high level of phosphorylated ATM in the lobules while all three wild type stained negatively (Figure 24 A). Interestingly, these two BRCA1-mutation carrier sections were also positive for RelB and strongly positive for p100/p52. Indeed, the pattern of ATM phosphorylation was the same for ALDH1, p100/p52, and RelB, where not all lobules stained positive (Figure 24 B). One possible explanation for this finding is that in BRCA1-mutation carriers, the elevated DNA damage may be responsible for NF-κB

activation (showed by strong p100/p52 and RelB staining) that in turn induces proliferation and expansion of progenitor cells (showed by elevated ALDH1 expression).

To test this hypothesis, the link between DNA damage and NF-κB activation was reviewed in the literature. It has been previously shown that NF-κB can be activated after DNA damage. DSBs induce ATM phosphorylation that in turns phosphorylates NEMO in the nucleus. Once phosphorylated, NEMO can be ubiquitylated and exported into the cytoplasm together with ATM. This ATM/NEMO complex can induce phosphorylation of IKKα and so activates alternative NF-κB pathway (Gapud et al., 2011; Hadian and Krappmann, 2011; Miyamoto, 2011). The role of ATM in the activation of alternative NF-κB pathway was first dissected using the BRCA1-mutated HCC1937 cell line. After 72 hours of transfection with siATM, western blot analysis showed that ATM inhibition in HCC1937 cells resulted in a 60% reduction in mature p52 (Figure 25 A). While this result confirmed a direct involvement of ATM in the alternative NF-κB induction, information on ATM/NEMO complex formation followed by BRCA1 loss or mutation were still missing. To test this, co-immunoprecipitation was performed to compare the level of NEMO/ATM complex in the BRCA1-wild type cell line MCF-7 versus the BRCA1-mutated cell line HCC1937. ATM was immunoprecipitated from lysate from both cell lines using two ATM antibodies followed by a western blot for NEMO. While MCF-7 cells contained a low level of NEMO associated with ATM, the BRCA1-mutated HCC1937 cells contained a much higher level of the NEMO/ATM complex (Figure 25 B). To confirm that the increase in the ATM/NEMO complex was a consequence of BRCA1 loss of function, BRCA1 was knocked down in MCF-7 cells using lenti-shBRCA1. Co-immunoprecipitation analysis was then performed and showed that after

BRCA1 knockdown the level of NEMO/ATM complex was increased (Figure 25 C). BRCA1 knockdown as well as ATM and IgG non-specific immunoprecipitates are shown in Figure 25 D and E respectively. This data confirms that BRCA1 loss or mutation results in increased ATM/NEMO complexes.

After confirming the role of ATM in the NF-κB activation, the role of ATM-mediated NF-κB activation was also studied in the formation of B27-independent acini from BRCA1-deficient luminal progenitor cells. Progenitor cells obtained from BRCA1 WT and BRCA1 KO mouse mammary glands were infected with lenti-shATM or lenti-shNT and Matrigel acini assay performed. Similar to the effect of shp100, the inhibition of ATM only reduced the acini size of BRCA1-deficient progenitor cells plated in the absence of B27 (Figure 26 A and Figure 40). Contrary to what was observed with the alternative NF-κB pathway inhibition by shp100, ATM inhibition did not affect the growth of either BRCA1-deficient or BRCA1-competent progenitor cells in the presence of B27. ATM knockdown in the progenitor cells was confirmed by qPCR and shown in Figure 26 B. Moreover, ATM knockdown in lin neg. cells obtained from BRCA1 KO mouse mammary glands resulted in a 80 % reduction in mature p52 (Figure 26 C), demonstrating that alternative NF-κB activation is mediated by ATM in BRCA1-deficient cells. Similar results were obtained when cells were treated with 5 μM of KU55933, a pharmacological ATM inhibitor (Figure 27 A and Figure 41), demonstrating that ATM-mediated NF-κB activation is important for progesterone-independent BRCA1-deficient progenitor cell expansion. KU-55933 was also tested on HCC1937 where it was able to reduce to 50% the level of p52 formation (Figure 27 B), confirming that ATM is necessary for the alternative NF-κB activation.

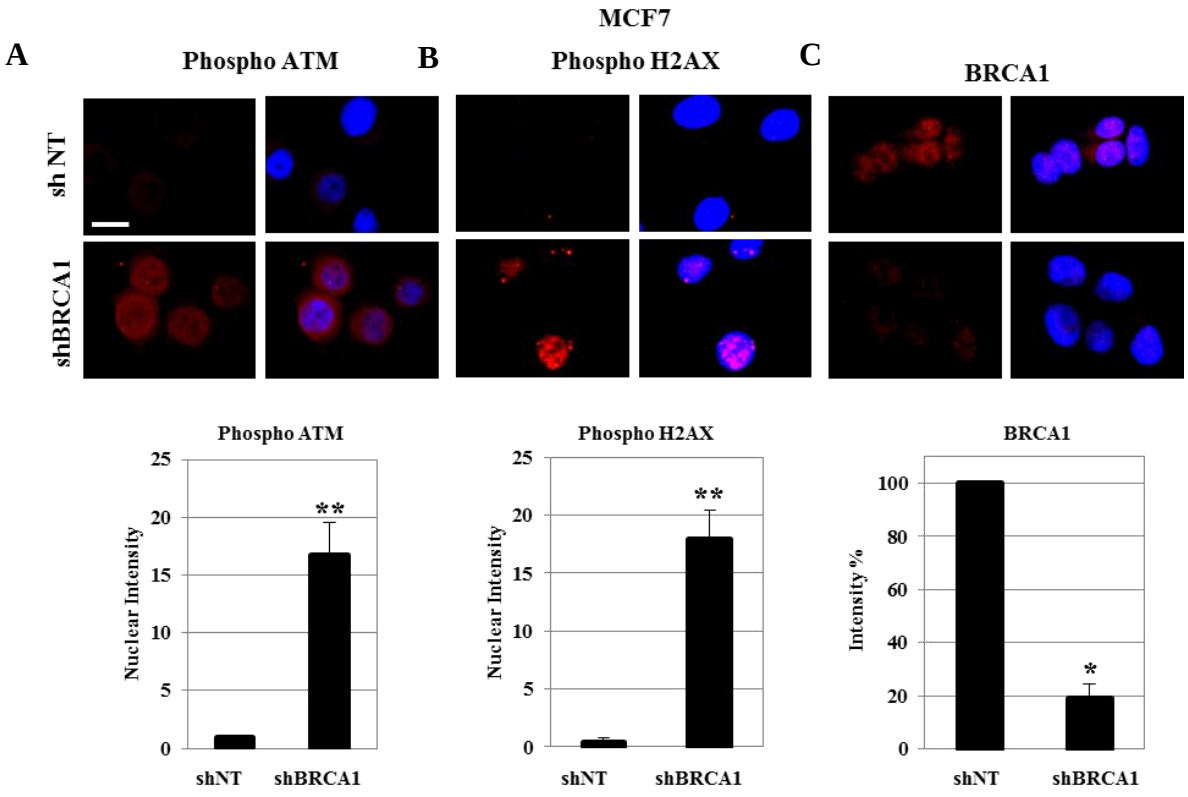

Figure 22: BRCA1 knockdown induces DNA damage in MCF-7 cells

MCF-7 were infected with lentivirus carrying non-targeting (NT) or BRCA1 shRNA for 72 hours, fixed, and immunofluorescence performed for **A.** phospho ATM (serine1981), **B.** phospho H2AX (serine 139), and **C.** BRCA1. The graph underneath each image represents the intensity of each staining calculated with ImageJ and normalized to shNT levels (mean ± S.E.). Scale bar 10 µm.(*) refers to $p<0.005$ and (**) refers to $p<0.01$. Images are representative of at least three independent experiments.

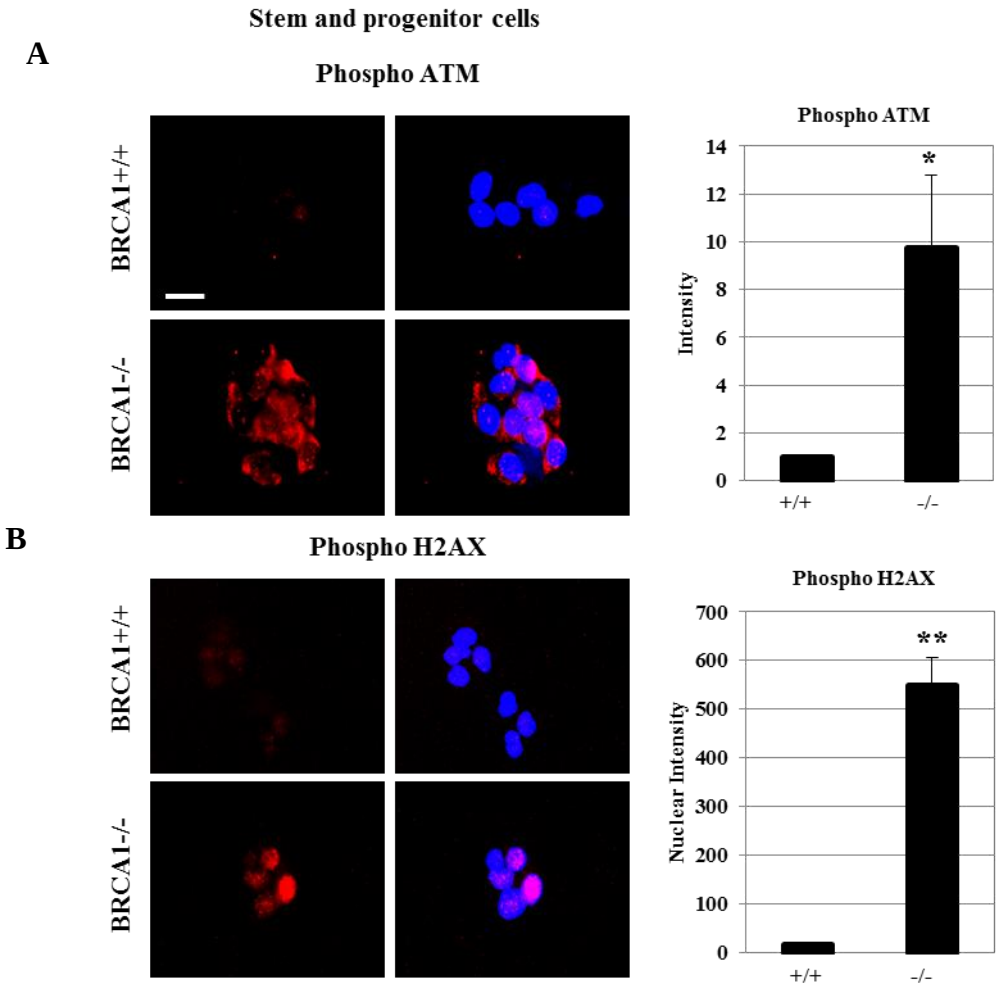

Figure 23: BRCA1-deficient stem and progenitor cells show high levels of DNA damage

Stem-enriched ($CD49f^{HI}$ $CD24^{LO}$) and progenitor-enriched ($CD49f^{LO}$ and $CD24^{HI}$) cell populations were isolated from BRCA1 wild type (+/+) and BRCA1 knockout (-/-) mouse mammary glands, sorted by FACS, and cytospun onto slides. Immunostaining for **A.** phospho ATM (serine1981) **B.** phospho H2AX (serine 139). The graph on right to each image represents the intensity of each staining calculated using ImageJ and normalized to BRCA1 +/+ levels (mean ± S.E.). Scale bar 10 µm. (*) refers to $p<0.05$ and (**) refers to $p<0.01$. Images are representative of at least three independent experiments.

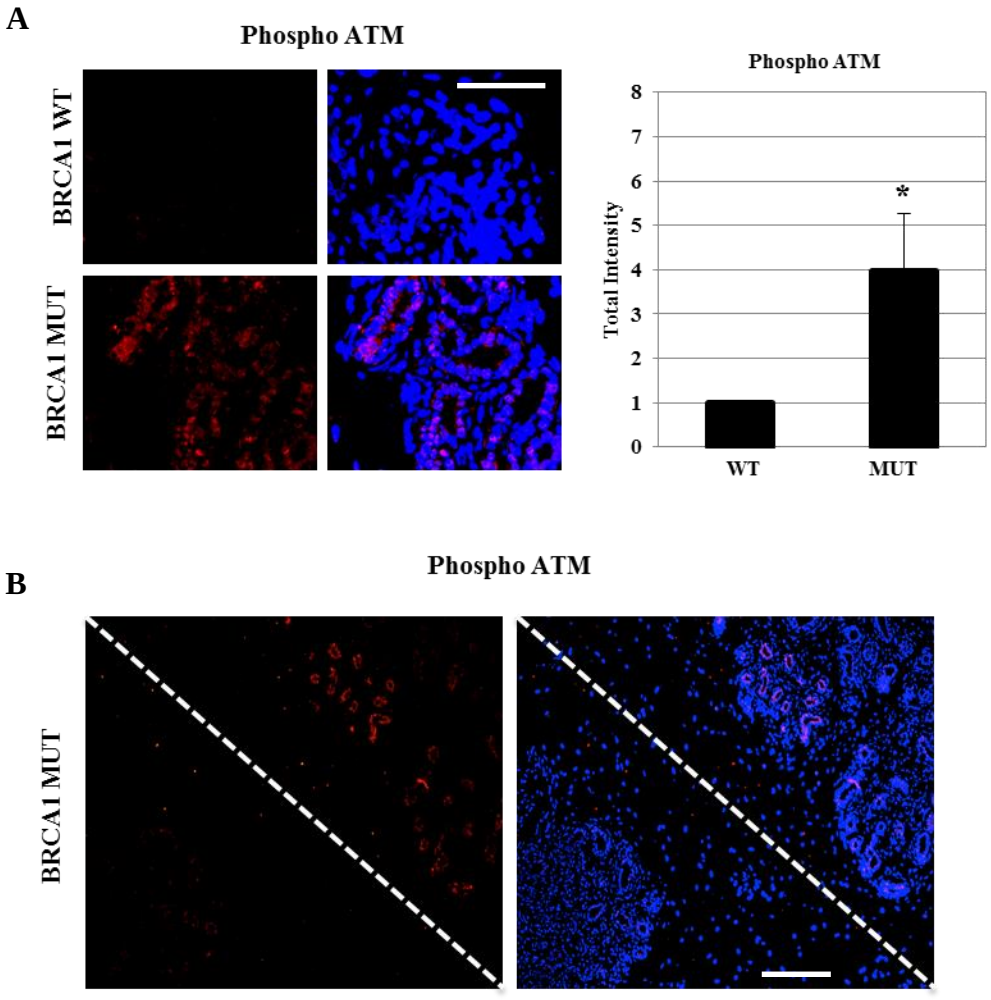

Figure 24: BRCA1-mutation carriers show sign of DNA damage in the mammary glands

Sections from BRCA1 wild type (WT) and BRCA1-mutation carriers (MUT) were immunostained for **A.** phospho ATM (serine 1981). The graph on right represents the intensity of staining calculated with ImageJ normalized to BRCA1 WT levels (mean ± S.E.). Scale bar 25 μm. **B.** Immunofluorescence for phospho ATM in BRCA1-mutation carrier sections. The dotted white line separates two areas with different staining of phospho ATM (positive versus negative). Scale bar 50 μm. (**) refers to $p<0.01$.

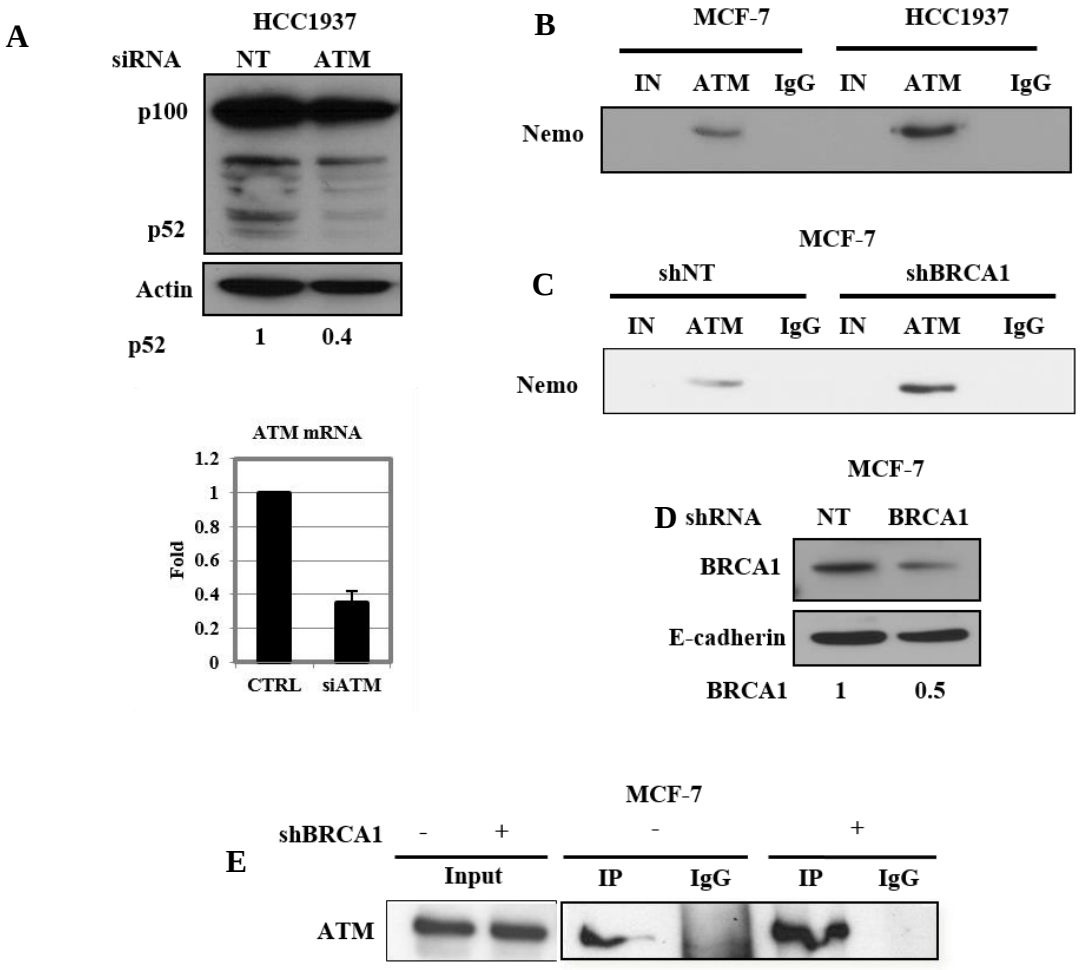

Figure 25: BRCA1 loss or mutation increases NEMO/ATM complex formation

A. HCC1937 cells were transfected with non-targeting (NT) or ATM siRNA for 72 hours. Whole cell lysates were collected and immunoblotted for p100/p52. Actin was used as loading control. Numbers underneath actin represent p52 protein levels quantification calculated with ImageJ and normalized to siNT levels. The graph underneath shows ATM knockdown by qRT-PCR. mRNA levels were quantified using primers specific for ATM and beta-actin (the endogenous control) **B.** Co-immunoprecipitation on MCF-7 and HCC1937 cell lines. Whole cell lysates were incubated with two ATM antibodies and immunoblotted for NEMO. IgG were used as negative control. **C.** Co-immunoprecipitation on MCF-7 infected for 72 hours with lentivirus carrying non-targeting (NT) or BRCA1 shRNA. Whole cell lysates were incubated with two ATM antibodies and immunoblotted for NEMO. IgG were used as negative control **D.** Confirmation of BRCA1 knockdown in MCF-7. E-cadherin was used as loading control. Numbers underneath E-cadherin represent BRCA1 protein levels calculated with ImageJ and normalized to shNT levels. **E.** Confirmation of ATM immunoprecipitation in MCF-7 cells. Inputs represent the ATM protein levels in the whole cell lysates before ATM antibodies were incubated overnight. IP represent the level of ATM immunoprecipitated after incubation of whole cell lysates over night with ATM antibodies. IgG were used as negative control.

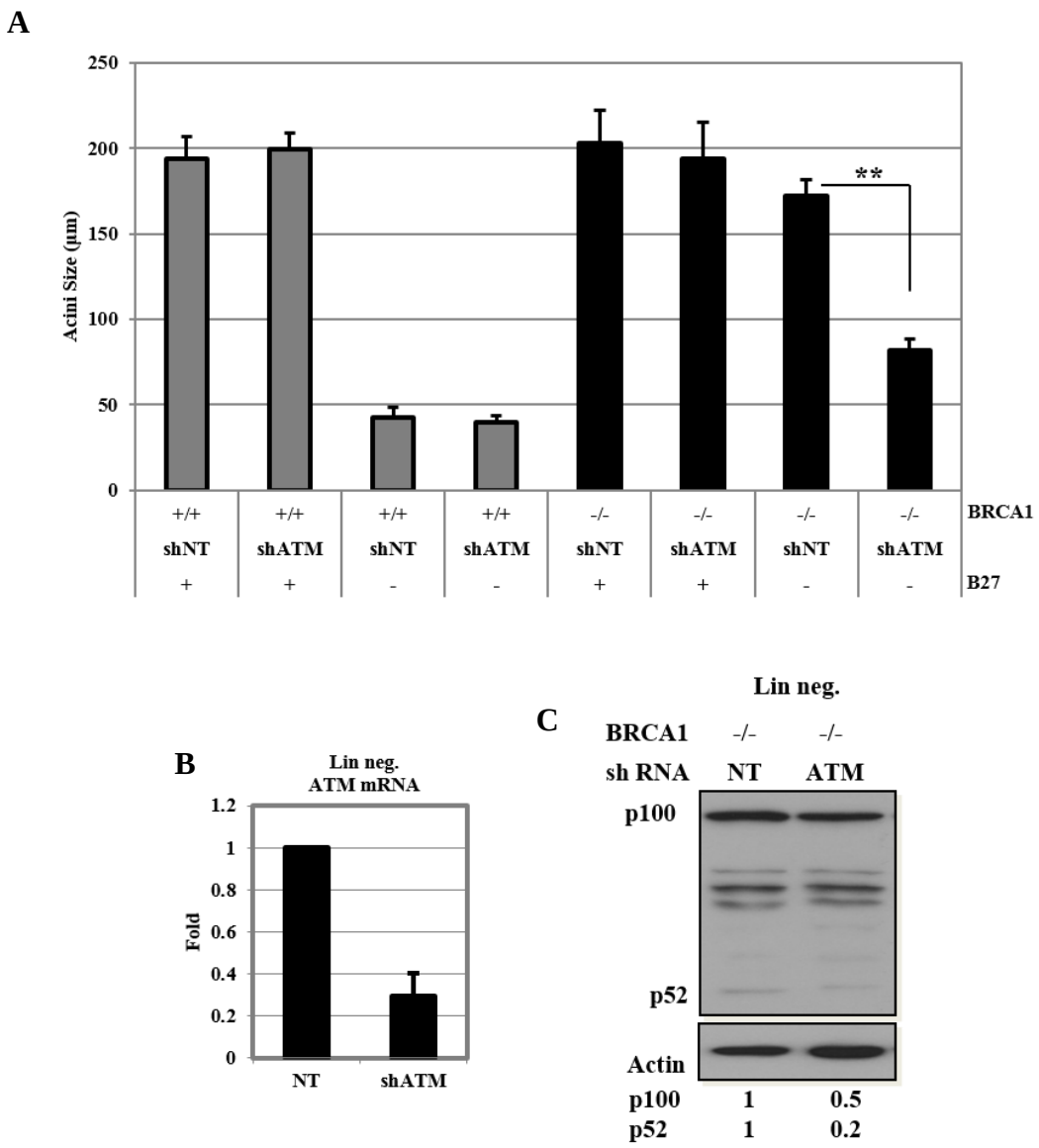

Figure 26: ATM inhibition blocks the progesterone-independent growth of BRCA1-deficient luminal progenitor cells in Matrigel

Lin neg. cells isolated from BRCA1 wild type (+/+) and BRCA1 knockout (-/-) mouse mammary glands were plated in Matrigel (2,000 cell in 20µL of Matrigel). **A.** Lin neg. cells were infected with lentivirus carrying non-targeting (NT) or ATM shRNA and grown in the presence (+) or absence (-) of B27. After 15 days acini size was measured using Northern Eclipse. The graph represents the average of the thirty largest acini in the microscopy field (mean ± S.E.). **B.** mRNA was isolated from lin neg. cells infected with shNT and shATM and qRT-PCR performed to confirm ATM knockdown. mRNA levels were quantified using primers specific for ATM and beta-actin (the endogenous control) **C.** Whole cell lysates from lin neg. cells infected with lenti shNT or shATM were immunoblotted for p100/p52. Actin was used as loading control. Numbers underneath the actin represent p52 protein quantification by ImageJ normalized to shNT levels. (**) refers to $p<0.01$ calculated by two-way ANOVA analysis, followed by Tukey test. Graph, immunoblot, and qPCR are representative of at least three independent experiments.

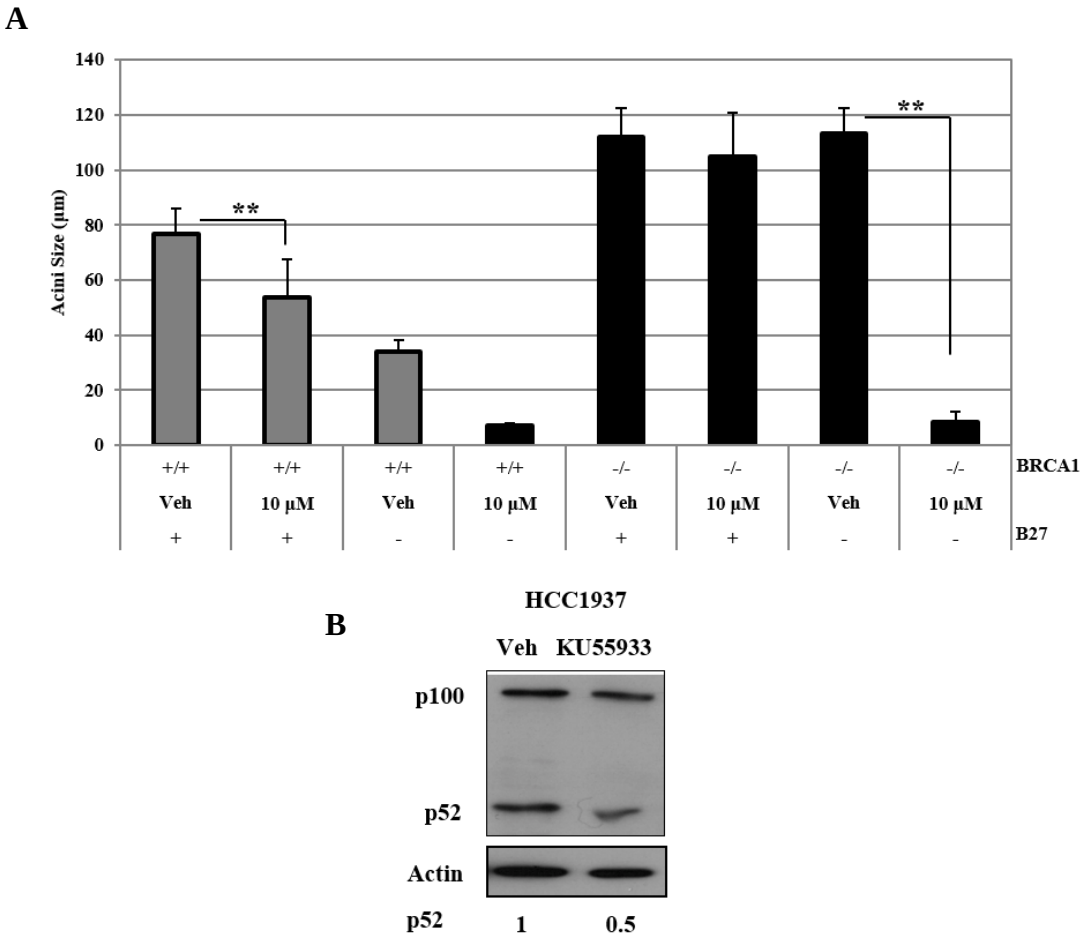

Figure 27: ATM pharmacological inhibition blocks the progesterone-independent growth of BRCA1-deficient luminal progenitor cells in Matrigel

Lin neg. cells were isolated from BRCA1 wild type (+/+) and BRCA1 knockout (-/-) mouse mammary glands and plated in Matrigel (2,000 cell in 20µL of Matrigel). **A.** Cells were treated with vehicle (Veh) or 10 µM KU-55933 and grown in the presence (+) or absence (-) of B27. After 15 days acini size was measured using Northern Eclipse. The graph represents the average of the thirty largest acini in the microscopy field (mean ± S.E.). **B.** Whole cell lysates from HCC1937 treated with vehicle (Veh) or 10 µM KU-55933 were immunoblotted for p100/p52. Actin was used as loading control. Numbers underneath actin represent p52 protein levels quantification calculated with ImageJ and normalized to veh levels. (**) refers to $p<0.01$ calculated by two-way ANOVA analysis, followed by Tukey test. Immunoblots are representative of at least three independent experiments.

Progesterone increases proliferation-mediated DNA damage in BRCA1-deficient progenitor cells

As previously mentioned, progesterone has a proliferative role in the human and mouse mammary glands, inducing proliferation not only in the PR-positive mammary epithelial cells, but also to PR-negative stem and progenitor cells (Beleut et al., 2010; Joshi et al., 2010). Moreover, it has recently brought back to light the key role of progesterone in the initiation and progression of breast cancer (Brisken, 2013).

To test if progesterone treatment was inducing increased proliferation in the mouse mammary epithelial cells, mice were injected with progesterone at a concentration of 10 mg/Kg or with vehicle for 3 consecutive days and then Ki-67 immunohistochemistry was performed on mouse mammary glands. Progesterone treatment increased the numbers of Ki67-positive cells across most ductal sections relative to vehicle (Figure 28 A). Interestingly, a marked difference between BRCA1 KO and BRCA1 WT mammary glands was also noted, wherein numerous mitotic cells were differentially detected in the basal regions of the BRCA1 KO glands as shown by the arrows in picture 28 A.

During normal cellular replication, a lesion in one of the single strand may cause the DNA polymerase to stall inducing the collapsing of replication forks that could result in DSBs (Nagaraju and Scully, 2007). While these breaks are normally repaired by the BRCA1-mediated error-free mechanism HR, in the absence of functional BRCA1, the error-prone mechanism NHEJ takes place instead, leading to genomic instability (Schlacher et al., 2012). To test if the elevated proliferation signal induced by progesterone could result in increased fork stalling and DSBs, immunohistochemistry on

progesterone and vehicle-treated mouse mammary glands was performed for the DNA damage marker phospho-H2AX. An overall increase in the levels of phosphorylated H2AX was found in the progesterone-treated mouse mammary glands of both BRCA1 KO and BRCA1 WT mice (Figure 28 B). However, the level and intensity of phosphorylated H2AX were higher in the BRCA1 KO mouse mammary glands, as shown by the arrows in Figure 28 B.

In order to quantify the level of H2AX phosphorylation, a western blot using protein collected from lin neg. cells from progesterone- or vehicle-treated mice was performed. Lin neg. cells obtained from vehicle-treated BRCA1 KO mouse mammary glands showed a 2 fold-increase in phosphorylated H2AX compared to the cells from vehicle-treated BRCA1 WT mice (Figure 29 A). This was in agreement with the previous finding of BRCA1-deficient mammary progenitor cells that showed presence of phosphorylated H2AX (Figure 23 B). Moreover, lin neg. cells from progesterone-treated BRCA1 WT mouse mammary glands showed a 5-fold increase in phosphorylated H2AX compared to the vehicle-treated cells. Interestingly, lin neg. cells from progesterone-treated BRCA1 KO mouse mammary glands had a 9 fold-increase in phosphorylated H2AX compared to cells from the vehicle-treated BRCA1 KO mice. This confirmed that progesterone exposure induces an overall increase in DNA damage, and that given the key role of BRCA1 in repairing DSBs caused by replication stress, BRCA1 KO mice were more susceptible to progesterone-induced DNA damage.

Based on our finding that the elevated NF-κB activity increased BRCA1-deficient luminal progenitor cell proliferation, it was tested whether inhibition of NF-κB could reduce the proliferation-mediated DNA damage found in BRCA1 KO mammary glands.

Indeed, DMAPT i.p injection reduced the level of phosphorylated H2AX in the BRCA1 KO mouse mammary glands (Figure 29 B). The reason behind this reduction in DNA damage could be explain by either a reduction in the proliferation of aberrant luminal progenitor cells or by an increase in their cell death due to DMAPT treatment. More experiments need to be performed in order to clarify this mechanism.

Increased DNA damage can induce cell death if lesions are not repaired (Ciccia and Elledge, 2010). PARP-1 is an important protein involved in the DNA damage repair machinery and cell death, known to be a hallmark of apoptosis. Indeed, when cell death is initiated, caspase-3 and caspase-7 can block PARP-1 activity by inducing its cleavage that results in the production of PARP-1 89 KDa fragment (Chaitanya et al., 2010). To see if DNA damage resulted in caspase activation, PARP-1 expression/cleavage was examined in lin neg. cells from progesterone- or vehicle-treated mouse mammary glands. Lin neg. cells from progesterone-treated BRCA1 WT mouse mammary glands showed increased level of PARP-1 89 KDa fragment (Figure 29 C), confirming that the high level of DNA damage resulted in caspase activation. Interestingly, lin neg. cells obtained from progesterone-treated BRCA1 KO mouse mammary glands contained a lower level of the 89 KDa fragment compared to the BRCA1 WT progesterone-treated, despite their higher level of DNA damage.

All together these findings demonstrate that progesterone induces an increase in proliferation that results in increased DNA damage in the mouse mammary glands. However, after progesterone treatment, BRCA1-deficient cells appear to block caspase activation, evade apoptosis and proliferate despite their higher level of DNA damage compared to BRCA-competent cells.

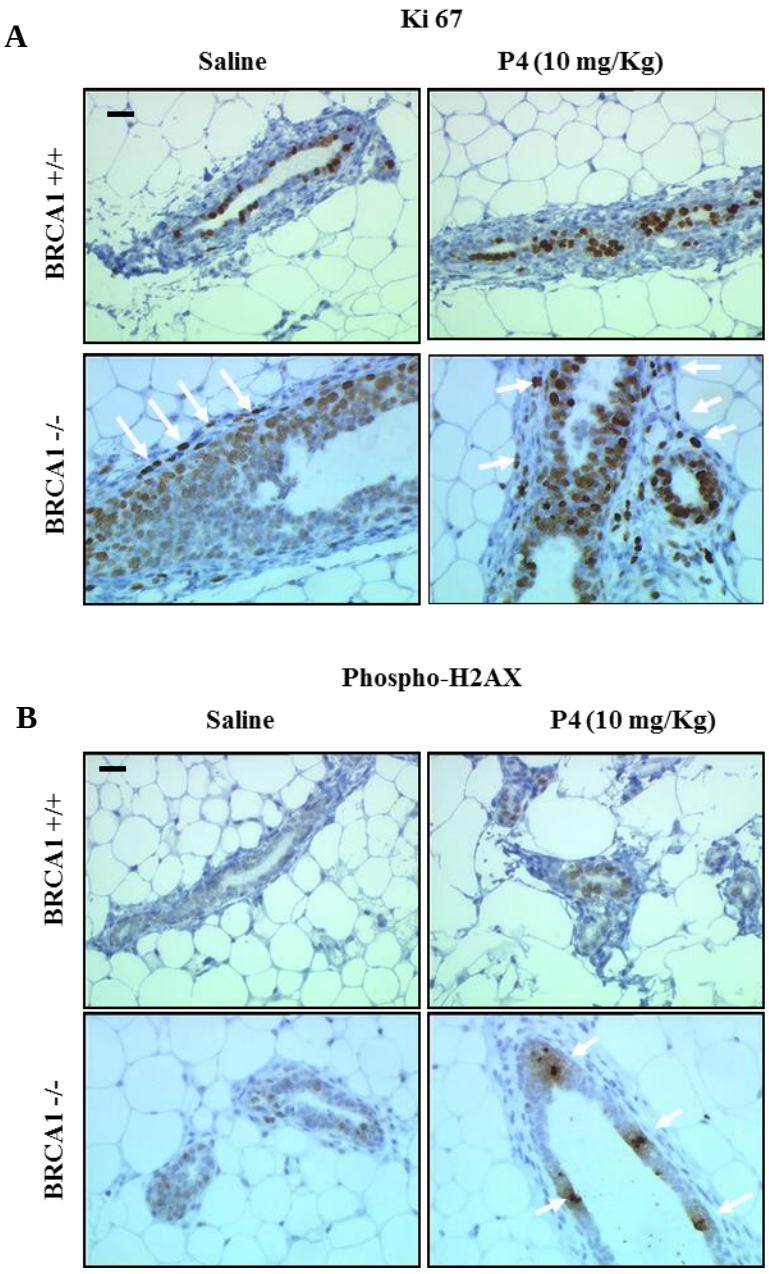

Figure 28: Progesterone treatment increases proliferation and DNA damage in mouse mammary glands

BRCA1 wild type (+/+) and BRCA1 knockout (-/-) mice were injected s.c. with 10 mg/Kg of progesterone (P4) or saline for 3 consecutive days. On the fourth day mammary glands were collected for paraffin-embedded sections. Immunohistochemistry on mouse mammary gland paraffin-embedded sections with **A.** Ki67 and **B.** phospho-H2AX (serine 139). Arrows indicate basal cells positive for Ki67 in **A.** and foci of high level of phosphorylated H2AX in **B.** Scale bar 25 μm. Images are representative of at least three independent experiments.

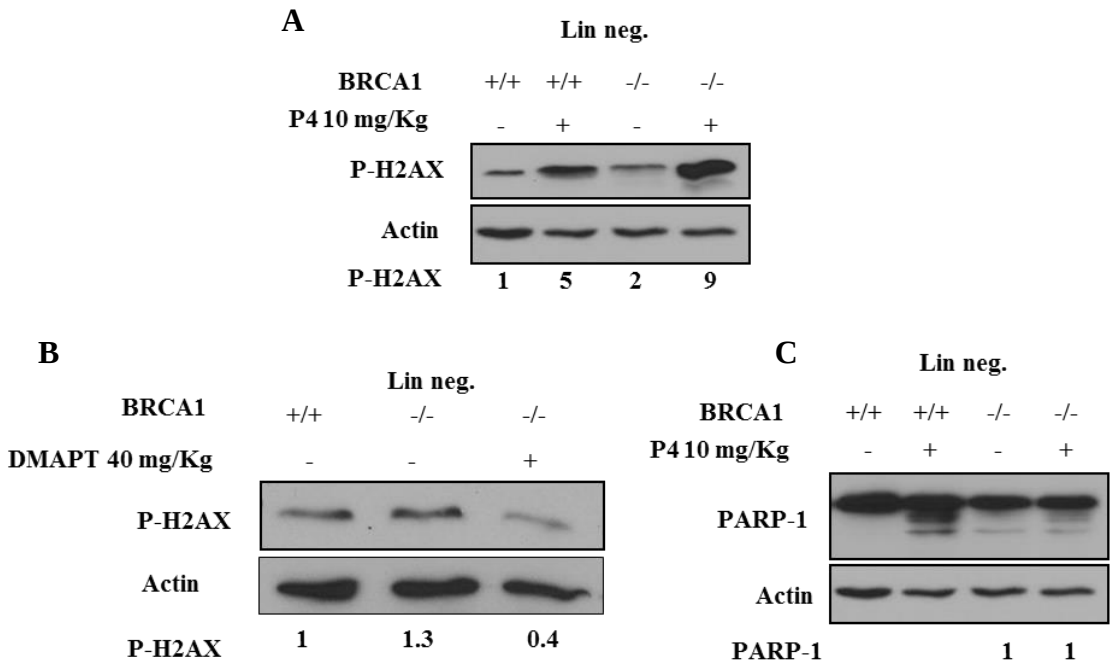

Figure 29: BRCA1-deficient lin neg. cells show high levels of DNA damage but low levels of caspase activation

BRCA1 wild type (+/+) and BRCA1 knockout (-/-) mice were injected s.c. with 10 mg/Kg of progesterone (P4) (+) or saline (-) for 3 consecutive days. The fourth day mammary glands were collected for lin neg. isolation. **A.** Whole cell lysates of lin neg. cells from mice injected with P4 or saline were immunoblotted for phospho-H2AX (serine 139). Actin was used as loading control. Numbers underneath actin represent phospho-H2AX protein levels calculated with ImageJ normalized to BRCA1 +/+ saline-treated levels. **B.** Whole cell lysates of lin neg. cells from mice treated with saline or 40 mg/Kg DMAPT were immunoblotted for phospho-H2AX (serine 139). Actin was used as loading control. Numbers underneath actin represent phospho-H2AX protein levels quantification calculated with ImageJ normalized to BRCA1 +/+ saline-treated levels. **C.** Whole cell lysates of lin neg. cells from mice treated with saline or P4 were immunoblotted for PARP-1. Actin was used as loading control. Numbers underneath actin represent PARP-1 89 KDa fragment quantification levels calculated with ImageJ normalized to BRCA1 +/+ saline-treated levels. Immunoblots are representative of at least three independent experiments.

Myc and cyclin D2 expression is increased and regulated by NF-κB in BRCA1-deficient cells

The MYC oncogene can be amplified in BRCA1-associated breast cancer (Grushko et al., 2004). It has also been reported that NF-κB can induce Myc transcription through p52/RelB complex (Demicco et al., 2005) and NEMO/IKKα complex can also directly interact with Myc and promote phosphorylation at serine 62 that stabilizes Myc protein (Duyao et al., 1990; Kim et al., 2010; Yeh et al., 2011). Therefore, Myc expression levels were examined in lin neg. cells from BRCA1 KO and BRCA1 WT mouse mammary glands. Western blot analysis of proteins collected from lin neg. cells revealed increased level of Myc in BRCA1 KO mice compared to BRCA1 WT (Figure 30 A). To assess whether Myc protein levels were also increased in the breast tissue from human BRCA1-mutation carriers, immunohistochemistry analysis was performed. Two out of the three BRCA1-mutation carriers had increased levels of Myc in their lobules, while low levels of Myc were found in the three BRCA1 wild type carriers (Figure 30 B).

To confirm that Myc was regulated by NF-κB, lin neg. cells isolated from BRCA1 WT and BRCA1 KO mouse mammary glands were plated and treated with 10 μM of BMS-345541 or vehicle and proteins collected for western blot analysis. BMS-345541-mediated NF-κB inhibition reduced Myc protein levels in lin neg. cells from BRCA1 KO mouse mammary glands while no effect was detected in those from BRCA1 WT (Figure 30 C). Since BMS-345541 can inhibit both the canonical and alternative NF-κB pathways, lenti-shp100 was used to specifically target the alternative NF-κB pathway. After infecting lin neg. cells from BRCA1 KO mouse mammary glands with lenti-shp100, Myc protein levels were found strongly reduced as a consequence of alternative

NF-κB inhibition (Figure 30 D). The same result was obtained when HCC1937 cells were infected with lenti-shp100 (Figure 30 E). This data confirms that the alternative NF-κB pathway induces the increased levels of Myc in BRCA1 KO mammary glands.

Myc has a well-known function in regulating cell proliferation, and it has been demonstrated that deregulated expression of Myc leads to uncontrolled proliferation and cancer (Bernard and Eilers, 2006). We therefore tested if Myc expression was playing a role in the BRCA1-deficient progenitor cell proliferation. Lin neg. cells isolated from BRCA1 KO and BRCA1 WT mouse mammary glands were plated in Matrigel and infected with lenti-shMyc or lenti-shNT. Myc knock-down induced an overall reduction of acini sizes of progenitor cells obtained from BRCA1 WT and BRCA1 KO mouse mammary glands in the presence and absence of B27. However, a slightly stronger effect was observed in progenitor cells obtained from BRCA1 KO mouse mammary glands plated in absence of B27 (Figure 31A). Confirmation of Myc knockdown is shown in Figure 31 B. This result demonstrates that, although Myc inhibition induces a delay in the proliferation of normal progenitor cells, BRCA1-deficient progenitor cells seem to rely more on Myc for their progesterone-independent growth in Matrigel.

A previous work published a list of genes differentially regulated in stem and luminal progenitor cells from patients with wild type BRCA1 and BRCA1 mutations (Lim et al., 2009). After cross-referencing this list of genes with known Myc targets, cyclin D2, which is strongly regulated by Myc, was found to be one of the most differentially expressed genes in BRCA1-mutated progenitor cells (6-fold induction). Cyclin D2 expression has been linked to stem and progenitor cell expansion and cell cycle progression (Becker et al., 2010; Bouchard et al., 1999; Sasaki et al., 2004).

To confirm the increased level of cyclin D2 in BRCA1 KO versus BRCA1 WT mice, western blot and qPCR analyses were performed. Cyclin D2 mRNA and protein levels were found to be 2-fold increase in the lin neg. cells obtained from BRCA1 KO compared to BRCA1 WT mouse mammary glands (Figure 32 A,B). To demonstrate NF-κB-mediated cyclin D2 regulation, proteins from HCC1937 cells infected with lenti-shp100 or lenti-shNT were immunoblot for cyclin D2. NF-κB alternative pathway inhibition strongly reduced the level of cyclin D2 by 80 % (Figure 32 C). Cyclin D2 protein levels were also examined on lin neg. cells obtained from BRCA1 KO mice injected i.p. with DMAPT. A 40 % reduction in cyclin D2 levels was observed after DMAPT injections (Figure 32 D), confirming the NF-κB-mediated regulation of cyclin D2 *in vivo*.

All together these findings demonstrate that NF-κB-directed Myc activation induces expansion of the mammary progenitor cell population and at the same time increases cyclin D2 expression levels.

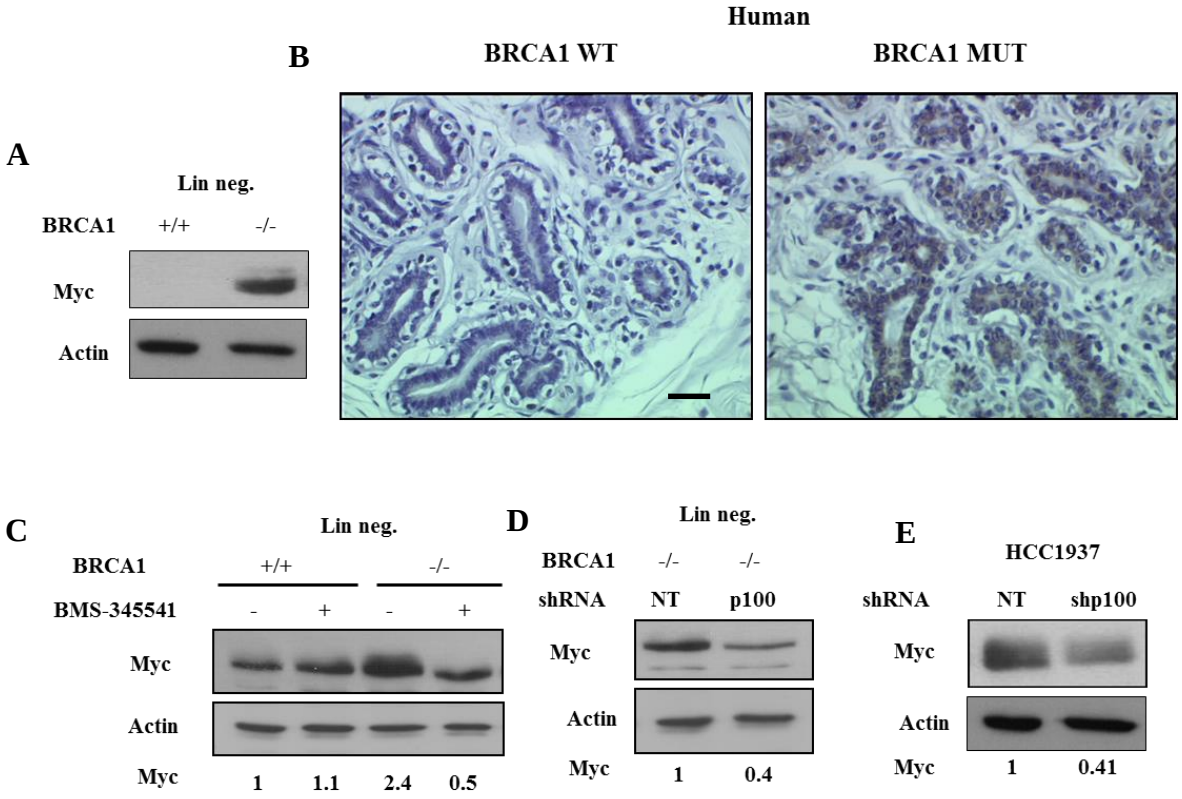

Figure 30: Myc expression is increased in BRCA1-deficient lin neg. cells and BRCA1-mutated human mammary glands

A. Whole cell lysates were immunoblotted for Myc in lin neg. cells from BRCA1 wild type (+/+) and BRCA1 knockout (-/-) mouse mammary glands. Actin was used as loading control. **B.** Paraffin-embedded sections of human mastectomies from BRCA1 wild type (WT) and BRCA1-mutation (MUT) carriers. Sections were immunostained for Myc. Scale bar 25 μm. Whole cell lysates were immunoblotted for Myc in **C.** lin neg. cells treated for 72 hours with 10 μM BMS-345541 (+) or vehicle (-), **D.** in lin neg. cells infected with lentivirus carrying non-targeting (NT) or p100 shRNA, **E.** HCC1937 cells infected with lentivirus carrying non-targeting (NT) or p100 shRNA. Actin was used as loading control. Numbers underneath actin represent Myc protein levels quantification calculated with ImageJ. In lin neg. values were normalized to BRCA1 +/+ protein levels. In HCC1937 values were normalized to shNT protein levels. Immunoblots and immunohistochemistry images are representative of at least three independent experiments.

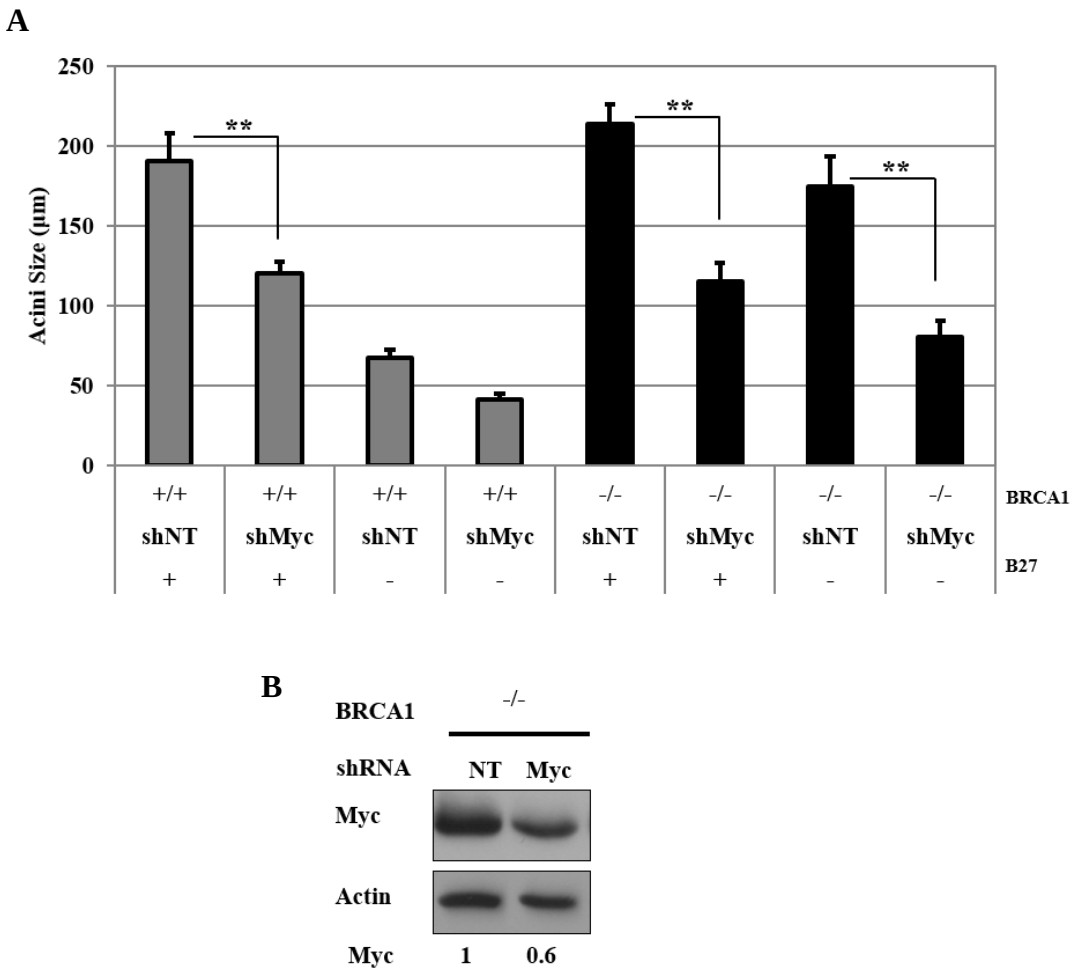

Figure 31: Myc inhibition blocks luminal progenitor cell proliferation in Matrigel

A. Lin neg. cells obtained from BRCA1 WT (+/+) and BRCA1 KO (-/-) mouse mammary gland were plated in Matrigel (2,000 cell in 20µL of Matrigel). Cells were infected with lentivirus carrying non-targeting (NT) or Myc shRNA and grown in the presence (+) or absence (-) of B27. After 15 days acini size was measured using Northern Eclipse. The graph represents the average of the thirty largest acini in the microscopy field (mean ± S.E.). **B.** Confirmation of Myc knockdown in lin neg. cells by immunoblot. Actin was used as loading control. Numbers underneath actin represent Myc protein levels quantification calculated with ImageJ normalized to shNT levels. (**) refers to $p<0.01$ calculated by two-way ANOVA analysis, followed by Tukey test. The graph and immunoblot are representative of at least three independent experiments.

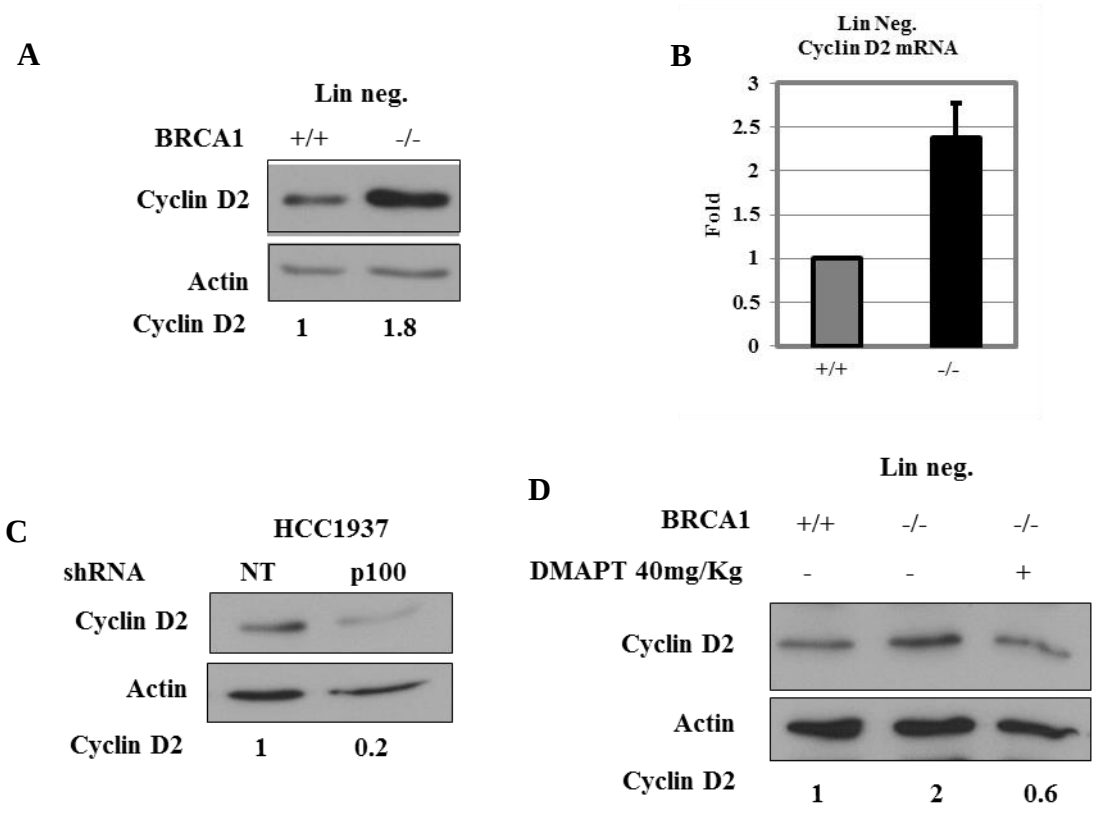

Figure 32: Cyclin D2 expression is increased in BRCA1-deficient lin neg. cells and regulated by NF-κB

Cylcin D2 levels in lin neg and. HCC1937cells. **A.** Whole cell lysates of lin neg cells from BRCA1 wild type (+/+) and BRCA1 knockout (-/-) mouse mammary glands were immunoblotted for cyclin D2. Actin was used as loading control. Numbers underneath actin represent cyclin D2 protein levels quantification calculated with ImageJ normalized to BRCA1 +/+ levels. **B.** qRT-PCR on mRNA extracted from lin neg. cells from BRCA1 +/+ and BRCA1-/- mouse mammary glands. mRNA levels were quantified using primers specific for cyclin D2 and beta-actin (the endogenous control). Cyclin D2 mRNA levels were normalized to the levels of BRCA1 +/+. **C.** Whole cell lysates from HCC1937 cells infected with lentivirus carrying non-targeting (NT) or p100 shRNA were immunoblotted for cycling D2. Actin was used as loading control. Numbers underneath actin represent cyclin D2 protein levels quantification calculated with ImageJ normalized to shNT levels. **D.** Whole cell lysates of lin neg. cells from BRCA1 +/+ and BRCA1 -/- mice treated with DMAPT at 40 mg/Kg (+) or saline (-) were immunoblotted for cyclin D2. Actin was used as loading control. Numbers underneath actin represent cyclin D2 protein levels quantification calculated with ImageJ normalized to BRCA1 +/+ saline-treated (-) levels. Immunoblots and qPCR are representative of at least three independent experiments.

DISCUSSION

Summary

This study shows for the first time a central role for autologous activation of the alternative NF-κB pathway in the expansion of BRCA1-deficient mammary progenitor cells. Down-regulation of BRCA1 using either siRNA or shRNA consistently resulted in activation of the alternative NF-κB pathway. Consistent with its role in DNA damage repair, BRCA1 loss or mutation resulted in increased DNA damage shown by increased phosphorylation of H2AX foci and ATM. Moreover, an elevated level of ATM/NEMO complexes and IKK-mediated p100 processing was observed in cells lacking BRCA1.

Alternative NF-κB pathway activation has been associated with increased cell proliferation but at the same time delayed differentiation (Connelly et al., 2007). Indeed, when p52 was overexpressed in the non-tumorigenic mouse mammary epithelial cell line HC11, a block in lactogenic differentiation was observed. DNA damage-mediated NF-κB activation in BRCA1 KO mouse mammary glands induced expansion of stem and progenitor cell compartments. When examined, these BRCA1-deficient mouse mammary progenitor cells exhibited high levels of nuclear p52 and RelB and had the ability to form acini in Matrigel in the absence of progesterone. Consequently, the use of NF-κB inhibitors such as BMS-345541, DMAPT, and shp100 inhibited the proliferation of these "aberrant" progenitor cells in acini formation assays in the absence of progesterone.

Progesterone induces proliferation of mammary epithelial stem and progenitor cells and it has recently been proposed to play a role in the initiation of breast cancer (Brisken, 2013; Joshi et al., 2010). Progesterone treatment increased proliferation and DNA damage in BRCA1 KO mouse mammary glands, suggesting a role for this hormone

in the DNA damage-mediated activation of NF-κB and aberrant progenitor cell expansion in the mammary glands. The findings of this study are summarized as model in Figure 33.

BRCA1 loss or mutation induces the alternative NF-κB pathway activation *in vitro* and *in vivo*

BRCA1 and NF-κB have both been found to regulate normal mammary gland development from the early embryonic stage to pregnancy and lactation (Connelly et al., 2007; Demicco et al., 2005; Furuta et al., 2005; Marquis et al., 1995). Gain and loss of function of NF-κB and BRCA1 respectively have been associated with breast cancer initiation and progression (Ginestier et al., 2009; Pratt et al., 2009). For the first time, the mechanism through which BRCA1 loss or mutation induces the alternative NF-κB activation has been dissected in progenitor cells, which may predispose them to breast cancer initiation.

Confirmation of NF-κB activation in BRCA1-deficient cells was first assayed by knockdown experiments in three different cell lines: the non-tumorigenic mammary epithelial cell line MCF-10A, the luminal breast cancer cell line MCF-7, and basal breast cancer cell line MDA-MB-231. BRCA1 knockdown resulted in increased p100 processing and p52/RelB nuclear localization, demonstrating the activation of the alternative NF-κB pathway following BRCA1 loss. To prove that this NF-κB activation was not simply a consequence of BRCA1 knockdown, the BRCA1-mutated breast cancer cell line HCC1937 was used. This cell line was originally established from a primary breast carcinoma from a 24 year-old patient with a germ-line BRCA1 mutation (homozygous BRCA1 5832insC mutation) (Tomlinson et al., 1998). Reconstitution of

wild type BRCA1 in HCC1937 caused a decrease in p100 processing and in p52/RelB nuclear localization, demonstrating that not only BRCA1 loss but also BRCA1 mutation induces activation of alternative NF-κB *in vitro*. To confirm that BRCA1-mediated NF-κB activation was also induced *in vivo*, the MMTV-Cre transgenic mouse model with BRCA1 deletion restricted to mammary glands was used. Immunofluorescence analysis on the whole mouse mammary gland revealed a uniform pattern of p100 and RelB expression mostly localized in the cytoplasm of basal and luminal cells in BRCA1 WT mammary glands while in BRCA1 KO mammary glands, nuclear localization of p52/RelB confirmed alternative NF-κB activation.

In the last decade, several studies have tried to determine the cells of origin for different subtypes of breast cancers. BRCA1-mutated cancer belongs to the basal-like subtype, and several studies have shown that this tumor type originates from mammary luminal progenitor cells (Lim et al., 2009; Molyneux et al., 2010; Visvader and Stingl, 2014). Immunofluorescence analysis on luminal progenitor cells isolated from BRCA1 WT and BRCA1 KO mouse mammary glands showed elevated p52/RelB nuclear localization only in the BRCA1-deficient and not in the BRCA1-wild type luminal progenitor cells. Moreover, western blot analysis showed an increased level of phosphorylated IKKα/β in the BRCA1-deficient compared to BRCA1 wild type progenitor cells, confirming the activation of alternative NF-κB pathway in this population. The IKK complex is normally localized in the cytoplasm of a cell; however, IKKα can also been found in the nucleus, where it phosphorylates histone H3 and induce survival and cell proliferation (Anest et al., 2003; Park et al., 2005). When examined, the presence of phosphorylated IKKα was found in the nucleus of BRCA1-deficient luminal

progenitor cell, while BRCA1 wild type progenitor cells did not show any detectable levels.

While IKKα phosphorylation can mediate the activation of the alternative NF-κB pathway through p100 processing, phosphorylated IKKβ can induce IκB degradation followed by the release of the canonical NF-κB components p65/p50 (Hayden and Ghosh, 2004). The IKKβ phosphorylation observed was not surprising since IKKα phosphorylation can in turn induce IKKβ phosphorylation as well (Hayden and Ghosh, 2008b). To exclude the activation of the canonical NF-κB pathway, the nuclear localization of p65 (the main components of the canonical NF-κB pathway) was analyzed in the luminal progenitor cells and in whole mouse mammary gland sections. Almost no nuclear p65 was found in the nuclei of BRCA1-deficient and competent luminal progenitor cells. Moreover, BRCA1 KO and BRCA1 WT mouse mammary glands showed similar levels of p65 in the cytoplasm of basal and luminal cells, without any presence in their nuclei. These data confirmed that the canonical NF-κB proteins were poorly expressed and not activated after loss of BRCA1 and thus, only the alternative NF-κB pathway is induced following BRCA1 ablation.

To confirm these immunofluorescence findings from the mouse model in human patient samples, histological sections from prophylactic mastectomies of BRCA1-mutation carriers and BRCA1 wild type carriers were analyzed. When stained with p100/p52 and RelB, two out of three BRCA1-mutation carriers showed strong expression of p100/p52 and RelB in the lobules, while all BRCA1 wild type carriers were negative for p100/p52 and RelB expression. Unfortunately, information about the specific BRCA1 mutational status in these patients was unavailable. One possible reason why one of the

three BRCA1-mutation carriers did not express high level of p100/p52 and RelB could be that a non-deleterious mutation allowed BRCA1 to function as wild type in the mammary gland of that patient. Moreover, the absence of NF-κB expression might also be a consequence of the neoadjuvant chemotherapy that was administered to this particular patient (see patient information in materials and methods).

Interestingly, not all lobules of the two BRCA1-mutation carriers were positive for RelB or p100/p52. Indeed, some areas showed lobules with strong expression of NF-κB while others were completely negative. Moreover, within the same lobule, some acini were positive while others were negative. This might be explained by the previous finding of BRCA1 loss of heterozygosity (LOH) only in some lobules of BRCA1-mutation carriers (Liu et al., 2008). Hence, it might be possible that only in the lobules/acini where BRCA1 LOH occurred is the NF-κB pathway strongly activated. However, BRCA1 is not the only protein responsible for the global genomic stability, and several other proteins collaborate with BRCA1 in the DNA damage repair system. Indeed, it has been shown that mutations in some of these proteins (such as RAD51, BARD1, p53, etc.) can increase DNA damage resulting in a similar risk of breast cancer as that found in BRCA1-mutation carriers (Ralhan et al., 2007). Based on these findings, the lobules and acini that showed high expression of NF-κB might have undergone de-novo mutation in one of those genes involved in DNA damage repair, increasing DNA damage thus activating IKK/NEMO resulting in p100/p52 and RelB activation (the link between DNA damage and alternative NF-κB pathway activation will be discussed in the following sections).

Although the expression of these NF-κB components was elevated in the BRCA1-mutation carriers, it was not possible to correlate a nuclear versus cytoplasmic localization within the lobules as clearly as that observed in BRCA1 KO mouse mammary glands. A possible explanation for the difference in the nuclear localization of p52/RelB in the BRCA1 KO mouse mammary glands versus the more broad overall increase in BRCA1-mutated human mammary glands could be attributed to several factors: i) the transgenic mouse model versus the human BRCA1 mutated mammary gland; ii) the age (mice were studied after puberty, between 9 and 12 weeks old, while the human sections were from women spanning 35 years old to menopause); iii) the number of mouse estrous versus human menstrual cycles; iv) the number of pregnancies (all mice used were virgin while BRCA1-mutation carriers may have gone through pregnancy). So far, our findings demonstrate that deleterious BRCA1 mutations are able to increase the alternative NF-κB proteins in human mammary tissue.

The alternative NF-κB pathway activation induces stem/progenitor cell proliferation and blocks their differentiation

Both the alternative and canonical NF-κB pathways have been found to regulate proliferation and differentiation in the mammary gland. It has been reported that p52/RelB can rescue a delay in mammary gland development in transgenic mice with targeted super repressor IκBα expression (Demicco et al., 2005) while p100 overexpression can reduce branching formation during pregnancy (Connelly et al., 2007). Moreover, p65/p50 canonical NF-κB activity increases gradually during pregnancy then decreases at parturition at the onset of lactation. Notably, p65/p50 inhibits the prolactin receptor pathway thereby preventing lactogenic differentiation (Geymayer and Doppler,

2000) and mice lacking the catalytic function of IKKα cannot lactate due to a block in mammary epithelial proliferation (Cao et al., 2001). These data demonstrate that the expression of the alternative and canonical NF-κB activity is spatially and temporally regulated to induce proliferation and differentiation in the mammary gland. Indeed, our bioinformatics analysis performed on microarray data derived from human bipotent, progenitor, and differentiated mammary epithelial cell populations (Raouf et al., 2008) revealed that p100/p52 expression was significantly higher in the early progenitor compared to differentiated cells, suggesting an important role for the alternative NF-κB pathway in the proliferation and differentiation of these cell populations.

BRCA1 has also been shown to regulate the fate of mammary stem cells, and its loss has been associated with decreased number of ER-positive luminal cells and increased number of cells expressing the stem-cell marker ALDH1 (Liu et al., 2008). Taken together, these data demonstrate that BRCA1 loss-induced alternative NF-κB activation can affect stem and progenitor cell differentiation and proliferation.

FACS analysis of mammary epithelial-enriched stem and progenitor cell populations demonstrated that BRCA1 KO mice had higher numbers of the enriched-stem cell population in their mammary glands compared to those of BRCA1 WT. Previous groups also reported similar findings, where BRCA1 mutation carriers showed enlarged stem and progenitor cell populations, demonstrating a defect in the differentiation process due to BRCA1 loss of function (Lim et al., 2009; Liu et al., 2008; Proia et al., 2011). However, the mechanism behind this event has not yet been characterized. Therefore, it can be hypothesized that the elevated alternative NF-κB activity could be the defect providing these stem and progenitor cells the proliferative

signal necessary for their expansion and blocks their further differentiation. Indeed, not only did BRCA1-deficient mammary epithelial cells form more secondary mammospheres (a sign of increased stem cell self-renewal), but the use of the IKK inhibitor BMS-345541 blocked primary mammosphere formation, demonstrating that NF-κB activation blocks progenitor cell proliferation. The increased number of secondary mammospheres in BRCA1-deficient cells was also followed by elevated mRNA and protein levels of the stem cell marker CD44, which is regulated by growth factors involved in proliferation and differentiation (Hebbard et al., 2000). This increase in CD44 levels could be due to two phenomena: the increase in the stem cell number (more stem cells expressing CD44 in BRCA1 KO mice compared to BRCA1 WT mice) or the increase in the CD44 expression (BRCA1-deficient cells express higher level of CD44 mRNA compared to BRCA1-competent cells). Moreover, it was noticed that after BRCA1-knockdown in the stem-like HC11 cell line, CD44 mRNA levels increased. Therefore, all these scenarios could be possible: the elevated number of stem cells, the increased protein expression, and the BRCA1-mediated increase of CD44 mRNA levels (as shown in HC11 cells) might be the mediators of this effect.

A previous study found that BRCA1-mutant carriers had expanded stem and progenitor cell populations with increased expression of the stem-cell marker ALDH1 in some acini. It was also found that the ALDH1-positive acini correlated with LOH at the BRCA1 locus, while ALDH1-negative acini did not (Liu et al., 2008). Immunofluorescence analysis of ALDH1 in the BRCA1-mutation carriers showed that in one of the three sections most lobules were positive showing various levels of ALDH1 expression in the acini, while none of the BRCA1-wild type carriers were positive for

ALDH1. More interestingly, this section positive for ALDH1 was the same section that was also positive for p100/p52. When serial sections were examined, ALDH1-positive lobules correlated with those also positive for p100/p52, suggesting that the activation of the alternative NF-κB pathway may also be involved for the expansion of the ALDH1-positive cell population found in BRCA1-mutation carriers.

While these data demonstrated the role of NF-κB in the regulation of stem and progenitor cell proliferation, confirmation that the alternative NF-κB pathway activation in BRCA1-deficient cells could prevent differentiation was still required. To accomplish this goal, the stem-like HC11 cell line, a well-known culture model to study mammary epithelial cell differentiation, was used. After lactogenic stimuli, these cells form dome-like structures and produce milk proteins including β-casein (Perotti et al., 2009). Overexpression of p52 in the HC11 cell line blocked dome formation and β-casein production, demonstrating that the alternative NF-κB pathway activation blocks lactogenic mammary epithelial cell differentiation. All together, these findings provide novel insights into the role played by BRCA1 and NF-κB in mammary glands development. BRCA1 inactivation is followed by the alternative NF-κB pathway activation that in turn induces proliferation in the stem cells but at the same time blocks progenitor cell differentiation.

The alternative NF-κB pathway activation is necessary for BRCA1-deficient progenitor cell proliferation in a three-dimensional acini assay

The link between progesterone, NF-κB, and stem/progenitor cell proliferation has been extensively studied in recent years. Previous findings showed that progesterone is able to induce stem and progenitor cell proliferation through the RANK-L/RANK axis.

Once inside PR-positive cells, progesterone induces the expression of RANK-L, which can signal in a paracrine fashion by binding its receptor RANK on the cellular membrane of PR-negative stem and progenitor cells, thus activating the IKK complex which leads to cell proliferation (Joshi et al., 2010; Schramek et al., 2010).

A common method used to study the link between progesterone and mammary progenitor cell proliferation is the three-dimensional acini assay. When epithelial cells are isolated from a mammary gland and plated in a thick layer of Matrigel, only progenitor cells are able to grow and form acini. The size of the acini is a reflection of the proliferative potential of luminal progenitor cells. Acini formation is B27-dependent, as acini cannot form in the absence of B27 (a media supplement composed by progesterone, fatty acids, insulin, BSA, etc.). It was demonstrated that, when progesterone is added to the media, luminal progenitor cells can form acini even in absence of B27. Therefore, progesterone has been considered the main component able to induce acini formation from luminal progenitor cells *in vitro*. The same group also found that BRCA1-mutation carriers possess a population of luminal progenitor cells able to grow and form acini even in absence of B27 (progesterone-independent growth). This ability to grow in the absence of progesterone is maintained also when progesterone inhibitors are added to the media, demonstrating that these BRCA1-deficient luminal progenitor cells have an intrinsic defect in one or more signaling pathways rather than a ligand-independent activation of progesterone receptor (Lim et al., 2009). However, the mechanism behind this progesterone-independent growth of BRCA1-deficient cells is not yet understood. Hence, autologous constitutive NF-κB activation could be the intrinsic defect that allows progenitor cells to grow in a progesterone-independent manner.

When primary cells obtained from BRCA1 KO and WT mouse mammary glands were treated with the IKK inhibitor BMS-345541, luminal progenitor cells no longer formed acini in Matrigel, demonstrating the reliance of this cell population on NF-κB activity to proliferate. This complete block in acini formation can be explained by the ability of BMS-345541 to inhibit IKKα/β, thus blocking both the canonical and alternative NF-κB pathways. Therefore, a different NF-κB inhibitor that had already been shown to be selective and for which more extensive *in vivo* testing had been done was used. DMAPT is an IKK inhibitor that also represses pathways important for stem cell proliferation such as MAPK and PI3K. Moreover, DMAPT has been approved for clinical trials in patients with leukemia (Ghantous et al., 2013; Neelakantan et al., 2009). DMAPT treatment *in vitro* had a stronger effect compared to BMS-345541 in reducing the cell viability of the BRCA1-mutated HCC1937 cell line. When tested in the Matrigel acini assay, DMAPT completely blocked the formation of acini of BRCA1-deficient luminal progenitor cells growing in absence of progesterone; however, BRCA1-deficient luminal progenitor cells were still able to form acini in the presence of progesterone showing only a slight but significant reduction in their size. While BMS-345541 was able to completely block acini formation in all culture conditions, DMAPT showed a stronger and more targeted effect on BRCA1-deficient progenitor cells growing in absence of progesterone. This may be due to the higher selectivity of DMAPT in inhibiting other cellular pathways important for the proliferation of BRCA1-deficient cells.

Since these pharmacological inhibitors (DMAPT and BMS-345541) block both the canonical and alternative NF-κB pathways, to understand which one was more important for progenitor cell proliferation, a selective inhibition of one or the other

pathway was performed. When the canonical NF-κB pathway was specifically inhibited by the over expression of IκBα^{SR}, acini size was not reduced in any conditions, demonstrating that neither BRCA1-deficient nor wild type luminal progenitor cells require the canonical NF-κB activity to proliferate. On the other hand, when the alternative NF-κB pathway was specifically targeted using p100 shRNA, acini formation of BRCA1-deficient progenitor cells was almost completely blocked in absence of progesterone. However, BRCA1-deficient progenitor cells were still able to form acini in the presence of progesterone. It is possible that progesterone/RANK-L axis might amplify the proliferative signal in BRCA1-deficient luminal progenitor cells through the canonical NF-κB pathway or other pathways, partially bypassing the inhibition of the alternative NF-κB pathway and inducing a partial rescue of proliferation. A possible way to confirm this phenomenon might be the sequential inhibition of the alternative and canonical NF-κB pathways, where first the alternative NF-κB pathway is blocked using p100 shRNA and then the canonical NF-κB pathway is inhibited using the IκBα^{SR}. If progesterone can amplify the proliferative signal through the canonical NF-κB pathway after the inhibition of the alternative NF-κB pathway in BRCA1-deficient luminal progenitor cells, then a block in acini formation after the canonical NF-κB pathway inhibition could be expected.

As mentioned previously, the activation of the alternative NF-κB pathway is mediated by IKKα homodimers. To study the effect of IKKα inhibition on luminal progenitor cell proliferation in Matrigel, primary cells were isolated from mouse mammary glands expressing the IKKα^{AA} knock-in mutation that inactivates IKKα catalytic activity. Differently from what was observed with p100 inhibition, luminal

progenitor cells lacking IKKα activity were not able to form acini in either the presence or absence of progesterone. One explanation for the inability of $IKK\alpha^{AA}$ luminal progenitor cells to proliferate in the presence of progesterone might be due to the important role of nuclear IKKα. Indeed, as showed here, phospho-IKKα is found in the nucleus of BRCA1-deficient luminal progenitor cells, and a previous study showed that nuclear IKKα mediates cyclin D1 and Myc-dependent proliferation (Park et al., 2005). Moreover, IKKα has also been shown to activate NF-κB target genes in a p52/RelB-independent manner through directed histone H3 phosphorylation (Anest et al., 2003; Park et al., 2006). Hence, inhibition of IKKα not only blocks the activation of the alternative NF-κB pathway but can also result in the alteration of other cellular processes.

Based on our previous finding that DMAPT blocks progesterone-independent luminal progenitor cell proliferation *in vitro*, an experiment was performed in order to test whether the same effect could be achieved *in vivo*. DMAPT was injected i.p. in BRCA1 KO and BRCA1 WT mice, and then the ability of luminal progenitor cells to form acini was assessed. DMAPT was more effective *in vivo* than *in vitro* in blocking acini formation of both BRCA1-deficient and wild type progenitor cells in the presence or absence of progesterone. This strongest inhibition observed *in vivo* could be a result of achieving higher DMAPT concentration in the luminal progenitor cells or affecting surrounding cells in the mammary gland.

As mentioned in the introduction, human and mouse mammary glands are subjected to cyclic stimulation of progesterone levels, which peak after ovulation (every 5 days in mice and 28 days in human). Progesterone has been implicated in breast cancer initiation (Brisken, 2013); indeed, several studies have demonstrated that bilateral

ovariectomy reduces the risk of BRCA1-associated breast cancers (Kauff et al., 2008; Rebbeck, 2000), while the progesterone antagonist, mifepristone, blocks tumor formation in BRCA1/p53-deficient mice (Poole et al., 2006). Hence, the effect of the physiological progesterone in recovering proliferation in the luminal progenitor cells was analyzed. Interestingly, when mice were left to recover for 2 weeks after the last injection of DMAPT, the acini formation was completely rescued in all conditions with the exception of BRCA1-deficient progenitor cells growing in absence of progesterone. One possible explanation for this result could be that when DMAPT injections were stopped, the BRCA1-deficient luminal progenitor cells were able to expand again due to the progesterone stimuli.

This finding could open the possibility for therapeutic intervention in patients with BRCA1 mutations. Indeed, the 2 week interval between DMAPT injection and assay for progesterone-independent progenitor cells corresponds to approximately 3 human menstrual cycles. Hence, cyclic DMAPT treatments (for example once every three months) may be sufficient to reduce the risk of breast cancer associated with proliferating pools of BRCA1-deficient luminal progenitor cells.

Taken together all these data demonstrate the key role of the alternative NF-κB activity in the luminal progenitor cells. Using pharmacological agents that inhibit both the canonical and alternative NF-κB pathways, BRCA1-deficient luminal progenitor cells are not able to form acini in Matrigel. However, the canonical NF-κB pathway appears to play a minor role in the proliferation of both BRCA1-competent and deficient luminal progenitor cells, while the alternative NF-κB pathway is fundamental for the BRCA1-

deficient luminal progenitor cells, providing the advantage of proliferating even in absence of progesterone stimulation.

DNA damage activates the alternative NF-κB pathway

BRCA1 plays a central role in maintaining genomic stability and its inactivation leads to replication fork stalling, DNA double strand breaks, genomic instability, and ultimately to cancer (Deng, 2006; Jasin, 2002; Konishi et al., 2011; Schlacher et al., 2012; Venkitaraman, 2014). When a DSB occurs, ATM is recruited, phosphorylated and in turn phosphorylates H2AX (necessary for the recruitment of several additional factors to the site of damage). For this reason ATM and H2AX are used as DNA damage markers (Harper and Elledge, 2007). As expected, BRCA1 knockdown in the MCF-7 cell line induced an elevated level of phosphorylated ATM and H2AX. When immunofluorescence was performed on cells isolated from mouse mammary glands, BRCA1-deficient stem and progenitor cells also showed a high level of phosphorylated ATM and H2AX, confirming that loss of BRCA1 function resulted in increased DNA damage *in vivo*. The same induction of DNA damage was also observed in BRCA1-mutation carriers. Indeed, two out of three BRCA1-mutation carriers showed high levels of phosphorylated ATM, while all BRCA1-wild type carriers were negative. Interestingly, if lobules were positive for p100/p52, RelB, and ALDH1, they were also positive for phosphorylated ATM. As discussed before, it is most likely that the lobules that show activation of ATM and NF-κB have undergone LOH for BRCA1 or de-novo mutation in those genes involved in DNA damage repair causing increased DNA damage.

The activation of NF-κB by DNA damage has been known since the late 90s (Piret et al., 1999) but only recently the molecular mechanism behind this has been

addressed. Indeed, it has been recently shown that after DNA damage, phosphorylated ATM can induce the nuclear export of NEMO, which in turn activates NF-κB (Gapud et al., 2011; Hadian and Krappmann, 2011; Miyamoto, 2011). Hence, ATM activation might be the link between BRCA1 loss of function, abnormal NF-κB activation, and the expansion of genetically unstable progenitor cells in the mammary gland. Co-immunoprecipitation analysis showed higher level of NEMO binding ATM in the BRCA1-mutated HCC1937 cells compared to BRCA1-wild type MCF-7 cells. When BRCA1 was knocked down in MCF-7 cells, an increase in ATM/NEMO complexes was also detected. However, this still did not prove that ATM-mediated NEMO nuclear export was leading to increased NF-κB activity. When ATM was knocked down in HCC1937 and lin neg. cells from BRCA1 KO mouse mammary glands, a strong decrease in p52 formation was observed, indicating that NF-κB activation is mediated by ATM in a BRCA1-deficient cells. Moreover, when ATM was blocked by either shRNA or the chemical inhibitor KU-55933, acini formation was only blocked in BRCA1-deficient progenitor cells in absence of progesterone (the same effect observed with shp100), but no effect was noticed in the presence of progesterone (differently from what was observed with shp100). As discussed previously, progesterone is able to activate NF-κB. Hence, even if ATM is knocked down, progesterone/RANK-L signaling can still activate the alternative NF-κB pathway and maintain luminal progenitor cell proliferation yielding acini formation in the presence of progesterone. However, without progesterone, acini formation depends on ATM-mediated NF-κB activation. These findings demonstrate how the DNA damage that follows BRCA1 inactivation is responsible for NF-κB activation, which promotes aberrant luminal progenitor cell proliferation.

Progesterone increases replication-mediated DNA damage in mouse mammary glands

Progesterone is a key hormone in the physiology of the mammary glands: after every ovulatory phase, human and mouse mammary glands are subjected to high levels of progesterone driving proliferation (Beleut et al., 2010; Joshi et al., 2010). Indeed, after injecting mice with progesterone, it was noticed an overall increase in the Ki-67 positive cells, demonstrating an increase in cell proliferation. Interestingly, while all Ki-67 positive cells in progesterone-treated BRCA1 WT mammary glands were localized to the luminal compartment, in progesterone and vehicle-treated BRCA1 KO mammary glands Ki-67 positive cells were mostly present in the basal compartment. The reason for this differential Ki-67 compartmental localization can be explained by our and others' findings (Lim et al., 2009; Liu et al., 2008; Proia et al., 2011) showing that BRCA1 loss or mutation induces expansion of progenitor cell population (that localize in the basal compartment) in the mammary glands. Hence, it is possible that the expanded aberrant luminal progenitor cell population found within the basal cell compartment in the BRCA1 KO mouse mammary glands also shows higher proliferation rates compared to that in the BRCA1 WT mouse mammary glands.

Recent evidence demonstrated that BRCA1 plays a key role during normal cellular replication, protecting stalled replication forks. Moreover, in cases where a DSB occurs, BRCA1 can activate HR and repair the lesion without any further damage. However, when BRCA1 function is lost, cells are more sensitive to stalled replication forks that lead to DSBs and genomic instability (Schlacher et al., 2012; Zhang and Powell, 2005). Hence, replication for a BRCA1-deficient cell can represent a big

challenge. All our previous findings demonstrated how BRCA1-deficient luminal progenitor cells have acquired the ability to proliferate in a progesterone-independent manner, even with more DNA damage than normal cells.

During normal replication, DNA breaks can occur and are normally repaired by BRCA1-directed HR (Nagaraju and Scully, 2007). Thus, in BRCA1-deficient cell, the progesterone-induced proliferation could lead to increased DNA damage. Indeed, when signs of replication-induced DNA damage were examined, progesterone differentially increased the level of phosphorylated H2AX in the lobules of mouse mammary glands. Moreover, while BRCA1 WT mice injected with progesterone showed a slight increase in phosphorylated H2AX, BRCA1 KO mice injected with progesterone showed a stronger increase in phosphorylated H2AX in the lobules of their mammary glands. This was probably a consequence of the progesterone-increased proliferation in BRCA1-deficient cells lacking the ability to repair DNA. Interestingly, the levels of phosphorylated H2AX were higher in vehicle-treated BRCA1 KO mouse mammary glands compared to those of vehicle-treated BRCA1 WT mice (in agreement with the role of BRCA1 in repairing DNA damage). When DMAPT was injected i.p, phosphorylated H2AX levels were strongly reduced in BRCA1-deficient cells. Two mechanisms can be proposed to explain this result: 1) DMAPT-mediated NF-κB inhibition could reduce luminal progenitor cell proliferation and as a consequence also reduce proliferation-related DNA damage. 2) DMAPT-mediated NF-κB inhibition could reduce the survival of these aberrant progenitor cells, inducing apoptosis and as a consequence reducing the cell number of this population. It is possible that either one or both mechanisms are induced by DMAPT in the BRCA1 KO mouse mammary glands.

However, more experiments need to be performed in order to clarify this effect of DMAPT in mouse mammary glands.

The elevated level of proliferation and DNA damage found in the BRCA1-deficient cells poses the question of how these cells persist since DNA damage often activates apoptosis. Two main options are available after DNA damage is encountered in a cell: repair it or, if the lesion is irreparable, apoptosis is the most common outcome (Roos and Kaina, 2006). The cleavage of the 116 kDa protein PARP-1 by activated caspase 3 and 7 results in the formation of the 89 kDa PARP-1 fragment, a well-known hallmark of apoptosis (Chaitanya et al., 2010; Herceg and Wang, 1999). BRCA1 WT mice injected with progesterone (under super physiological level of this hormone) showed an increase in the amount of the 89 kDa PARP-1 fragment, demonstrating that proliferation-induced DNA damage was activating the apoptotic pathway. However, BRCA1 KO mice injected with progesterone did not show any difference in the cleaved PARP-1 levels compared to BRCA1 KO mice vehicle-injected. Despite the higher level of DNA damage, BRCA1-deficient cells were able to block the apoptotic pathway and survive. It has recently been found that the 53BP1 protein is down-regulated in BRCA1-mutated breast cancer and its inhibition can promote viability of BRCA1-deficient cells through the rescue of HR function (Bouwman et al., 2010). It was also demonstrated that BRCA1 loss activates cathepsin L-mediated degradation of 53BP1 (Grotsky et al., 2013). Since cathepsin L has a κB site in its promoter (Seth et al., 2003), it might be possible that the increased activity of NF-κB found in BRCA1-deficient cells can induce cathepsin L-mediated 53BP1 degradation and rescue HR function, allowing the survival of this cell

population. However, more experimental evidence needs to be collected in order to confirm this hypothesis.

NF-κB activates Myc and cyclin D2

All the experiments performed so far focused on alternative NF-κB pathway activation and its function in luminal progenitor cells. However, since NF-κB is a transcription factor, NF-κB target genes that might explain the expanded BRCA1-deficient cell population were also considered. One of the potential candidates NF-κB target genes was the proto-oncogene Myc. Indeed, it has been demonstrated that Myc can be regulated by NF-κB and IKK at both the transcriptional and post transcriptional levels (Duyao et al., 1990; Kim et al., 2010; Yeh et al., 2011). Myc has long been linked to cellular growth (Dang, 2013), and its expression has been found elevated in BRCA1-associated cancers (Grushko et al., 2004). Hence, the possibility that NF-κB might be inducing the expansion of luminal progenitor cells through Myc activation was considered. Indeed, Myc levels were increased in BRCA1 KO mouse mammary gland and in BRCA1-mutation carriers. Moreover, Myc expression was regulated by NF-κB activity since both BMS-345541 and shp100 notably reduced Myc levels in HCC1937 and in BRCA1-deficient mouse progenitor cells. The use of shp100 confirmed that Myc expression was mostly regulated by the alternative NF-κB activation. However, confirmation that this NF-κB-directed Myc expression was inducing luminal progenitor cell proliferation had still to be proved. When mouse luminal progenitor cells were plated on Matrigel and Myc expression inhibited with Myc shRNA, an overall reduction of acini size was observed (reflecting the same trend found with shp100). Moreover, the strongest reduction was noticed in the acini size from BRCA1-deficient cells grown in absence of

progesterone, demonstrating that these cells rely in part on NF-κB-mediated Myc activation in order to proliferate.

Examination of gene signature of stem and luminal progenitor cells from patients with wild type BRCA1 and BRCA1 mutations (Liu et al., 2008) showed 6-fold increased expression in cyclin D2 in BRCA1-mutation carriers. Cyclin D2 is a protein with a key role in stem cell proliferation (Becker et al., 2010; Sasaki et al., 2004), and it has also been found to regulate mammary gland development. Indeed, cyclin D2 overexpression during pregnancy blocks lobuloalveolar proliferation and differentiation (Kong et al., 2002) having the same effect as p100 overexpression (Connelly et al., 2007). Currently, there is no evidence that NF-κB can regulate cyclin D2 at the transcriptional or protein levels; however, Myc is also a transcription factor and can regulate cyclin D2 expression (Bouchard et al., 1999). BRCA1-deficient primary cells isolated from mouse mammary glands showed increased cyclin D2 mRNA and protein levels compared to BRCA1-wild type cells. Moreover, cyclin D2 levels were regulated by NF-κB; indeed, when BMS-345541 was added to BRCA1-deficient primary cells, cyclin D2 mRNA levels were reduced. An even stronger reduction in cyclin D2 protein levels was achieved by blocking the alternative NF-κB pathway in HCC1937 cells using shp100. When DMAPT was used *in vivo*, a strong reduction in cyclin D2 protein levels was observed, confirming that the alternative NF-κB pathway was mediating the cyclin D2 expression in BRCA1 KO mouse mammary glands. Taken together these results demonstrate that the alternative NF-κB pathway activation is associated with increased Myc and cyclin D2 expression in BRCA1-deficient cells.

Conclusion and implication for diagnosis and treatment

In this work it was showed for the first time how the alternative NF-κB pathway is activated by DNA damage. After BRCA1 loss or mutation, the increased level in DNA damage causes NEMO-dependent IKK activation, that in turns leads to the nuclear RelB/p52 localization. The activation of the alternative NF-κB pathway increases the proliferation of the mouse mammary luminal progenitor cell population and blocks differentiation, allowing the expansion of the stem and progenitor cell compartments in the mammary glands. NF-κB induces the proliferation of these luminal progenitor cells even in absence of proliferative stimuli, such as progesterone. In the absence of functional BRCA1, these luminal progenitor cells acquire genomic instability but continue to expand as a consequence of the constitutive NF-κB activation.

Currently screening for mutation in the complete BRCA1 sequence is used as a standard method for breast cancer risk assessment. However, not all BRCA1 mutations are deleterious and assigning risk to the numerous mutations found in the gene is difficult (Borg et al., 2010). Moreover, several studies have demonstrated that inactivation of other proteins involved in the DNA damage repair machinery can contribute to or modify BRCA1-mutational cancer risk (Ralhan et al., 2007). Today, our understanding of breast cancer is moving from the concept of a single-gene disease to a multigenic disorder, where the combined effect of different altered pathways can drive breast cancer initiation. More efficient markers that could be used to predict breast cancer risk are needed. As such, alternative NF-κB activation in the presence of various BRCA1 or other DNA damage gene mutations could represent a promising assay for increased DNA damage and aberrant cell proliferation within a standardized mammary epithelial cell assay.

Finally, it was found that DMAPT treatment *in vivo* blocked the expansion of BRCA1-deficient luminal progenitor cells, suggesting an exciting new approach for the prevention of breast cancer initiation. Indeed, intermittent or cyclic therapy using DMAPT has the potential to mitigate breast cancer risk in BRCA1-mutation carriers through acute reduction of aberrant progenitor cell activity. As such, NF-κB-directed chemopreventive therapies may provide promising alternatives to prophylactic mastectomy in this high-risk patient population.

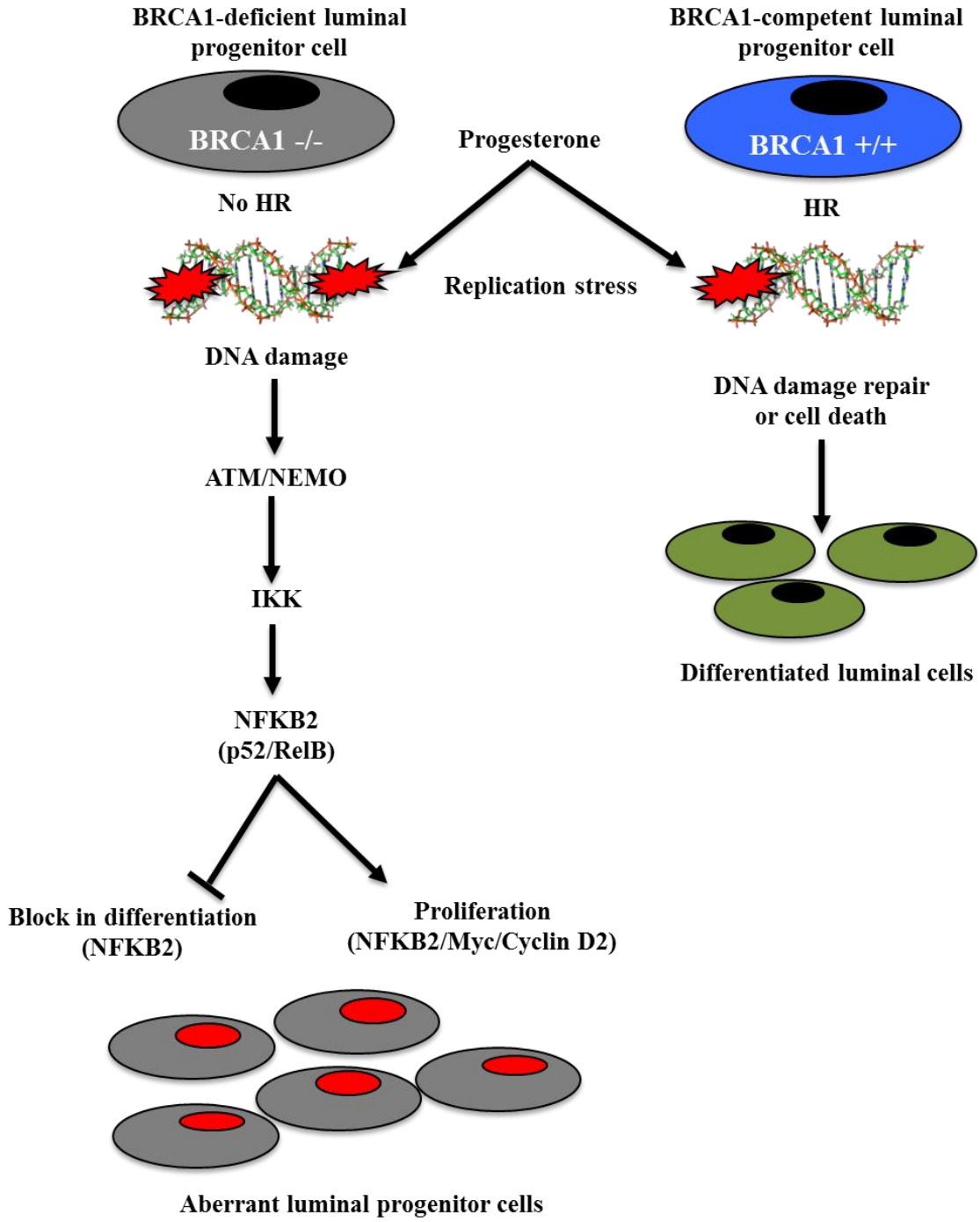

Figure 33: Proposed model of alternative NF-κB activation in BRCA1-deficient luminal progenitor cells

REFERENCES

Ak, P., and Levine, A.J. (2010). p53 and NF-κB: different strategies for responding to stress lead to a functional antagonism. FASEB J. Off. Publ. Fed. Am. Soc. Exp. Biol. *24*, 3643–3652.

Anderson, G.L., Chlebowski, R.T., Aragaki, A.K., Kuller, L.H., Manson, J.E., Gass, M., Bluhm, E., Connelly, S., Hubbell, F.A., Lane, D., et al. (2012). Conjugated equine oestrogen and breast cancer incidence and mortality in postmenopausal women with hysterectomy: extended follow-up of the Women's Health Initiative randomised placebo-controlled trial. Lancet Oncol. *13*, 476–486.

Andrechek, E.R., Hardy, W.R., Siegel, P.M., Rudnicki, M.A., Cardiff, R.D., and Muller, W.J. (2000). Amplification of the neu/erbB-2 oncogene in a mouse model of mammary tumorigenesis. Proc. Natl. Acad. Sci. U. S. A. *97*, 3444–3449.

Anest, V., Hanson, J.L., Cogswell, P.C., Steinbrecher, K.A., Strahl, B.D., and Baldwin, A.S. (2003). A nucleosomal function for IkappaB kinase-alpha in NF-kappaB-dependent gene expression. Nature *423*, 659–663.

Asselin-Labat, M.-L., Shackleton, M., Stingl, J., Vaillant, F., Forrest, N.C., Eaves, C.J., Visvader, J.E., and Lindeman, G.J. (2006). Steroid hormone receptor status of mouse mammary stem cells. J. Natl. Cancer Inst. *98*, 1011–1014.

Asselin-Labat, M.-L., Vaillant, F., Sheridan, J.M., Pal, B., Wu, D., Simpson, E.R., Yasuda, H., Smyth, G.K., Martin, T.J., Lindeman, G.J., et al. (2010). Control of mammary stem cell function by steroid hormone signalling. Nature *465*, 798–802.

Bai, F., Smith, M.D., Chan, H.L., and Pei, X.-H. (2013). Germline mutation of Brca1 alters the fate of mammary luminal cells and causes luminal-to-basal mammary tumor transformation. Oncogene *32*, 2715–2725.

Beatson, G. (1896). On the treatment of inoperable cases of carcinoma of the mamma: suggestions for a new method of treatment, with illustrative cases.1. The Lancet *148*, 104–107.

Becker, K.A., Ghule, P.N., Lian, J.B., Stein, J.L., van Wijnen, A.J., and Stein, G.S. (2010). Cyclin D2 and the CDK substrate p220(NPAT) are required for self-renewal of human embryonic stem cells. J. Cell. Physiol. *222*, 456–464.

Beleut, M., Rajaram, R.D., Caikovski, M., Ayyanan, A., Germano, D., Choi, Y., Schneider, P., and Brisken, C. (2010). Two distinct mechanisms underlie progesterone-induced proliferation in the mammary gland. Proc. Natl. Acad. Sci. U. S. A. *107*, 2989–2994.

Bendall, H.H., Sikes, M.L., Ballard, D.W., and Oltz, E.M. (1999). An intact NF-κB signaling pathway is required for maintenance of mature B cell subsets. Mol. Immunol. *36*, 187–195.

Bernard, S., and Eilers, M. (2006). Control of cell proliferation and growth by Myc proteins. Results Probl. Cell Differ. *42*, 329–342.

Biswas, D.K., Shi, Q., Baily, S., Strickland, I., Ghosh, S., Pardee, A.B., and Iglehart, J.D. (2004). NF-kappa B activation in human breast cancer specimens and its role in cell proliferation and apoptosis. Proc. Natl. Acad. Sci. U. S. A. *101*, 10137–10142.

Booth, B.W., Boulanger, C.A., Anderson, L.H., Jimenez-Rojo, L., Brisken, C., and Smith, G.H. (2010). Amphiregulin mediates self-renewal in an immortal mammary epithelial cell line with stem cell characteristics. Exp. Cell Res. *316*, 422–432.

Borg, A., Haile, R.W., Malone, K.E., Capanu, M., Diep, A., Torngren, T., Teraoka, S., Begg, C.B., Thomas, D.C., Concannon, P., et al. (2010). Characterization of BRCA1 and BRCA2 Deleterious Mutations and Variants of Unknown Clinical Significance in Unilateral and Bilateral Breast Cancer: The WECARE Study. Hum. Mutat. *31*, E1200–E1240.

Bouchard, C., Thieke, K., Maier, A., Saffrich, R., Hanley-Hyde, J., Ansorge, W., Reed, S., Sicinski, P., Bartek, J., and Eilers, M. (1999). Direct induction of cyclin D2 by Myc contributes to cell cycle progression and sequestration of p27. EMBO J. *18*, 5321–5333.

Boulanger, C.A., Wagner, K.-U., and Smith, G.H. (2005). Parity-induced mouse mammary epithelial cells are pluripotent, self-renewing and sensitive to TGF-beta1 expression. Oncogene *24*, 552–560.

Bouwman, P., Aly, A., Escandell, J.M., Pieterse, M., Bartkova, J., van der Gulden, H., Hiddingh, S., Thanasoula, M., Kulkarni, A., Yang, Q., et al. (2010). 53BP1 loss rescues BRCA1 deficiency and is associated with triple-negative and BRCA-mutated breast cancers. Nat. Struct. Mol. Biol. *17*, 688–695.

Boyd, N.F., Guo, H., Martin, L.J., Sun, L., Stone, J., Fishell, E., Jong, R.A., Hislop, G., Chiarelli, A., Minkin, S., et al. (2007). Mammographic density and the risk and detection of breast cancer. N. Engl. J. Med. *356*, 227–236.

Brantley, D.M., Yull, F.E., Muraoka, R.S., Hicks, D.J., Cook, C.M., and Kerr, L.D. (2000). Dynamic expression and activity of NF-kappaB during post-natal mammary gland morphogenesis. Mech. Dev. *97*, 149–155.

Bray, F., Ren, J.-S., Masuyer, E., and Ferlay, J. (2013). Global estimates of cancer prevalence for 27 sites in the adult population in 2008. Int. J. Cancer *132*, 1133–1145.

Brisken, C. (2013). Progesterone signalling in breast cancer: a neglected hormone coming into the limelight. Nat. Rev. Cancer *13*, 385–396.

Brisken, C. (2014). Reply to Is progesterone a neutral or protective factor for breast cancer? Nat. Rev. Cancer *14*, 146.

Brisken, C., Heineman, A., Chavarria, T., Elenbaas, B., Tan, J., Dey, S.K., McMahon, J.A., McMahon, A.P., and Weinberg, R.A. (2000). Essential function of Wnt-4 in mammary gland development downstream of progesterone signaling. Genes Dev. *14*, 650–654.

Buckley, N.E., Conlon, S.J., Jirstrom, K., Kay, E.W., Crawford, N.T., O'Grady, A., Sheehan, K., Mc Dade, S.S., Wang, C.-W., McCance, D.J., et al. (2011). The DeltaNp63 proteins are key allies of BRCA1 in the prevention of basal-like breast cancer. Cancer Res. *71*, 1933–1944.

Cao, Y., Bonizzi, G., Seagroves, T.N., Greten, F.R., Johnson, R., Schmidt, E.V., and Karin, M. (2001). IKKalpha provides an essential link between RANK signaling and cyclin D1 expression during mammary gland development. Cell *107*, 763–775.

Chaitanya, G.V., Alexander, J.S., and Babu, P.P. (2010). PARP-1 cleavage fragments: signatures of cell-death proteases in neurodegeneration. Cell Commun. Signal. *8*, 31.

Chlebowski, R.T., Anderson, G.L., Gass, M., Lane, D.S., Aragaki, A.K., Kuller, L.H., Manson, J.E., Stefanick, M.L., Ockene, J., Sarto, G.E., et al. (2010). Estrogen plus progestin and breast cancer incidence and mortality in postmenopausal women. JAMA J. Am. Med. Assoc. *304*, 1684–1692.

Chua, H.L., Bhat-Nakshatri, P., Clare, S.E., Morimiya, A., Badve, S., and Nakshatri, H. (2007). NF-kappaB represses E-cadherin expression and enhances epithelial to mesenchymal transition of mammary epithelial cells: potential involvement of ZEB-1 and ZEB-2. Oncogene *26*, 711–724.

Ciccia, A., and Elledge, S.J. (2010). The DNA damage response: making it safe to play with knives. Mol. Cell *40*, 179–204.

Clark, S.L., Rodriguez, A.M., Snyder, R.R., Hankins, G.D.V., and Boehning, D. (2012). Structure-Function of the Tumor Suppressor BRCA1. Comput. Struct. Biotechnol. J. *1*.

Clark-Knowles, K.V., Garson, K., Jonkers, J., and Vanderhyden, B.C. (2007). Conditional inactivation of Brca1 in the mouse ovarian surface epithelium results in an increase in preneoplastic changes. Exp. Cell Res. *313*, 133–145.

Clarkson, R.W.E., Heeley, J.L., Chapman, R., Aillet, F., Hay, R.T., Wyllie, A., and Watson, C.J. (2000). NF-κB Inhibits Apoptosis in Murine Mammary Epithelia. J. Biol. Chem. *275*, 12737–12742.

Claudio, E., Brown, K., Park, S., Wang, H., and Siebenlist, U. (2002). BAFF-induced NEMO-independent processing of NF-kappa B2 in maturing B cells. Nat. Immunol. *3*, 958–965.

Cogswell, P.C., Guttridge, D.C., Funkhouser, W.K., and Baldwin, A.S. (2000). Selective activation of NF-kappa B subunits in human breast cancer: potential roles for NF-kappa B2/p52 and for Bcl-3. Oncogene *19*, 1123–1131.

Cohnheim, J. (1875). Congenitales, quergestreiftes Muskelsarkom der Nieren. Arch. Für Pathol. Anat. Physiol. Für Klin. Med. *65*, 64–69.

Connelly, L., Robinson-Benion, C., Chont, M., Saint-Jean, L., Li, H., Polosukhin, V.V., Blackwell, T.S., and Yull, F.E. (2007). A transgenic model reveals important roles for the NF-kappa B alternative pathway (p100/p52) in mammary development and links to tumorigenesis. J. Biol. Chem. *282*, 10028–10035.

Connelly, L., Barham, W., Onishko, H.M., Sherrill, T., Chodosh, L.A., Blackwell, T.S., and Yull, F.E. (2011). Inhibition of NF-kappa B activity in mammary epithelium increases tumor latency and decreases tumor burden. Oncogene *30*, 1402–1412.

Coussens, L.M., and Werb, Z. (2002). Inflammation and cancer. Nature *420*, 860–867.

Dang, C.V. (2013). MYC, Metabolism, Cell Growth, and Tumorigenesis. Cold Spring Harb. Perspect. Med. *3*, a014217.

Daniel, C.W., Silberstein, G.B., and Strickland, P. (1987). Direct action of 17 beta-estradiol on mouse mammary ducts analyzed by sustained release implants and steroid autoradiography. Cancer Res. *47*, 6052–6057.

David, H. (1988). Rudolf Virchow and modern aspects of tumor pathology. Pathol. Res. Pract. *183*, 356–364.

Dejardin, E., Bonizzi, G., Bellahcène, A., Castronovo, V., Merville, M.P., and Bours, V. (1995). Highly-expressed p100/p52 (NFKB2) sequesters other NF-kappa B-related proteins in the cytoplasm of human breast cancer cells. Oncogene *11*, 1835–1841.

Demicco, E.G., Kavanagh, K.T., Romieu-Mourez, R., Wang, X., Shin, S.R., Landesman-Bollag, E., Seldin, D.C., and Sonenshein, G.E. (2005). RelB/p52 NF-kappaB complexes rescue an early delay in mammary gland development in transgenic mice with targeted superrepressor IkappaB-alpha expression and promote carcinogenesis of the mammary gland. Mol. Cell. Biol. *25*, 10136–10147.

Deng, C.-X. (2006). BRCA1: cell cycle checkpoint, genetic instability, DNA damage response and cancer evolution. Nucleic Acids Res. *34*, 1416–1426.

Deng, C.X., and Brodie, S.G. (2000). Roles of BRCA1 and its interacting proteins. BioEssays News Rev. Mol. Cell. Dev. Biol. *22*, 728–737.

Deome, K.B., Faulkin, L.J., Bern, H.A., and Blair, P.B. (1959). Development of mammary tumors from hyperplastic alveolar nodules transplanted into gland-free mammary fat pads of female C3H mice. Cancer Res. *19*, 515–520.

Dontu, G., Al-Hajj, M., Abdallah, W.M., Clarke, M.F., and Wicha, M.S. (2003a). Stem cells in normal breast development and breast cancer. Cell Prolif. *36*, 59–72.

Dontu, G., Abdallah, W.M., Foley, J.M., Jackson, K.W., Clarke, M.F., Kawamura, M.J., and Wicha, M.S. (2003b). In vitro propagation and transcriptional profiling of human mammary stem/progenitor cells. Genes Dev. *17*, 1253–1270.

Duyao, M.P., Buckler, A.J., and Sonenshein, G.E. (1990). Interaction of an NF-kappa B-like factor with a site upstream of the c-myc promoter. Proc. Natl. Acad. Sci. U. S. A. *87*, 4727–4731.

Easton, D.F., Ford, D., and Bishop, D.T. (1995). Breast and ovarian cancer incidence in BRCA1-mutation carriers. Breast Cancer Linkage Consortium. Am. J. Hum. Genet. *56*, 265–271.

Fabbro, M., Savage, K., Hobson, K., Deans, A.J., Powell, S.N., McArthur, G.A., and Khanna, K.K. (2004). BRCA1-BARD1 complexes are required for p53Ser-15 phosphorylation and a G1/S arrest following ionizing radiation-induced DNA damage. J. Biol. Chem. *279*, 31251–31258.

Fata, J.E., Kong, Y.Y., Li, J., Sasaki, T., Irie-Sasaki, J., Moorehead, R.A., Elliott, R., Scully, S., Voura, E.B., Lacey, D.L., et al. (2000). The osteoclast differentiation

factor osteoprotegerin-ligand is essential for mammary gland development. Cell *103*, 41–50.

Fernández-Ramires, R., Solé, X., De Cecco, L., Llort, G., Cazorla, A., Bonifaci, N., Garcia, M.J., Caldés, T., Blanco, I., Gariboldi, M., et al. (2009). Gene expression profiling integrated into network modelling reveals heterogeneity in the mechanisms of BRCA1 tumorigenesis. Br. J. Cancer *101*, 1469–1480.

Fillmore, C., and Kuperwasser, C. (2007). Human breast cancer stem cell markers CD44 and CD24: enriching for cells with functional properties in mice or in man? Breast Cancer Res. BCR *9*, 303.

Foreman, K.E., Rizzo, P., Osipo, C., and Miele, L. (2009). The Cancer Stem Cell Hypothesis. In Stem Cells and Cancer, B.A. Teicher, and R.G. Bagley, eds. (Humana Press), pp. 3–14.

Foulkes, W.D., Stefansson, I.M., Chappuis, P.O., Bégin, L.R., Goffin, J.R., Wong, N., Trudel, M., and Akslen, L.A. (2003). Germline BRCA1 Mutations and a Basal Epithelial Phenotype in Breast Cancer. J. Natl. Cancer Inst. *95*, 1482–1485.

Furth, P.A. (1999). Mammary Gland Involution and Apoptosis of Mammary Epithelial Cells. J. Mammary Gland Biol. Neoplasia *4*, 123–127.

Furuta, S., Jiang, X., Gu, B., Cheng, E., Chen, P.-L., and Lee, W.-H. (2005). Depletion of BRCA1 impairs differentiation but enhances proliferation of mammary epithelial cells. Proc. Natl. Acad. Sci. U. S. A. *102*, 9176–9181.

Gapud, E.J., Dorsett, Y., Yin, B., Callen, E., Bredemeyer, A., Mahowald, G.K., Omi, K.Q., Walker, L.M., Bednarski, J.J., McKinnon, P.J., et al. (2011). Ataxia telangiectasia mutated (Atm) and DNA-PKcs kinases have overlapping activities during chromosomal signal joint formation. Proc. Natl. Acad. Sci. U. S. A. *108*, 2022–2027.

Garber, J.E. (2009). BRCA1/2-Associated and Sporadic Breast Cancers: Fellow Travelers or Not? Cancer Prev. Res. (Phila. Pa.) *2*, 100–103.

Geymayer, S., and Doppler, W. (2000). Activation of NF-kappaB p50/p65 is regulated in the developing mammary gland and inhibits STAT5-mediated beta-casein gene expression. FASEB J. Off. Publ. Fed. Am. Soc. Exp. Biol. *14*, 1159–1170.

Ghantous, A., Sinjab, A., Herceg, Z., and Darwiche, N. (2013). Parthenolide: from plant shoots to cancer roots. Drug Discov. Today *18*, 894–905.

Ghosh, S., and Karin, M. (2002). Missing pieces in the NF-kappaB puzzle. Cell *109 Suppl*, S81–S96.

Ginestier, C., Liu, S., and Wicha, M.S. (2009). Getting to the root of BRCA1-deficient breast cancer. Cell Stem Cell *5*, 229–230.

Gonzalez-Suarez, E., Branstetter, D., Armstrong, A., Dinh, H., Blumberg, H., and Dougall, W.C. (2007). RANK overexpression in transgenic mice with mouse mammary tumor virus promoter-controlled RANK increases proliferation and impairs alveolar differentiation in the mammary epithelia and disrupts lumen formation in cultured epithelial acini. Mol. Cell. Biol. *27*, 1442–1454.

Greenberg, R.A. (2011). BRCA1, Everything But the RING? Science *334*, 459–460.

Grotsky, D.A., Gonzalez-Suarez, I., Novell, A., Neumann, M.A., Yaddanapudi, S.C., Croke, M., Martinez-Alonso, M., Redwood, A.B., Ortega-Martinez, S., Feng, Z., et al. (2013). BRCA1 loss activates cathepsin L–mediated degradation of 53BP1 in breast cancer cells. J. Cell Biol. *200*, 187–202.

Grushko, T.A., Dignam, J.J., Das, S., Blackwood, A.M., Perou, C.M., Ridderstråle, K.K., Anderson, K.N., Wei, M.-J., Adams, A.J., Hagos, F.G., et al. (2004). MYC is amplified in BRCA1-associated breast cancers. Clin. Cancer Res. Off. J. Am. Assoc. Cancer Res. *10*, 499–507.

Guo, W., Keckesova, Z., Donaher, J.L., Shibue, T., Tischler, V., Reinhardt, F., Itzkovitz, S., Noske, A., Zürrer-Härdi, U., Bell, G., et al. (2012). Slug and Sox9 cooperatively determine the mammary stem cell state. Cell *148*, 1015–1028.

Hadian, K., and Krappmann, D. (2011). Signals from the nucleus: activation of NF-kappaB by cytosolic ATM in the DNA damage response. Sci. Signal. *4*, pe2.

Hall, J.M., Lee, M.K., Newman, B., Morrow, J.E., Anderson, L.A., Huey, B., and King, M.C. (1990). Linkage of early-onset familial breast cancer to chromosome 17q21. Science *250*, 1684–1689.

Hanahan, D., and Weinberg, R.A. (2011). Hallmarks of cancer: the next generation. Cell *144*, 646–674.

Harper, J.W., and Elledge, S.J. (2007). The DNA damage response: ten years after. Mol. Cell *28*, 739–745.

Haslam, S.Z., and Shyamala, G. (1979). Effect of oestradiol on progesterone receptors in normal mammary glands and its relationship with lactation. Biochem. J. *182*, 127–131.

Hayden, M.S., and Ghosh, S. (2004). Signaling to NF-kappaB. Genes Dev. *18*, 2195–2224.

Hayden, M.S., and Ghosh, S. (2008a). Shared principles in NF-kappaB signaling. Cell *132*, 344–362.

Hayden, M.S., and Ghosh, S. (2008b). Shared principles in NF-kappaB signaling. Cell *132*, 344–362.

Hebbard, L., Steffen, A., Zawadzki, V., Fieber, C., Howells, N., Moll, J., Ponta, H., Hofmann, M., and Sleeman, J. (2000). CD44 expression and regulation during mammary gland development and function. J. Cell Sci. *113*, 2619–2630.

Herceg, Z., and Wang, Z.-Q. (1999). Failure of Poly(ADP-Ribose) Polymerase Cleavage by Caspases Leads to Induction of Necrosis and Enhanced Apoptosis. Mol. Cell. Biol. *19*, 5124–5133.

Hofseth, L.J., Raafat, A.M., Osuch, J.R., Pathak, D.R., Slomski, C.A., and Haslam, S.Z. (1999). Hormone replacement therapy with estrogen or estrogen plus

medroxyprogesterone acetate is associated with increased epithelial proliferation in the normal postmenopausal breast. J. Clin. Endocrinol. Metab. *84*, 4559–4565.

Hosey, A.M., Gorski, J.J., Murray, M.M., Quinn, J.E., Chung, W.Y., Stewart, G.E., James, C.R., Farragher, S.M., Mulligan, J.M., Scott, A.N., et al. (2007). Molecular basis for estrogen receptor alpha deficiency in BRCA1-linked breast cancer. J. Natl. Cancer Inst. *99*, 1683–1694.

Hu, Y., Baud, V., Delhase, M., Zhang, P., Deerinck, T., Ellisman, M., Johnson, R., and Karin, M. (1999). Abnormal Morphogenesis But Intact IKK Activation in Mice Lacking the IKKα Subunit of IκB Kinase. Science *284*, 316–320.

Huang, S., Robinson, J.B., Deguzman, A., Bucana, C.D., and Fidler, I.J. (2000). Blockade of nuclear factor-kappaB signaling inhibits angiogenesis and tumorigenicity of human ovarian cancer cells by suppressing expression of vascular endothelial growth factor and interleukin 8. Cancer Res. *60*, 5334–5339.

Huang, T.T., Wuerzberger-Davis, S.M., Wu, Z.-H., and Miyamoto, S. (2003). Sequential modification of NEMO/IKKgamma by SUMO-1 and ubiquitin mediates NF-kappaB activation by genotoxic stress. Cell *115*, 565–576.

Huber, M.A., Azoitei, N., Baumann, B., Grunert, S., Sommer, A., Pehamberger, H., Kraut, N., Beug, H., and Wirth, T. (2004). NF-?B is essential for epithelial-mesenchymal transition and metastasis in a model of breast cancer progression. J. Clin. Invest. *114*, 569–581.

Janssens, S., and Tschopp, J. (2006). Signals from within: the DNA-damage-induced NF-kappaB response. Cell Death Differ. *13*, 773–784.

Jasin, M. (2002). Homologous repair of DNA damage and tumorigenesis: the BRCA connection. Oncogene *21*, 8981–8993.

Joshi, P.A., Jackson, H.W., Beristain, A.G., Di Grappa, M.A., Mote, P.A., Clarke, C.L., Stingl, J., Waterhouse, P.D., and Khokha, R. (2010). Progesterone induces adult mammary stem cell expansion. Nature *465*, 803–807.

Karamboulas, C., and Ailles, L. (2013). Developmental signaling pathways in cancer stem cells of solid tumors. Biochim. Biophys. Acta *1830*, 2481–2495.

Karin, M. (2006). Nuclear factor-kappaB in cancer development and progression. Nature *441*, 431–436.

Karin, M., and Lin, A. (2002). NF-kappaB at the crossroads of life and death. Nat. Immunol. *3*, 221–227.

Karin, M., and Ben-Neriah, Y. (2000). Phosphorylation meets ubiquitination: the control of NF-[kappa]B activity. Annu. Rev. Immunol. *18*, 621–663.

Kauff, N.D., Domchek, S.M., Friebel, T.M., Robson, M.E., Lee, J., Garber, J.E., Isaacs, C., Evans, D.G., Lynch, H., Eeles, R.A., et al. (2008). Risk-reducing salpingo-oophorectomy for the prevention of BRCA1- and BRCA2-associated breast and gynecologic cancer: a multicenter, prospective study. J. Clin. Oncol. Off. J. Am. Soc. Clin. Oncol. *26*, 1331–1337.

Kendellen, M.F., Bradford, J.W., Lawrence, C.L., Clark, K.S., and Baldwin, A.S. (2014). Canonical and non-canonical NF-κB signaling promotes breast cancer tumor-initiating cells. Oncogene *33*, 1297–1305.

Khaw, K.-T., Wareham, N., Bingham, S., Welch, A., Luben, R., and Day, N. (2008). Combined impact of health behaviours and mortality in men and women: the EPIC-Norfolk prospective population study. PLoS Med. *5*, e12.

Kim, B.-Y., Yang, J.-S., Kwak, S.-Y., Zhang, X., and Han, Y.-H. (2010). NEMO stabilizes c-Myc through direct interaction in the nucleus. FEBS Lett. *584*, 4524–4530.

Kim, J.-S., Krasieva, T.B., Kurumizaka, H., Chen, D.J., Taylor, A.M.R., and Yokomori, K. (2005). Independent and sequential recruitment of NHEJ and HR factors to DNA damage sites in mammalian cells. J. Cell Biol. *170*, 341–347.

King, M.-C. (2014). "The race" to clone BRCA1. Science *343*, 1462–1465.

Knoops, K.T.B., de Groot, L.C.P.G.M., Kromhout, D., Perrin, A.-E., Moreiras-Varela, O., Menotti, A., and van Staveren, W.A. (2004). Mediterranean diet, lifestyle factors, and 10-year mortality in elderly European men and women: the HALE project. JAMA J. Am. Med. Assoc. *292*, 1433–1439.

Komiya, Y., and Habas, R. (2008). Wnt signal transduction pathways. Organogenesis *4*, 68–75.

Kong, G., Chua, S.S., Yijun, Y., Kittrell, F., Moraes, R.C., Medina, D., and Said, T.K. (2002). Functional analysis of cyclin D2 and p27(Kip1) in cyclin D2 transgenic mouse mammary gland during development. Oncogene *21*, 7214–7225.

Konishi, H., Mohseni, M., Tamaki, A., Garay, J.P., Croessmann, S., Karnan, S., Ota, A., Wong, H.Y., Konishi, Y., Karakas, B., et al. (2011). Mutation of a single allele of the cancer susceptibility gene BRCA1 leads to genomic instability in human breast epithelial cells. Proc. Natl. Acad. Sci. *108*, 17773–17778.

Kordon, E.C., and Smith, G.H. (1998). An entire functional mammary gland may comprise the progeny from a single cell. Development *125*, 1921–1930.

Kouros-Mehr, H., Slorach, E.M., Sternlicht, M.D., and Werb, Z. (2006). GATA-3 maintains the differentiation of the luminal cell fate in the mammary gland. Cell *127*, 1041–1055.

Kubista, M., Rosner, M., Kubista, E., Bernaschek, G., and Hengstschläger, M. (2002). Brca1 regulates in vitro differentiation of mammary epithelial cells. Oncogene *21*, 4747–4756.

Laemmli, U.K. (1970). Cleavage of structural proteins during the assembly of the head of bacteriophage T4. Nature *227*, 680–685.

Leung, C.C.Y., and Glover, J.M. (2011). BRCT domains. Cell Cycle *10*, 2461–2470.

Li, N., Banin, S., Ouyang, H., Li, G.C., Courtois, G., Shiloh, Y., Karin, M., and Rotman, G. (2001). ATM is required for IkappaB kinase (IKKk) activation in response to DNA double strand breaks. J. Biol. Chem. *276*, 8898–8903.

Lim, E., Vaillant, F., Wu, D., Forrest, N.C., Pal, B., Hart, A.H., Asselin-Labat, M.-L., Gyorki, D.E., Ward, T., Partanen, A., et al. (2009). Aberrant luminal progenitors as the candidate target population for basal tumor development in BRCA1 mutation carriers. Nat. Med. *15*, 907–913.

Liu, S., Ginestier, C., Charafe-Jauffret, E., Foco, H., Kleer, C.G., Merajver, S.D., Dontu, G., and Wicha, M.S. (2008). BRCA1 regulates human mammary stem/progenitor cell fate. Proc. Natl. Acad. Sci. U. S. A. *105*, 1680–1685.

Longacre, T.A., and Bartow, S.A. (1986). A correlative morphologic study of human breast and endometrium in the menstrual cycle. Am. J. Surg. Pathol. *10*, 382–393.

Mallepell, S., Krust, A., Chambon, P., and Brisken, C. (2006). Paracrine signaling through the epithelial estrogen receptor alpha is required for proliferation and morphogenesis in the mammary gland. Proc. Natl. Acad. Sci. U. S. A. *103*, 2196–2201.

Mann, G.J., Thorne, H., Balleine, R.L., Butow, P.N., Clarke, C.L., Edkins, E., Evans, G.M., Fereday, S., Haan, E., Gattas, M., et al. (2006). Analysis of cancer risk and BRCA1 and BRCA2 mutation prevalence in the kConFab familial breast cancer resource. Breast Cancer Res. BCR *8*, R12.

Marquis, S.T., Rajan, J.V., Wynshaw-Boris, A., Xu, J., Yin, G.Y., Abel, K.J., Weber, B.L., and Chodosh, L.A. (1995). The developmental pattern of Brca1 expression implies a role in differentiation of the breast and other tissues. Nat. Genet. *11*, 17–26.

Masters, J.R., Drife, J.O., and Scarisbrick, J.J. (1977). Cyclic Variation of DNA synthesis in human breast epithelium. J. Natl. Cancer Inst. *58*, 1263–1265.

Medina, D. (1996). The mammary gland: a unique organ for the study of development and tumorigenesis. J. Mammary Gland Biol. Neoplasia *1*, 5–19.

Miki, Y., Swensen, J., Shattuck-Eidens, D., Futreal, P.A., Harshman, K., Tavtigian, S., Liu, Q., Cochran, C., Bennett, L.M., Ding, W., et al. (1994). A strong candidate for the breast and ovarian cancer susceptibility gene BRCA1. Science *266*, 66+.

Miyamoto, S. (2011). Nuclear initiated NF-κB signaling: NEMO and ATM take center stage. Cell Res. *21*, 116–130.

Molyneux, G., Geyer, F.C., Magnay, F.-A., McCarthy, A., Kendrick, H., Natrajan, R., Mackay, A., Grigoriadis, A., Tutt, A., Ashworth, A., et al. (2010). BRCA1 basal-like breast cancers originate from luminal epithelial progenitors and not from basal stem cells. Cell Stem Cell *7*, 403–417.

Mukharjee, S. (2010). Emperor of All Maladies: A Biography of Cancer (Scribner).

Mukherjee, A., Soyal, S.M., Li, J., Ying, Y., He, B., DeMayo, F.J., and Lydon, J.P. (2010). Targeting RANKL to a specific subset of murine mammary epithelial cells induces ordered branching morphogenesis and alveologenesis in the absence of

progesterone receptor expression. FASEB J. Off. Publ. Fed. Am. Soc. Exp. Biol. *24*, 4408–4419.

Mulac-Jericevic, B., Lydon, J.P., DeMayo, F.J., and Conneely, O.M. (2003). Defective mammary gland morphogenesis in mice lacking the progesterone receptor B isoform. Proc. Natl. Acad. Sci. U. S. A. *100*, 9744–9749.

Muti, P. (2014). Is progesterone a neutral or protective factor for breast cancer? Nat. Rev. Cancer *14*, 146.

Nagaraju, G., and Scully, R. (2007). Minding the gap: the underground functions of BRCA1 and BRCA2 at stalled replication forks. DNA Repair *6*, 1018–1031.

Nakshatri, H., Bhat-Nakshatri, P., Martin, D.A., Goulet, R.J., and Sledge, G.W. (1997). Constitutive activation of NF-kappaB during progression of breast cancer to hormone-independent growth. Mol. Cell. Biol. *17*, 3629–3639.

Naylor, M.J., Lockefeer, J.A., Horseman, N.D., and Ormandy, C.J. (2003). Prolactin regulates mammary epithelial cell proliferation via autocrine/paracrine mechanism. Endocrine *20*, 111–114.

Neelakantan, S., Nasim, S., Guzman, M.L., Jordan, C.T., and Crooks, P.A. (2009). Aminoparthenolides as novel anti-leukemic agents: Discovery of the NF-kappaB inhibitor, DMAPT (LC-1). Bioorg. Med. Chem. Lett. *19*, 4346–4349.

Nielsen, M., Thomsen, J.L., Primdahl, S., Dyreborg, U., and Andersen, J.A. (1987). Breast cancer and atypia among young and middle-aged women: a study of 110 medicolegal autopsies. Br. J. Cancer *56*, 814–819.

Park, G.Y., Wang, X., Hu, N., Pedchenko, T.V., Blackwell, T.S., and Christman, J.W. (2006). NIK is involved in nucleosomal regulation by enhancing histone H3 phosphorylation by IKKalpha. J. Biol. Chem. *281*, 18684–18690.

Park, K.-J., Krishnan, V., O'Malley, B.W., Yamamoto, Y., and Gaynor, R.B. (2005). Formation of an IKKalpha-dependent transcription complex is required for estrogen receptor-mediated gene activation. Mol. Cell *18*, 71–82.

Perotti, C., Wiedl, T., Florin, L., Reuter, H., Moffat, S., Silbermann, M., Hahn, M., Angel, P., and Shemanko, C.S. (2009). Characterization of mammary epithelial cell line HC11 using the NIA 15k gene array reveals potential regulators of the undifferentiated and differentiated phenotypes. Differ. Res. Biol. Divers. *78*, 269–282.

Perou, C.M., Sørlie, T., Eisen, M.B., van de Rijn, M., Jeffrey, S.S., Rees, C.A., Pollack, J.R., Ross, D.T., Johnsen, H., Akslen, L.A., et al. (2000). Molecular portraits of human breast tumours. Nature *406*, 747–752.

Piret, B., Schoonbroodt, S., and Piette, J. (1999). The ATM protein is required for sustained activation of NF-kappaB following DNA damage. Oncogene *18*, 2261–2271.

Poole, A.J., Li, Y., Kim, Y., Lin, S.-C.J., Lee, W.-H., and Lee, E.Y.-H.P. (2006). Prevention of Brca1-mediated mammary tumorigenesis in mice by a progesterone antagonist. Science *314*, 1467–1470.

Prat, A., Parker, J.S., Karginova, O., Fan, C., Livasy, C., Herschkowitz, J.I., He, X., and Perou, C.M. (2010). Phenotypic and molecular characterization of the claudin-low intrinsic subtype of breast cancer. Breast Cancer Res. BCR *12*, R68.

Pratt, M.A.C., Bishop, T.E., White, D., Yasvinski, G., Ménard, M., Niu, M.Y., and Clarke, R. (2003). Estrogen withdrawal-induced NF-kappaB activity and bcl-3 expression in breast cancer cells: roles in growth and hormone independence. Mol. Cell. Biol. *23*, 6887–6900.

Pratt, M.A.C., Tibbo, E., Robertson, S.J., Jansson, D., Hurst, K., Perez-Iratxeta, C., Lau, R., and Niu, M.Y. (2009). The canonical NF-kappaB pathway is required for formation of luminal mammary neoplasias and is activated in the mammary progenitor population. Oncogene *28*, 2710–2722.

Proia, T.A., Keller, P.J., Gupta, P.B., Klebba, I., Jones, A.D., Sedic, M., Gilmore, H., Tung, N., Naber, S.P., Schnitt, S., et al. (2011). Genetic predisposition directs breast cancer phenotype by dictating progenitor cell fate. Cell Stem Cell *8*, 149–163.

Rajan, J.V., Wang, M., Marquis, S.T., and Chodosh, L.A. (1996). Brca2 is coordinately regulated with Brca1 during proliferation and differentiation in mammary epithelial cells. Proc. Natl. Acad. Sci. U. S. A. *93*, 13078–13083.

Rajan, J.V., Marquis, S.T., Gardner, H.P., and Chodosh, L.A. (1997). Developmental expression of Brca2 colocalizes with Brca1 and is associated with proliferation and differentiation in multiple tissues. Dev. Biol. *184*, 385–401.

Ralhan, R., Kaur, J., Kreienberg, R., and Wiesmüller, L. (2007). Links between DNA double strand break repair and breast cancer: Accumulating evidence from both familial and nonfamilial cases. Cancer Lett. *248*, 1–17.

Raouf, A., Zhao, Y., To, K., Stingl, J., Delaney, A., Barbara, M., Iscove, N., Jones, S., McKinney, S., Emerman, J., et al. (2008). Transcriptome analysis of the normal human mammary cell commitment and differentiation process. Cell Stem Cell *3*, 109–118.

Rebbeck, T.R. (2000). Prophylactic oophorectomy in BRCA1 and BRCA2 mutation carriers. J. Clin. Oncol. Off. J. Am. Soc. Clin. Oncol. *18*, 100S – 3S.

Roos, W.P., and Kaina, B. (2006). DNA damage-induced cell death by apoptosis. Trends Mol. Med. *12*, 440–450.

Roy, R., Chun, J., and Powell, S.N. (2012). BRCA1 and BRCA2: different roles in a common pathway of genome protection. Nat. Rev. Cancer *12*, 68–78.

Sasaki, Y., Jensen, C.T., Karlsson, S., and Jacobsen, S.E.W. (2004). Enforced expression of cyclin D2 enhances the proliferative potential of myeloid progenitors, accelerates in vivo myeloid reconstitution, and promotes rescue of mice from lethal myeloablation. Blood *104*, 986–992.

Schlacher, K., Wu, H., and Jasin, M. (2012). A distinct replication fork protection pathway connects Fanconi anemia tumor suppressors to RAD51-BRCA1/2. Cancer Cell *22*, 106–116.

Schramek, D., Leibbrandt, A., Sigl, V., Kenner, L., Pospisilik, J.A., Lee, H.J., Hanada, R., Joshi, P.A., Aliprantis, A., Glimcher, L., et al. (2010). Osteoclast differentiation factor RANKL controls development of progestin-driven mammary cancer. Nature *468*, 98–102.

Scully, R., Ganesan, S., Vlasakova, K., Chen, J., Socolovsky, M., and Livingston, D.M. (1999). Genetic analysis of BRCA1 function in a defined tumor cell line. Mol. Cell *4*, 1093–1099.

Sen, R., and Baltimore, D. (1986). Multiple nuclear factors interact with the immunoglobulin enhancer sequences. Cell *46*, 705–716.

Senftleben, U., Cao, Y., Xiao, G., Greten, F.R., Krähn, G., Bonizzi, G., Chen, Y., Hu, Y., Fong, A., Sun, S.C., et al. (2001). Activation by IKKalpha of a second, evolutionary conserved, NF-kappa B signaling pathway. Science *293*, 1495–1499.

Seth, P., Mahajan, V.S., and Chauhan, S.S. (2003). Transcription of human cathepsin L mRNA species hCATL B from a novel alternative promoter in the first intron of its gene. Gene *321*, 83–91.

Shackleton, M., Vaillant, F., Simpson, K.J., Stingl, J., Smyth, G.K., Asselin-Labat, M.-L., Wu, L., Lindeman, G.J., and Visvader, J.E. (2006). Generation of a functional mammary gland from a single stem cell. Nature *439*, 84–88.

Shehata, M., Teschendorff, A., Sharp, G., Novcic, N., Russell, I.A., Avril, S., Prater, M., Eirew, P., Caldas, C., Watson, C.J., et al. (2012). Phenotypic and functional characterisation of the luminal cell hierarchy of the mammary gland. Breast Cancer Res. BCR *14*, R134.

Singh, H., Sen, R., Baltimore, D., and Sharp, P.A. (1986). A nuclear factor that binds to a conserved sequence motif in transcriptional control elements of immunoglobulin genes. Nature *319*, 154–158.

Sleeman, K.E., Kendrick, H., Robertson, D., Isacke, C.M., Ashworth, A., and Smalley, M.J. (2007). Dissociation of estrogen receptor expression and in vivo stem cell activity in the mammary gland. J. Cell Biol. *176*, 19–26.

Smalley, M.J., Kendrick, H., Sheridan, J.M., Regan, J.L., Prater, M.D., Lindeman, G.J., Watson, C.J., Visvader, J.E., and Stingl, J. (2012). Isolation of mouse mammary epithelial subpopulations: a comparison of leading methods. J. Mammary Gland Biol. Neoplasia *17*, 91–97.

Smith, A.P., Verrecchia, A., Fagà, G., Doni, M., Perna, D., Martinato, F., Guccione, E., and Amati, B. (2009). A positive role for Myc in TGFbeta-induced Snail transcription and epithelial-to-mesenchymal transition. Oncogene *28*, 422–430.

Solan, N.J., Miyoshi, H., Carmona, E.M., Bren, G.D., and Paya, C.V. (2002). RelB cellular regulation and transcriptional activity are regulated by p100. J. Biol. Chem. *277*, 1405–1418.

Solt, L.A., Madge, L.A., Orange, J.S., and May, M.J. (2007). Interleukin-1-induced NF-kappaB activation is NEMO-dependent but does not require IKKbeta. J. Biol. Chem. *282*, 8724–8733.

Sørlie, T., Tibshirani, R., Parker, J., Hastie, T., Marron, J.S., Nobel, A., Deng, S., Johnsen, H., Pesich, R., Geisler, S., et al. (2003). Repeated observation of breast tumor subtypes in independent gene expression data sets. Proc. Natl. Acad. Sci. *100*, 8418–8423.

Sovak, M.A., Bellas, R.E., Kim, D.W., Zanieski, G.J., Rogers, A.E., Traish, A.M., and Sonenshein, G.E. (1997). Aberrant nuclear factor-kappaB/Rel expression and the pathogenesis of breast cancer. J. Clin. Invest. *100*, 2952–2960.

Stingl, J. (2011). Estrogen and progesterone in normal mammary gland development and in cancer. Horm. Cancer *2*, 85–90.

Stingl, J., Eirew, P., Ricketson, I., Shackleton, M., Vaillant, F., Choi, D., Li, H.I., and Eaves, C.J. (2006). Purification and unique properties of mammary epithelial stem cells. Nature *439*, 993–997.

Tanaka, M., Fuentes, M.E., Yamaguchi, K., Durnin, M.H., Dalrymple, S.A., Hardy, K.L., and Goeddel, D.V. (1999). Embryonic lethality, liver degeneration, and impaired NF-kappa B activation in IKK-beta-deficient mice. Immunity *10*, 421–429.

Till, J.E., and McCulloch, E.A. (1961). A direct measurement of the radiation sensitivity of normal mouse bone marrow cells. Radiat. Res. *14*, 213–222.

Tkocz, D., Crawford, N.T., Buckley, N.E., Berry, F.B., Kennedy, R.D., Gorski, J.J., Harkin, D.P., and Mullan, P.B. (2012). BRCA1 and GATA3 corepress FOXC1 to inhibit the pathogenesis of basal-like breast cancers. Oncogene *31*, 3667–3678.

Tomlinson, G.E., Chen, T.T., Stastny, V.A., Virmani, A.K., Spillman, M.A., Tonk, V., Blum, J.L., Schneider, N.R., Wistuba, I.I., Shay, J.W., et al. (1998). Characterization of a breast cancer cell line derived from a germ-line BRCA1 mutation carrier. Cancer Res. *58*, 3237–3242.

Trichopoulou, A., Costacou, T., Bamia, C., and Trichopoulos, D. (2003). Adherence to a Mediterranean Diet and Survival in a Greek Population. N. Engl. J. Med. *348*, 2599–2608.

Tu, S.-M., Lin, S.-H., and Logothetis, C.J. (2002). Stem-cell origin of metastasis and heterogeneity in solid tumours. Lancet Oncol. *3*, 508–513.

Tuma, R.S. (2012). Cancer Stem Cell Hypothesis and Trastuzumab in HER2-Negative Tumors. J. Natl. Cancer Inst.

Vachon, C.M., Sellers, T.A., Vierkant, R.A., Wu, F.-F., and Brandt, K.R. (2002). Case-control study of increased mammographic breast density response to hormone replacement therapy. Cancer Epidemiol. Biomark. Prev. Publ. Am. Assoc. Cancer Res. Cosponsored Am. Soc. Prev. Oncol. *11*, 1382–1388.

Vargo-Gogola, T., and Rosen, J.M. (2007). Modelling breast cancer: one size does not fit all. Nat. Rev. Cancer *7*, 659–672.

Venkitaraman, A.R. (2014). Cancer Suppression by the Chromosome Custodians, BRCA1 and BRCA2. Science *343*, 1470–1475.

Visvader, J.E., and Stingl, J. (2014). Mammary stem cells and the differentiation hierarchy: current status and perspectives. Genes Dev. *28*, 1143–1158.

Walmer, D.K., Wrona, M.A., Hughes, C.L., and Nelson, K.G. (1992). Lactoferrin expression in the mouse reproductive tract during the natural estrous cycle: correlation with circulating estradiol and progesterone. Endocrinology *131*, 1458–1466.

Wang, S., Counterman, L.J., and Haslam, S.Z. (1990). Progesterone action in normal mouse mammary gland. Endocrinology *127*, 2183–2189.

Wang, X., Belguise, K., Kersual, N., Kirsch, K.H., Mineva, N.D., Galtier, F., Chalbos, D., and Sonenshein, G.E. (2007). Oestrogen signalling inhibits invasive phenotype by repressing RelB and its target BCL2. Nat. Cell Biol. *9*, 470–478.

Wicha, M.S., Liu, S., and Dontu, G. (2006). Cancer Stem Cells: An Old Idea—A Paradigm Shift. Cancer Res. *66*, 1883–1890.

Willis, N.A., Chandramouly, G., Huang, B., Kwok, A., Follonier, C., Deng, C., and Scully, R. (2014). BRCA1 controls homologous recombination at Tus/Ter-stalled mammalian replication forks. Nature *advance online publication*.

Wu, Z.-H., and Miyamoto, S. (2007). Many faces of NF-kappaB signaling induced by genotoxic stress. J. Mol. Med. Berl. Ger. *85*, 1187–1202.

Wu, Z.-H., and Miyamoto, S. (2008). Induction of a pro-apoptotic ATM-NF-kappaB pathway and its repression by ATR in response to replication stress. EMBO J. *27*, 1963–1973.

Wu, Z.-H., Shi, Y., Tibbetts, R.S., and Miyamoto, S. (2006). Molecular linkage between the kinase ATM and NF-kappaB signaling in response to genotoxic stimuli. Science *311*, 1141–1146.

Wu, Z.-H., Wong, E.T., Shi, Y., Niu, J., Chen, Z., Miyamoto, S., and Tergaonkar, V. (2010). ATM- and NEMO-dependent ELKS ubiquitination coordinates TAK1-mediated IKK activation in response to genotoxic stress. Mol. Cell *40*, 75–86.

Xu, X., Wagner, K.U., Larson, D., Weaver, Z., Li, C., Ried, T., Hennighausen, L., Wynshaw-Boris, A., and Deng, C.X. (1999). Conditional mutation of Brca1 in mammary epithelial cells results in blunted ductal morphogenesis and tumour formation. Nat. Genet. *22*, 37–43.

Yamane, K., Katayama, E., and Tsuruo, T. (2000). The BRCT regions of tumor suppressor BRCA1 and of XRCC1 show DNA end binding activity with a multimerizing feature. Biochem. Biophys. Res. Commun. *279*, 678–684.

Yeh, P.-Y., Lu, Y.-S., Ou, D.-L., and Cheng, A.-L. (2011). IκB kinases increase Myc protein stability and enhance progression of breast cancer cells. Mol. Cancer *10*, 53.

Zeman, M.K., and Cimprich, K.A. (2014). Causes and consequences of replication stress. Nat. Cell Biol. *16*, 2–9.

Zhang, J., and Powell, S.N. (2005). The Role of the BRCA1 Tumor Suppressor in DNA Double-Strand Break Repair. Mol. Cancer Res. *3*, 531–539.

(1996). Breast cancer and hormonal contraceptives: collaborative reanalysis of individual data on 53 297 women with breast cancer and 100 239 women without breast cancer from 54 epidemiological studies. The Lancet *347*, 1713–1727.

APPENDIX – SUPPLEMENTARY DATA

Paired t-tests

	Gene	Affy ID	p-value	Overexpressed in:
		Bipotent enriched vs Early/Commited Luminal progenitor		
[Alternative p100/p52]	**NFKB2**	g4505382_3p_x_at	0.04868619	Early/ Com Luminal
		Early/Com Luminal vs Mature Luminal Progenitor		
[Alternative p100/p52]	**NFKB2**	g4505382_3p_x_at	0.03715145	Early/Com Luminal

Figure 34: Analysis of expression of the NFKB2 gene in microarrays derived from Raouf et al., 2008 (GEO accession number GSE11395)

Expression levels derived from Affymetrix array analysis of 3 samples of human bipotent and committed luminal progenitor cells. Log2 expression values for the indicated probe sets were subjected to a paired t-test. Luminal progenitor enriched fraction expresses higher levels of p100/p52 than the bipotent cells and maintained a higher expression level than the mature luminal progenitor cells.

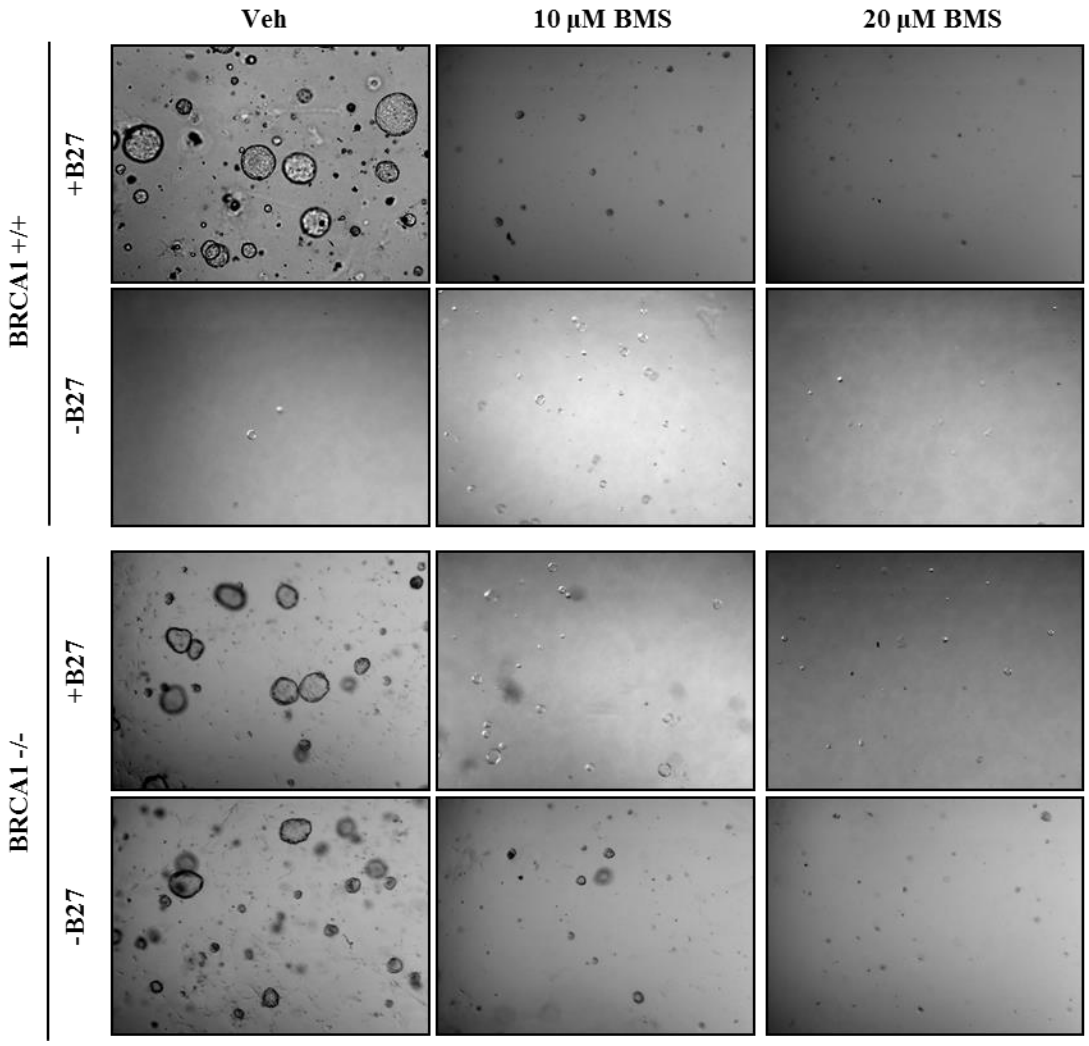

Figure 35: BMS-345541-treated lin neg. cells plated for acini assay

Lin neg. cells plated in Matrigel (2,000 cell in 20µL of Matrigel) were grown in the presence or absence of B27 for 15 days. Acini size was measured using Northern Eclipse. Objective 2.5X.

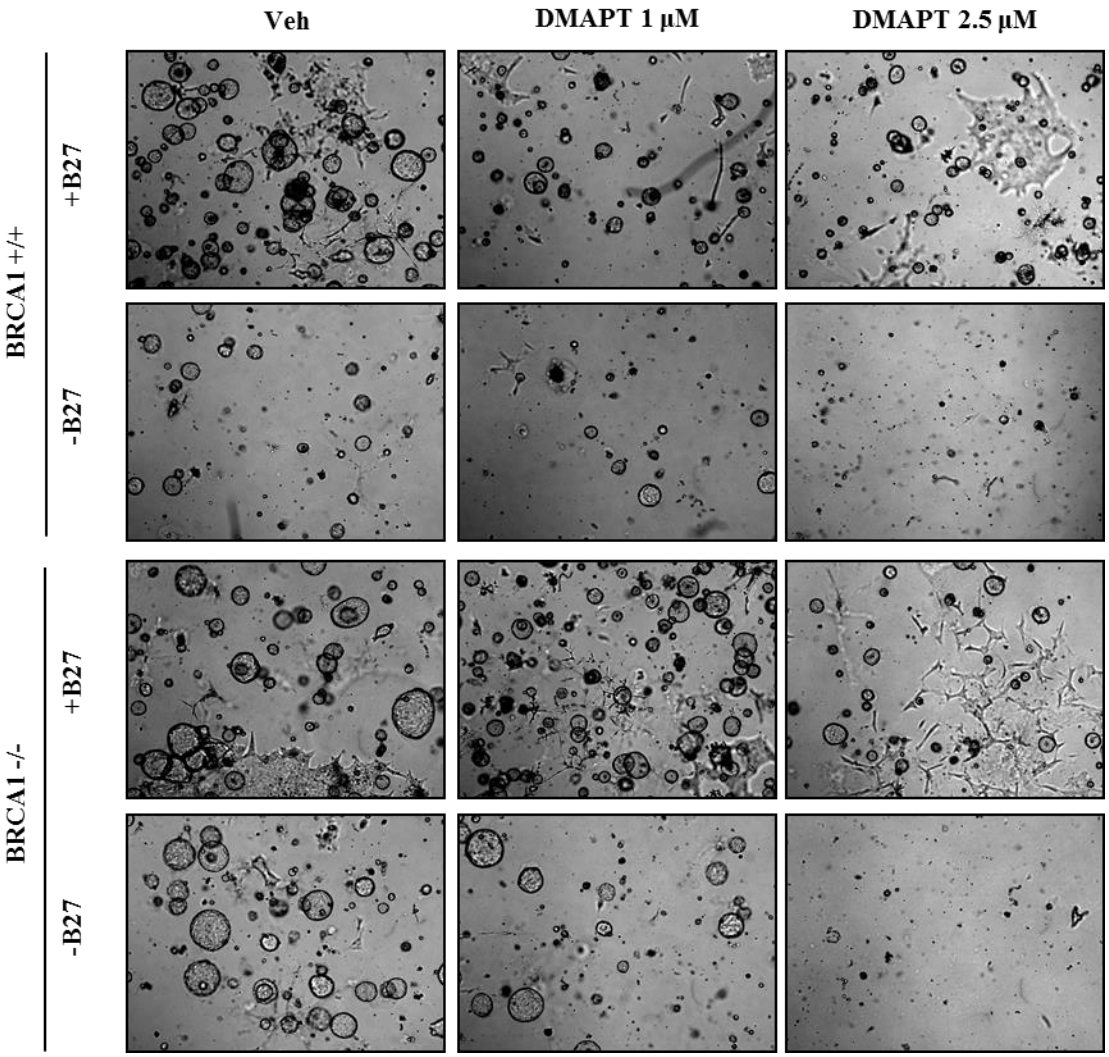

Figure 36: DMAPT-treated lin neg. cells plated for acini assay

Lin neg. cells plated in Matrigel (2,000 cell in 20µL of Matrigel) were grown in the presence or absence of B27 for 15 days. Acini size was measured using Northern Eclipse. Objective 2.5X.

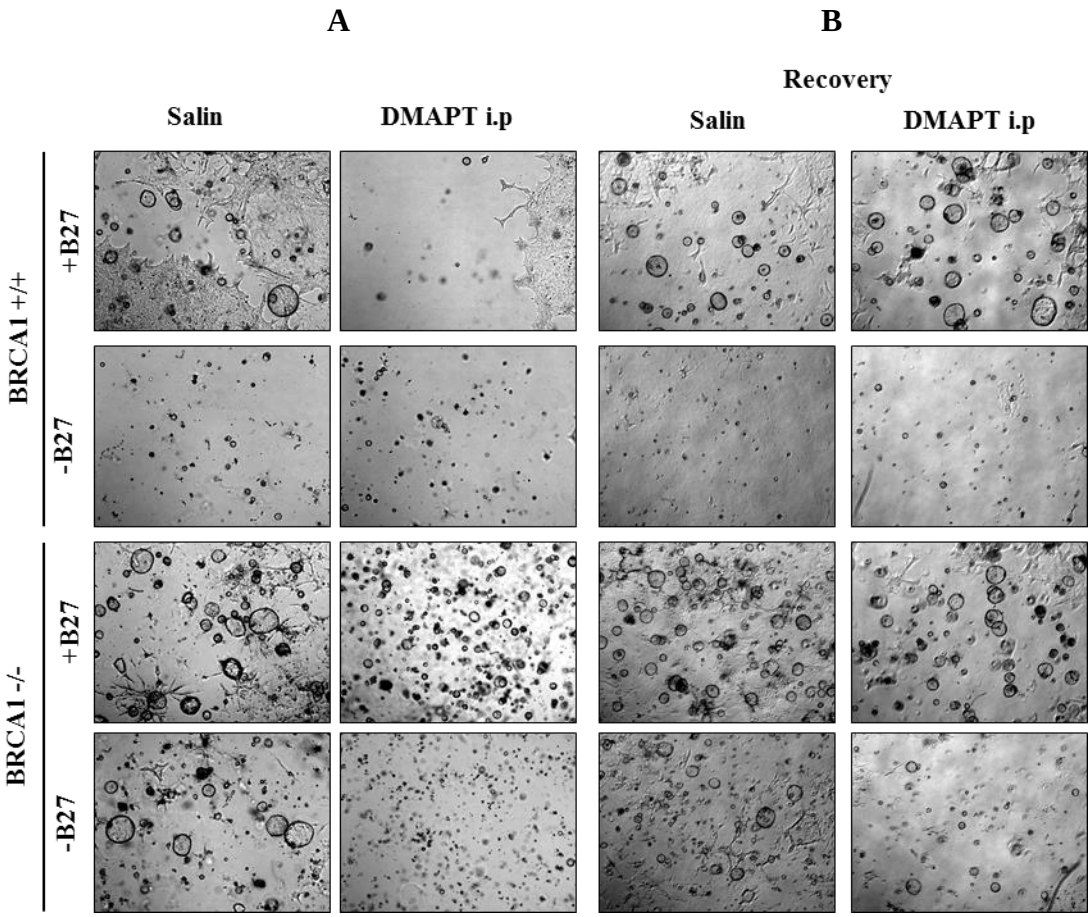

Figure 37: Lin neg. cells from mouse mammary glands DMAPT-injected plated for acini assay

Lin neg. cells plated in Matrigel (2,000 cell in 20µL of Matrigel) were grown in the presence or absence of B27 for 15 days. Lin neg. cells were collected **A**. the day after the last injection and **B**. two weeks after the last injection. Acini size was measured using Northern Eclipse. Objective 2.5X.

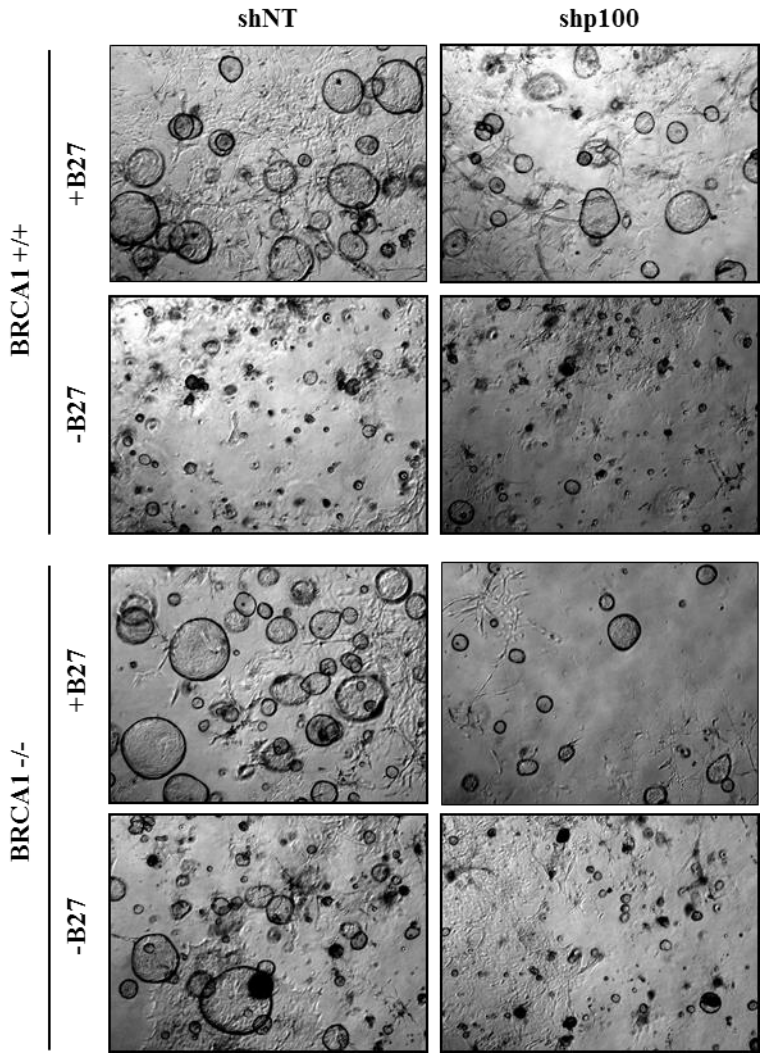

Figure 38: The effect of p100 inhibition on lin neg. cells plated for acini assay

Lin neg. cells plated in Matrigel (2,000 cell in 20μL of Matrigel) were grown in the presence or absence of B27 for 15 days. Acini size was measured using Northern Eclipse. Objective 2.5X.

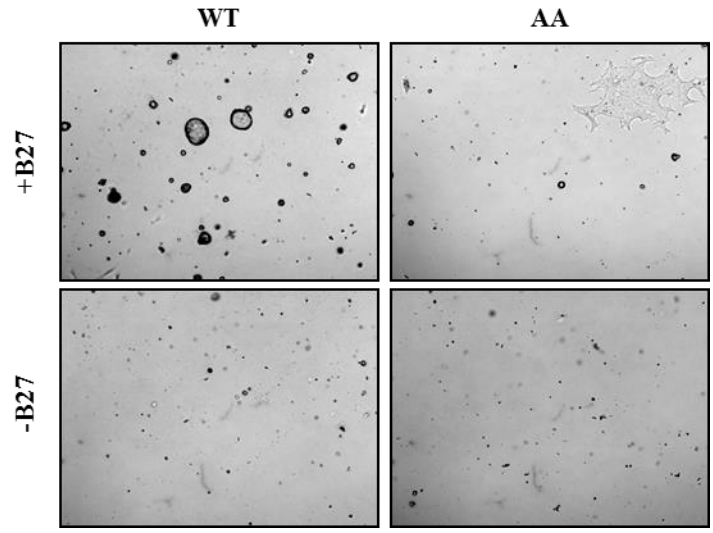

Figure 39: Lin neg. cells from IKKα^{AA} and IKKα^{WT} mouse mammary glands plated for acini assay

Lin neg. cells plated in Matrigel (2,000 cell in 20μL of Matrigel) were grown in the presence or absence of B27 for 15 days. Acini size was measured using Northern Eclipse. Objective 2.5X.

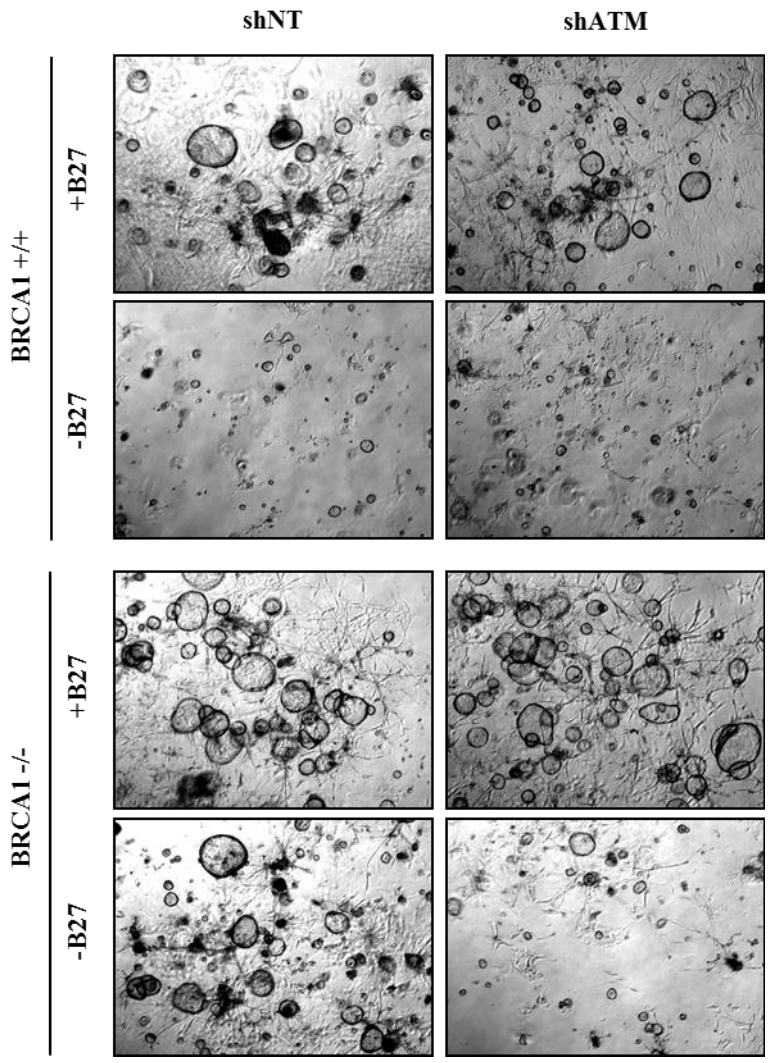

Figure 40: Effect of ATM inhibition on lin neg. cells plated for acini assay

Lin neg. cells plated in Matrigel (2,000 cell in 20μL of Matrigel) were grown in the presence or absence of B27 for 15 days. Acini size was measured using Northern Eclipse. Objective 2.5X.

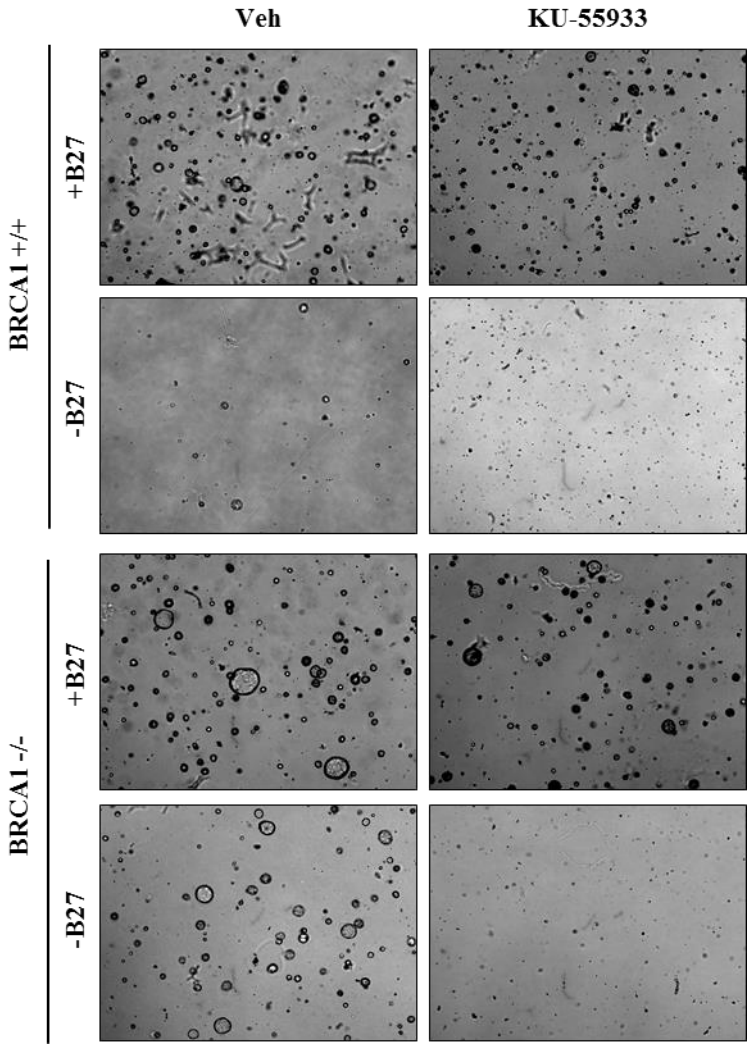

Figure 41: KU-55933-treated lin neg. cells plated for acini assay

Lin neg. cells plated in Matrigel (2,000 cell in 20μL of Matrigel) were grown in the presence or absence of B27 for 15 days. Acini size was measured using Northern Eclipse. Objective 2.5X.

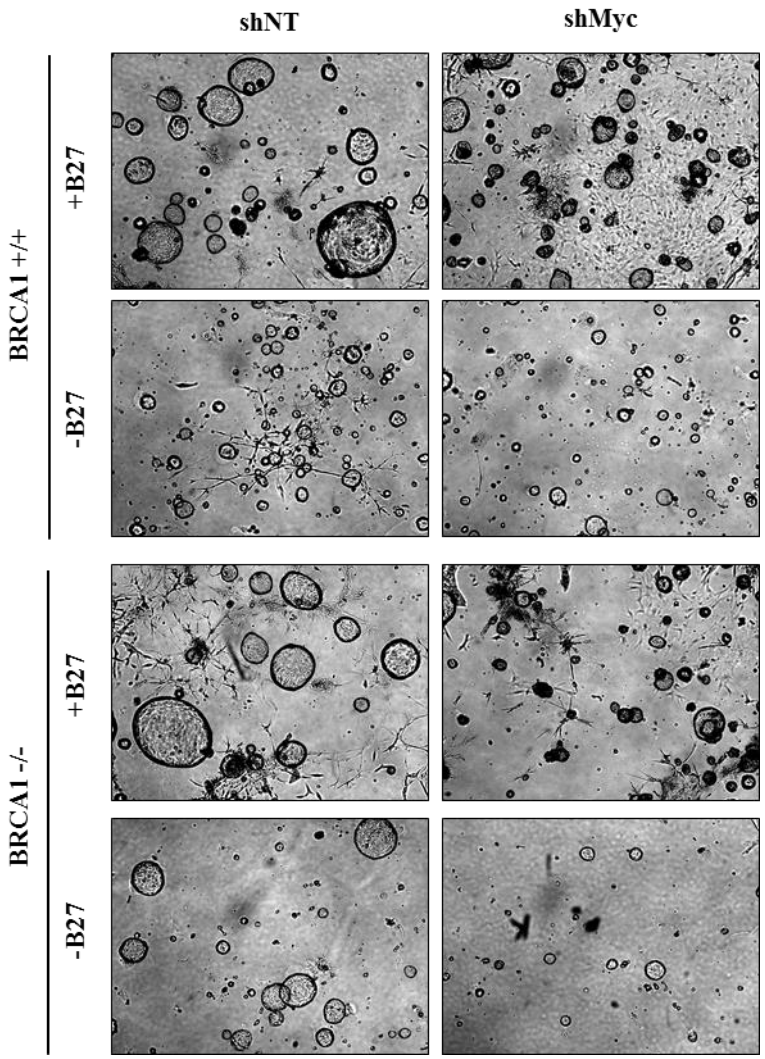

Figure 42: Effect of Myc inhibition on lin neg. cells plated for acini assay

Lin neg. cells plated in Matrigel (2,000 cell in 20μL of Matrigel) were grown in the presence or absence of B27 for 15 days. Acini size was measured using Northern Eclipse. Objective 2.5X.

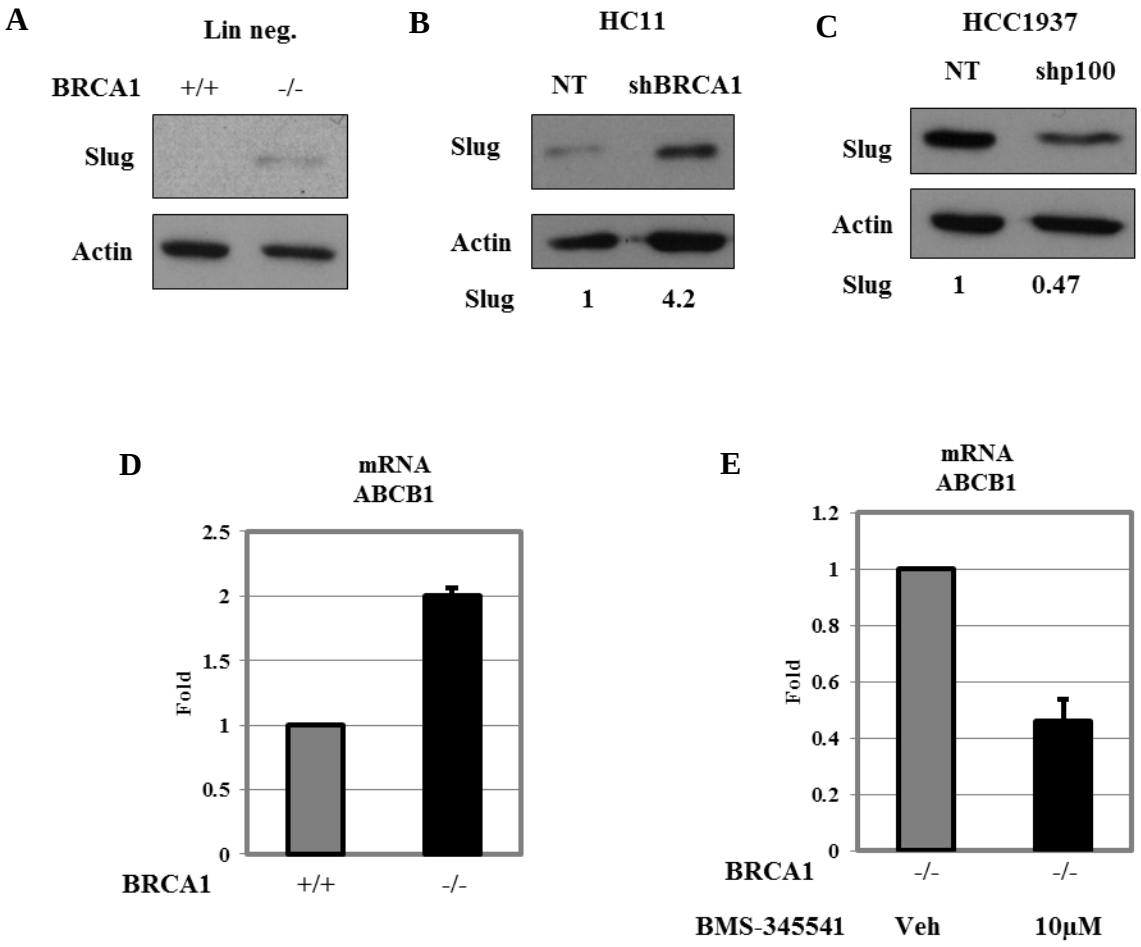

Figure 43: Slug protein levels and ABCB1 mRNA levels are increased in BRCA1-deficient cells

A. Whole cell lysates from lin neg. cells were immunoblotted for slug. BRCA1-deficient mouse mammary epithelial cells showed an increase in slug protein levels. **B.** Whole cell lysates from HC11 cells infected with lentivirus carrying non-targeting (NT) or BRCA1 shRNA were immunoblotted for slug. Actin was used as loading control. Numbers underneath actin represent slug protein levels quantification by ImageJ normalized to shNT levels. **C.** Whole cell lysates from HCC1937 cells infected with lentivirus carrying non-targeting (NT) or p100 shRNA were immunoblotted for slug. Actin was used as loading control. Numbers underneath actin represent slug protein levels quantification by ImageJ normalized to shNT levels. **D.** and **E.** mRNA was extracted from lin neg. cells treated with vehicle (Veh) or 10 μM BMS-345541 and qPCR performed for ABCB1. Actin was used as the housekeeping gene control. Immunoblots and graphs are representative of at least three independent experiments.